

# **BOI Zandige Waterkeringen: XBeach testbed BOI Phase 2 release 2022**

**skillbed quality status report**

Version: BOI release  
SVN Revision: 5924

21 July 2022

**BOI Zandige Waterkeringen:  
XBeach testbed  
BOI Phase 2 release 2022 ,**

**Published and printed by:**

Deltares  
Boussinesqweg 1  
2629 HV Delft  
P.O. 177  
2600 MH Delft  
The Netherlands

telephone: +31 88 335 82 73  
fax: +31 88 335 85 82  
e-mail: [info@deltares.nl](mailto:info@deltares.nl)  
www: <https://www.deltares.nl>

**For sales contact:**

telephone: +31 88 335 81 88  
fax: +31 88 335 81 11  
e-mail: [software@deltares.nl](mailto:software@deltares.nl)  
www: <https://www.deltares.nl/software>

**For support contact:**

telephone: +31 88 335 81 00  
fax: +31 88 335 81 11  
e-mail: [software.support@deltares.nl](mailto:software.support@deltares.nl)  
www: <https://www.deltares.nl/software>

Copyright © 2022 Deltares

All rights reserved. No part of this document may be reproduced in any form by print, photo print, photo copy, microfilm or any other means, without written permission from the publisher: Deltares.

## Contents

<b>List of Figures</b>	<b>v</b>
<b>List of Tables</b>	<b>xi</b>
<b>1 Introduction</b>	<b>1</b>
1.1 BOI settings . . . . .	1
1.2 Reader's guide . . . . .	1
<b>2 Laboratory experiments: hydrodynamics</b>	<b>5</b>
2.1 Long wave propagation . . . . .	5
2.2 1D wave runup (analytical solution) . . . . .	7
2.3 High- and low-frequency wave transformation over a barred beach . . . . .	8
2.4 High- and low-frequency wave transformation over a gentle sloping beach . . . . .	11
<b>3 Laboratory experiments: morphodynamics</b>	<b>15</b>
3.1 H4357: Delta Flume 2006 . . . . .	17
3.2 M1797: Delta Flume 1981 . . . . .	22
3.3 M1263 III: Delta Flume 1980-1981 . . . . .	24
3.4 LIP11D: Delta Flume 1994 . . . . .	31
3.5 Deltaflume H4731 . . . . .	33
3.6 Grosse Wellen Kanal 1998 . . . . .	34
<b>4 Field validation</b>	<b>41</b>
4.1 Schiermonnikoog . . . . .	41
4.2 Saint-Trojan . . . . .	47
4.3 Egmond . . . . .	51
4.4 Vlaanderen . . . . .	57
4.5 Vedersoe . . . . .	60
4.6 Fire-Island . . . . .	63
4.7 Langeoog . . . . .	67
4.8 Holland 1976 . . . . .	70
4.9 Holland 1953 . . . . .	74
<b>5 References</b>	<b>77</b>
<b>A Model Performance Statistics</b>	<b>81</b>
A.1 Introduction . . . . .	81
A.2 MPS parameters . . . . .	81
A.3 Mean Error & Standard Deviation . . . . .	81
A.4 Relative Bias . . . . .	82
A.5 Scatter Index . . . . .	82
<b>B Morphology indicators</b>	<b>83</b>
B.1 Erosion volume . . . . .	83
B.2 Dune front retreat . . . . .	83
B.3 Berm slope . . . . .	84
<b>C Detailed analysis</b>	<b>85</b>
C.1 Deltagoot 2006 . . . . .	85
C.2 LIP . . . . .	93



## List of Figures

2.1	Water levels and velocities from the start of the experiment until the wave just reaches the end of the flume. The amplitude of the analytical solution is shown with a red line. . . . .	6
2.2	Snapshots of water levels and velocities showing a standing wave pattern. The amplitude of the analytical solution is shown with a red line. . . . .	6
2.3	Snapshots of water level and velocity . . . . .	7
2.4	Locations of surface elevation measurements . . . . .	8
2.5	Wave hydrodynamics during experiment 1A. The observed short-wave height (dots) and observed infragravity wave height (triangles) are compared to the XBeach results (blue and red line) in the upper panel. The observed setup (dots) is compared to the setup computed with XBeach (blue line) in the second panel and the bathymetry is shown in the third panel. . . . .	9
2.6	Wave hydrodynamics during experiment 1B. The observed short-wave height (dots) and observed infragravity wave height (triangles) are compared to the XBeach results (blue and red line) in the upper panel. The observed setup (dots) is compared to the setup computed with XBeach (blue line) in the second panel and the bathymetry is shown in the third panel. . . . .	10
2.7	Wave hydrodynamics during experiment 1C. The observed short-wave height (dots) and observed infragravity wave height (triangles) are compared to the XBeach results (blue and red line) in the upper panel. The observed setup (dots) is compared to the setup computed with XBeach (blue line) in the second panel and the bathymetry is shown in the third panel. . . . .	10
2.8	Overview of the statistical scores of the Boers experiments. The relative error and scatter index for the short-wave height (upper panel), infragravity wave height (second panel) and setup (third panel) are shown for the different Boers experiments. . . . .	11
2.9	Elevation $z$ versus cross-shore distance $x$ in the Scheldegoot during the GLOBEX project. Here, $x = 0$ is the location of the wave-maker at rest, and $z = 0$ corresponds to the still water level. At $x = 84.6$ m the still water level intersected with the bed. The 190 dots are the positions of the wave gauges. . . . .	12
2.10	Wave hydrodynamics during experiment A1. The observed short-wave height (dots) and observed infragravity wave height (triangles) are compared to the XBeach results (blue and red line) in the upper panel. The observed setup (dots) is compared to the setup computed with XBeach (blue line) in the second panel and the bathymetry is shown in the third panel. . . . .	12
2.11	Wave hydrodynamics during experiment A2. The observed short-wave height (dots) and observed infragravity wave height (triangles) are compared to the XBeach results (blue and red line) in the upper panel. The observed setup (dots) is compared to the setup computed with XBeach (blue line) in the second panel and the bathymetry is shown in the third panel. . . . .	13
2.12	Wave hydrodynamics during experiment A3. The observed short-wave height (dots) and observed infragravity wave height (triangles) are compared to the XBeach results (blue and red line) in the upper panel. The observed setup (dots) is compared to the setup computed with XBeach (blue line) in the second panel and the bathymetry is shown in the third panel. . . . .	13
2.13	Overview of the statistical scores of the GLOBEX experiments. The relative error and scatter index for the short-wave height (upper panel), infragravity wave height (second panel) and setup (third panel) are shown for the different GLOBEX experiments. . . . .	14
3.1	Dune retreat indicator. See the Appendix for the definition of this indicator. . .	16
3.2	Definition of erosion volume. See the Appendix for the definition of this indicator.	16

3.3	Berm slope indicator. See the Appendix for the definition of this indicator. . . . .	16
3.4	Comparisons of profiles from experiment T01 for different moments in time. Observed profiles are shown with a dashed line and the XBeach profiles with a solid line. The storm surge level is shown with a black dashed line. . . . .	18
3.5	Temporal development of the relative error for the three indicators. . . . .	18
3.6	Comparisons of profiles from experiment T02 for different moments in time. Observed profiles are shown with a dashed line and the XBeach profiles with a solid line. The storm surge level is shown with a black dashed line. . . . .	19
3.7	Temporal development of the relative error for the three indicators. . . . .	19
3.8	Comparisons of profiles from experiment T03 for different moments in time. Observed profiles are shown with a dashed line and the XBeach profiles with a solid line. The storm surge level is shown with a black dashed line. . . . .	20
3.9	Temporal development of the relative error for the three indicators. . . . .	20
3.10	Comparisons of profiles from experiment T08 for different moments in time. Observed profiles are shown with a dashed line and the XBeach profiles with a solid line. The storm surge level is shown with a black dashed line. . . . .	21
3.11	Temporal development of the relative error for the three indicators. . . . .	21
3.12	Overview of statistical scores for the Deltagoot 2006 experiments. . . . .	22
3.13	Comparison of profile during experiment T01. Observed profiles are shown with a dashed line and the XBeach profiles with a solid line. The storm surge level is shown with a black dashed line. . . . .	23
3.14	Temporal development of the relative error for the three indicators. . . . .	23
3.15	Boundary conditions for test 3. The storm development is shown for the water level (upper panel), the wave height (second panel) and the peak period (lower panel) as a function of time. . . . .	25
3.16	Boundary conditions for test 4. The storm development is shown for the water level (upper panel), the wave height (second panel) and the peak period (lower panel) as a function of time. . . . .	25
3.17	Comparisons of profiles from experiment Test-1 for different moments in time. Observed profiles are shown with a dashed line and the XBeach profiles with a solid line. The storm surge level is shown with a black dashed line. . . . .	26
3.18	Temporal development of the relative error for the three indicators. . . . .	26
3.19	Comparisons of profiles from experiment Test-2 for different moments in time. Observed profiles are shown with a dashed line and the XBeach profiles with a solid line. The storm surge level is shown with a black dashed line. . . . .	27
3.20	Temporal development of the relative error for the three indicators. . . . .	27
3.21	Comparisons of profiles from experiment Test-3 for different moments in time. Observed profiles are shown with a dashed line and the XBeach profiles with a solid line. The storm surge level is shown with a black dashed line. . . . .	28
3.22	Temporal development of the relative error for the three indicators. . . . .	28
3.23	Comparisons of profiles from experiment Test-4 for different moments in time. Observed profiles are shown with a dashed line and the XBeach profiles with a solid line. The storm surge level is shown with a black dashed line. . . . .	29
3.24	Temporal development of the relative error for the three indicators. . . . .	29
3.25	Comparisons of profiles from experiment Test-5 for different moments in time. Observed profiles are shown with a dashed line and the XBeach profiles with a solid line. The storm surge level is shown with a black dashed line. . . . .	30
3.26	Temporal development of the relative error for the three indicators. . . . .	30
3.27	Overview of the statistical scores for M1263 experiments. . . . .	31
3.28	Comparisons of profiles from experiment LIP 2E for different moments in time. Observed profiles are shown with a dashed line and the XBeach profiles with a solid line. The storm surge level is shown with a black dashed line. . . . .	32
3.29	Temporal development of the relative error for the three indicators. . . . .	33

3.30	Comparison of profile during experiment T14 Observed profiles are shown with a dashed line and the XBeach profiles with a solid line. The storm surge level is shown with a black dashed line. . . . .	33
3.31	Temporal development of the relative error for the three indicators. . . . .	34
3.32	Comparisons of profiles from experiment A9 for different moments in time. Observed profiles are shown with a dashed line and the XBeach profiles with a solid line. The storm surge level is shown with a black dashed line. . . . .	35
3.33	Temporal development of the relative error for the three indicators. . . . .	35
3.34	Comparisons of profiles from experiment B2 for different moments in time. Observed profiles are shown with a dashed line and the XBeach profiles with a solid line. The storm surge level is shown with a black dashed line. . . . .	36
3.35	Temporal development of the relative error for the three indicators. . . . .	36
3.36	Comparisons of profiles from experiment C2 for different moments in time. Observed profiles are shown with a dashed line and the XBeach profiles with a solid line. The storm surge level is shown with a black dashed line. . . . .	37
3.37	Temporal development of the relative error for the three indicators. . . . .	37
3.38	Comparisons of profiles from experiment F1 for different moments in time. Observed profiles are shown with a dashed line and the XBeach profiles with a solid line. The storm surge level is shown with a black dashed line. . . . .	38
3.39	Temporal development of the relative error for the three indicators. . . . .	38
3.40	Comparisons of profiles from experiment H2 for different moments in time. Observed profiles are shown with a dashed line and the XBeach profiles with a solid line. The storm surge level is shown with a black dashed line. . . . .	39
3.41	Temporal development of the relative error for the three indicators. . . . .	39
3.42	GWK overview . . . . .	40
4.1	Overview of the Schiermonnikoog study area. Right: elevation at and surrounding Schiermonnikoog (mosaic of the ‘Vaklodingen’ of 2012-2015) and the location of the (offshore) hydraulic stations of RWS (black dots) and the transect (red line) with measurement equipment locations (red dots). Left: aerial photograph of the tail of Schiermonnikoog at 04-20-2014 (Google Earth). The coordinates are in meter (RD-new projection). . . . .	43
4.2	Cross-section with the modelled and measured water level and spectral significant wave height ( $H_{m0}$ ) of high and low frequency waves during the storm peak (11-01-2015 13:00-13:30). The grey zone around the modelled $H_{m0,hf}$ indicates the minimum and maximum $H_{m0,hf}$ . Note the difference between the modelled low frequency $H_{m0}$ (no frequency domain filter) (black line) and the measured infragravity $H_{m0}$ (0.005 and 0.05 Hz) at the point locations (grey-green dots). . . . .	44
4.3	Timeseries of measured and modelled water depth, short and infragravity spectral significant wave height including goodness-of-fit indicators for measurement location P1. . . . .	45
4.4	Scatter plot of the measured versus modelled water depth, spectral significant wave height ( $H_{m0}$ ) of short waves (G) and infragravity waves (IG) for all measurement locations at Schiermonnikoog. The dashed line indicates a perfect fit, the continuous line represents a linear fit through the point cloud . . . . .	46
4.5	Location of the Saint Trojan study area in the Bay of Biscay, with the Biscay buoy (x) and Chassiron Meteorological station (x). (b) Detailed bathymetry of the study area (m relative to mean sea level), showing the location of the offshore ADCP1 (x) and the instrumented cross-shore profile (dashed line). The coordinates are in meter (Lambert-93 projection). Source: Bertin <i>et al.</i> (2020) . . . . .	47

4.6	Cross-section at the transect location during storm peak (3rd of February 2017 at 8 AM) of the water level (upper panel), short-wave height (middle panel) and low-frequency (IG and VLF) wave height (middle panel). In blue the model results, and the observations are represented by circles. In grey the predicted minimum and maximum short-wave heights during the half hour around the peak of the storm. . . . .	48
4.7	Modeled (blue line) against observed (circles) water depth (top), short-wave height (middle) and low-frequency wave height (bottom) at PT3. . . . .	49
4.8	Modeled (blue line) against observed (circles) water depth (top), short-wave height (middle) and low-frequency wave height (bottom) at PT7. . . . .	50
4.9	Observed versus predicted (left) water levels, (middle) short-wave height $H_{m0,HF}$ and (right) low-frequency wave-height $H_{m0,LF}$ . . . . .	51
4.10	Location of study site (left panel). The beach poles form an alongshore reference line, with the km number referring to the distance to the zero point at the northern end of the Holland coast. The origin of the local coordinate system used (right panel) here is beach pole 41.25, with positive x and y in the seaward and southern direction, respectively. The crosses ('x') indicate the different pressure sensors. . . . .	52
4.11	Observed water levels (black circles) against the modelled water levels (orange) for all pressure sensors. The panel in the middle shows the location of the pressure sensors, and the surrounding subpanels follow the order from North to South (top to bottom) and from sea (left) to the beach (right). . . . .	53
4.12	Observed short-wave heights (black circles) against the modelled short-wave heights (orange) for all pressure sensors. The panel in the middle shows the location of the pressure sensors, and the surrounding subpanels follow the order from North to South (top to bottom) and from sea (left) to the beach (right). . . . .	54
4.13	Observed infragravity wave heights (black circles) against the modelled infragravity wave heights (orange) for all pressure sensors. The panel in the middle shows the location of the pressure sensors, and the surrounding subpanels follow the order from North to South (top to bottom) and from sea (left) to the beach (right). . . . .	55
4.14	XBeach results for cross-shore transect 0 at Egmond aan Zee. Initial bed levels are depicted by the black dotted line, observed post-storm bed levels by the black solid line and XBeach model results are presented in red. The modelled dune erosion is shown by the red shaded area. . . . .	56
4.15	XBeach results for cross-shore transect -1755 at Egmond aan Zee. Initial bed levels are depicted by the black dotted line, observed post-storm bed levels by the black solid line and XBeach model results are presented in red. The modelled dune erosion is shown by the red shaded area. . . . .	57
4.16	Overview of the Belgian coastline with the location of the analyzed cross-shore profiles measured before and after the Sint Nicholas storm and the water level (WL) and wave measurement locations used for this case. . . . .	58
4.17	Cross-section profile nr. 119 before and after the Sint Nicholas storm based on the measurements and XBeach, including dune erosion volumes and retreat distances. Bottom: entire XBeach profile, top: zoom of beach and dune profile. . . . .	60
4.18	Location of the study area near Vedersoe (Denmark). The two different transects considered in this study are located close to each other, but different morphological behaviour is observed. Source: Kystdirektoratet (2021) . . . . .	61
4.19	XBeach results for cross-shore transect Vedersoe 01 Initial bed levels are depicted by the black dashed line, observed post-storm bed levels by the black solid line and XBeach model results are presented in red. The modelled dune erosion is shown by the red shaded area, whereas the observed dune erosion is depicted with the grey shaded area. . . . .	62

4.20	XBeach results for cross-shore transect Vedersoe 02. Initial bed levels are depicted by the black dashed line, observed post-storm bed levels by the black solid line and XBeach model results are presented in red. The modelled dune erosion is shown by the red shaded area, whereas the observed dune erosion is depicted with the grey shaded area. . . . .	63
4.21	Left: Model domain extent of the nested regional D-Flow FM/SWAN model (in grey) and the XBeach model (in red): Wilderness breach. Right: observed pre- (top) and post-(middle) bathymetry and sedimentation/erosion (bottom). . . . .	64
4.22	XBeach results for cross-shore transect 005 at Fire Island. Initial bed levels are depicted by the black dotted line, observed post-storm bed levels by the black solid line and XBeach model results are presented in red. The modelled dune erosion is shown by the red shaded area. . . . .	65
4.23	XBeach results for cross-shore transect 305 at Fire Island. Initial bed levels are depicted by the black dotted line, observed post-storm bed levels by the black solid line and XBeach model results are presented in red. The modelled dune erosion is shown by the red shaded area. . . . .	66
4.24	XBeach results for cross-shore transect 405 at Fire Island. Initial bed levels are depicted by the black dotted line, observed post-storm bed levels by the black solid line and XBeach model results are presented in red. The modelled dune erosion is shown by the red shaded area. . . . .	66
4.25	Location of the study site in Langeoog, Germany and location of the XBeach model. Model input bathymetry (right panel) with the location of the beach nourishment and the six transects A to F. Source: Hillmann and Frederiksen (2021) . . . . .	68
4.26	XBeach results for cross-shore transect A at Langeoog. Initial bed levels are depicted by the black dotted line, observed post-storm bed levels by the black solid line and XBeach model results are presented in red. The modelled dune erosion is shown by the red shaded area. . . . .	69
4.27	XBeach results for cross-shore transect D at Langeoog. Initial bed levels are depicted by the black dotted line, observed post-storm bed levels by the black solid line and XBeach model results are presented in red. The modelled dune erosion is shown by the red shaded area. . . . .	69
4.28	Indication of assessed coastal profiles in red, from 568 in the north to 7100 in the south. . . . .	71
4.29	Cross-section for JarKus profile 648 before and after the 1976 storm based on the measurements and XBeach, including dune erosion volumes and retreat distances. . . . .	73
4.30	Cross-section for JarKus profile 5000 before and after the 1976 storm based on the measurements and XBeach, including dune erosion volumes and retreat distances. . . . .	73
4.31	Cross-section for JarKus profile 7100 before and after the 1976 storm based on the measurements and XBeach, including dune erosion volumes and retreat distances. . . . .	74
4.32	Overview of the extent of the southern part of the Dutch coast (Hoek van Holland to IJmuiden) and the location of the ERA5 data. . . . .	75
4.33	Pre and post storm surge profile as computed by XBeach. Upper frame shows the dune erosion section, the lower frame shows the entire XBeach profile. . . . .	76
B.1	Definition of erosion volume . . . . .	83
B.2	Dune retreat indicator. . . . .	83
B.3	Berm slope indicator . . . . .	84

C.1	Computed and observed short wave height transformation, infragravity wave height transformation and mean water level (upper panel) for test T01. The lower panel shows the initial and final computed profiles. . . . .	85
C.2	Computed and observed short wave height transformation, infragravity wave height transformation and mean water level (upper panel) for test T02. The lower panel shows the initial and final computed profiles. . . . .	86
C.3	Computed and observed short wave height transformation, infragravity wave height transformation and mean water level (upper panel) for test T03. The lower panel shows the initial and final computed profiles. . . . .	86
C.4	Computed and observed high and low frequency root-mean-squared velocity and mean velocity (upper panel) for test T01. The lower panel shows the initial and final computed profiles. . . . .	87
C.5	Computed and observed high and low frequency root-mean-squared velocity and mean velocity (upper panel) for test T03. The lower panel shows the initial and final computed profiles. . . . .	87
C.6	Computed and observed wave shape as a function of the cross-shore distance (upper panel). . . . .	88
C.7	Computed and observed wave shape as a function of the cross-shore distance (upper panel) . . . . .	88
C.8	Computed and observed wave shape as a function of the cross-shore distance (upper panel) . . . . .	89
C.9	Sediment concentrations . . . . .	89
C.10	Sediment concentrations . . . . .	90
C.11	Erosion and sedimentation patterns (upper panel) and profiles (lower panel) for test T01 . . . . .	90
C.12	Erosion and sedimentation patterns (upper panel) and profiles (lower panel) for test T02 . . . . .	91
C.13	Erosion and sedimentation patterns (upper panel) and profiles (lower panel) for test T03 . . . . .	91
C.14	Erosion volumes as a function of time for test T01 . . . . .	92
C.15	Erosion volumes as a function of time for test T02 . . . . .	92
C.16	Erosion volumes as a function of time for test T03 . . . . .	93
C.17	Computed and observed short wave height transformation, infragravity wave height transformation and mean water level (upper panel) for test 2E. The lower panel shows the initial and final computed profiles. . . . .	93
C.18	Erosion pattern and volumes and retreat distance during test 2E . . . . .	94
C.19	Erosion volumes as a function of time for test E2 . . . . .	94

## List of Tables

1.1	Overview of the BOI parameters and XBeachX default parameters . . . . .	2
1.2	Overview of the tests in this report. . . . .	3
2.1	The XBeach and analytical wave heights and wave lengths. The amplitude without reflection is computed for the period $t=0$ to $t=600$ s. The amplitude for the standing wave pattern is computed for the period $t=500$ to $t=1200$ . The amplitude is defined as the maximum water level/velocity in the domain for the given time period. . . . .	7
2.2	The maximum and minimum surface elevation and velocities in the runup. . . .	8
2.3	The Boers (1996) wave conditions. . . . .	8
2.4	The statistical scores for the Boers experiments. The scatter index (SCI) and relative bias (rel. bias) are shown for the short-wave height, infragravity wave height and setup. . . . .	11
2.5	The statistical scores for the GLOBEX experiments. The scatter index (SCI) and relative bias (rel. bias) are shown for the short-wave height, infragravity wave height and setup. . . . .	14
3.1	Overview of experiments . . . . .	17
3.2	The computed and observed volume ( $V$ ) and berm slopes ( $S$ ) for T01. Volumes ( $V$ ) are given in $m^3/m$ . The relative error is expressed in a percentage. Both the relative error in terms of the same time ( $rel, t$ ) and the final time are shown ( $rel$ ). . . . .	18
3.3	The computed and observed volume ( $V$ ) and berm slopes ( $S$ ) for T02. Volumes ( $V$ ) are given in $m^3/m$ . The relative error is expressed in a percentage. Both the relative error in terms of the same time ( $rel, t$ ) and the final time are shown ( $rel$ ). . . . .	19
3.4	The computed and observed volume ( $V$ ) and berm slopes ( $S$ ) for T03. Volumes ( $V$ ) are given in $m^3/m$ . The relative error is expressed in a percentage. Both the relative error in terms of the same time ( $rel, t$ ) and the final time are shown ( $rel$ ). . . . .	20
3.5	The computed and observed volume ( $V$ ) and berm slopes ( $S$ ) for T08. Volumes ( $V$ ) are given in $m^3/m$ . The relative error is expressed in a percentage. Both the relative error in terms of the same time ( $rel, t$ ) and the final time are shown ( $rel$ ). . . . .	21
3.6	Deltagoot 2006 statistical scores. . . . .	22
3.7	The computed and observed volume ( $V$ ) and berm slopes ( $S$ ) for T01. Volumes ( $V$ ) are given in $m^3/m$ . The relative error is expressed in a percentage. Both the relative error in terms of the same time ( $rel, t$ ) and the final time are shown ( $rel$ ). . . . .	23
3.8	Overview of experiments . . . . .	24
3.9	The computed and observed volume ( $V$ ) and berm slopes ( $S$ ) for Test-1. Volumes ( $V$ ) are given in $m^3/m$ . The relative error is expressed in a percentage. Both the relative error in terms of the same time ( $rel, t$ ) and the final time are shown ( $rel$ ). . . . .	26
3.10	The computed and observed volume ( $V$ ) and berm slopes ( $S$ ) for Test-2. Volumes ( $V$ ) are given in $m^3/m$ . The relative error is expressed in a percentage. Both the relative error in terms of the same time ( $rel, t$ ) and the final time are shown ( $rel$ ). . . . .	27
3.11	The computed and observed volume ( $V$ ) and berm slopes ( $S$ ) for Test-3. Volumes ( $V$ ) are given in $m^3/m$ . The relative error is expressed in a percentage. Both the relative error in terms of the same time ( $rel, t$ ) and the final time are shown ( $rel$ ). . . . .	28

3.12	The computed and observed volume ( $V$ ) and berm slopes ( $S$ ) for Test-4. Volumes ( $V$ ) are given in $m^3/m$ . The relative error is expressed in a percentage. Both the relative error in terms of the same time ( $rel, t$ ) and the final time are shown ( $rel$ ).	29
3.13	The computed and observed volume ( $V$ ) and berm slopes ( $S$ ) for Test-5. Volumes ( $V$ ) are given in $m^3/m$ . The relative error is expressed in a percentage. Both the relative error in terms of the same time ( $rel, t$ ) and the final time are shown ( $rel$ ).	30
3.14	M1263 III statistical scores.	31
3.15	The computed and observed volume ( $V$ ) and berm slopes ( $S$ ) for 2E. Volumes ( $V$ ) are given in $m^3/m$ . The relative error is expressed in a percentage. Both the relative error in terms of the same time ( $rel, t$ ) and the final time are shown ( $rel$ ).	32
3.16	The computed and observed volume ( $V$ ) and berm slopes ( $S$ ) for T14. Volumes ( $V$ ) are given in $m^3/m$ . The relative error is expressed in a percentage. Both the relative error in terms of the same time ( $rel, t$ ) and the final time are shown ( $rel$ ).	34
3.17	The computed and observed volume ( $V$ ) and berm slopes ( $S$ ) for A9. Volumes ( $V$ ) are given in $m^3/m$ . The relative error is expressed in a percentage. Both the relative error in terms of the same time ( $rel, t$ ) and the final time are shown ( $rel$ ).	35
3.18	The computed and observed volume ( $V$ ) and berm slopes ( $S$ ) for B2. Volumes ( $V$ ) are given in $m^3/m$ . The relative error is expressed in a percentage. Both the relative error in terms of the same time ( $rel, t$ ) and the final time are shown ( $rel$ ).	36
3.19	The computed and observed volume ( $V$ ) and berm slopes ( $S$ ) for C2. Volumes ( $V$ ) are given in $m^3/m$ . The relative error is expressed in a percentage. Both the relative error in terms of the same time ( $rel, t$ ) and the final time are shown ( $rel$ ).	37
3.20	The computed and observed volume ( $V$ ) and berm slopes ( $S$ ) for F1. Volumes ( $V$ ) are given in $m^3/m$ . The relative error is expressed in a percentage. Both the relative error in terms of the same time ( $rel, t$ ) and the final time are shown ( $rel$ ).	38
3.21	The computed and observed volume ( $V$ ) and berm slopes ( $S$ ) for H2. Volumes ( $V$ ) are given in $m^3/m$ . The relative error is expressed in a percentage. Both the relative error in terms of the same time ( $rel, t$ ) and the final time are shown ( $rel$ ).	39
3.22	Statistical scores for the Grosse Wellen Kanal experiments.	40
4.1	Overview of the validation case studies and characteristics.	42
4.2	Erosion volume and dune retreat at 3m+NAP for the Egmond case	46
4.3	Erosion volume and dune retreat at 3m+NAP for the Egmond case	50
4.4	A quantitative comparison of modelled and observed erosion volumes [ $m^3/m$ ] and dune retreat [m] at 3m + NAP for all 7 profiles.	56
4.5	Erosion volume and dune retreat at 3m+NAP for the Egmond case	59
4.6	Erosion volume and dune retreat at 3m+NAP for the Egmond case	63
4.7	Erosion volume and dune retreat at 3m+NAP for the Egmond case	65
4.8	Erosion volume and dune retreat at 3m+NAP for the Egmond case	68
4.9	Erosion volume and dune retreat at 3m+NAP for the Egmond case	72
A.1	MPS parameters	81

# 1 Introduction

This document reports on the hydrodynamic and morphodynamic accuracy of the XBeach model that is to be applied in the BOI Zandige Waterkeringen project. This document is part of the XBeach testbed (alongside the trunk default skillbed) and is generated automatically any time the model code is updated. The XBeach testbed is an environment, which automatically executes simulations, analyses simulations and generates reports with the results. The XBeach source code is hosted on a SVN repository, which is publicly available (open source). A new commit to this repository starts the trigger to create this report. The date and revision number of the XBeach model code used in this report is given on the cover of this skillbed report.

The function of this skillbed report is twofold. The testbed cases show the performance of the BOI XBeach model for multiple applications in terms of quantitative statistical scores and visualizations. Apart from the performance, this report can also be used to track the code development and verify the impact of a commit in the source code.

The accuracy of the XBeach model is determined by comparison to laboratory experiments and field measurements. The BOI parameter settings presented in [De Bakker \*et al.\* \(2021\)](#) and given below in [Table 1.1](#) are applied. This report provides quantitative insight into the ability of the model skill with a uniform set of model parameters. In [Table 1.2](#) it is indicated which tests are applied to calibrate the parameters. The derived BOI settings are applied in all the described validation cases to show the performance of the BOI XBeach model. Note that these parameters are derived for the Dutch coast and, therefore, do not always correspond to the XBeach default parameters.

In this report the results are not discussed since the results can change between different versions of XBeach.

The validation cases and source code are publicly available in the OSS XBeach repository: <https://svn.oss.deltares.nl/repos/xbeach>. Moreover, after each commit the skillbed reports are published on the XBeach website: <https://oss.deltares.nl/web/xbeach/>.

## 1.1 BOI settings

The BOI settings are a set of hydrodynamic and morphodynamic parameters that have been derived using laboratory and a limited number of field datasets. The Boers and GLOBEX experiments were applied in the optimization of the hydrodynamic parameters, and the morphodynamic parameters were derived from experiments and nine field measurement cross-shore profiles. [Table 1.1](#) shows the BOI parameters of XBeach.

The XBeach defaults are applied for the other parameters, except for case specific parameters, such as the boundary conditions and grid related parameters. Note that the reduction of the short-wave group signal (`wbcEvarreduce`) is only applied in the field validation since we this reduction is only required when modelling 2D cases with a 1D model.

## 1.2 Reader's guide

The hydrodynamic validation is shown in [chapter 2](#) and the the morphodynamic validation in [chapter 3](#). The field validation of both hydrodynamics and morphodynamics is shown in [chapter 4](#). An explanation of the model performance statistics is shown in [Appendix A](#). Furthermore, in [Appendix C](#) a comparison of detailed properties is shown for selected cases.

Keyword	BOI parameters	XBeachX default parameters
bedfriction	Manning	Chezy
bedfriccoef	0.02	55
form	VanThiel VanRijn	VanThiel VanRijn
waveform	vanthiel	vanthiel
facSk	0.15	0.1
facAs	0.20	0.1
wetslp	0.15	0.3
beta	0.08	0.1
break	roelvink daly	roelvink2
gamma	0.46	0.55
gamma2	0.34	0.3
alpha	1.38	1.0
wbcEvarreduce (only for field validation of 2D cases with a 1D model)	0.3	-
alfaD50	0.4	-

**Table 1.1:** Overview of the BOI parameters and XBeachX default parameters. See the online manual for the explanation of the parameters ([https://xbeach.readthedocs.io/en/latest/user\\_manual.html](https://xbeach.readthedocs.io/en/latest/user_manual.html)).

Test	Type	Applied in the calibration
Long wave propagation	Hydrodynamics	no
1D wave runup	Hydrodynamics	no
High- and low-frequency wave transformation over a barred beach	Hydrodynamics	yes
High- and low-frequency wave transformation over a gentle sloping beach	Hydrodynamics	yes
H4357: Delta Flume 2006	Morphodynamics	yes
M1797: Delta Flume 1981	Morphodynamics	yes
M1263 III: Delta Flume 1984	Morphodynamics	yes
LIP11D: Delta Flume 1994	Morphodynamics	yes
LIP11D: Delta Flume 1994	Morphodynamics	yes
H4731: Delta flume 1998	Morphodynamics	yes
Grosse Wellen Kanal 1998	Morphodynamics	no
Schiermonnikoog	Hydrodynamics	no
Saint-Trojan	Hydrodynamics	no
Egmond	Morphodynamics and Hydrodynamics	no
Vlaanderen	Morphodynamics	partially (three profiles)
Vedersoe	Morphodynamics	no
Fire-Island	Morphodynamics	partially (three profiles)
Langeoog	Morphodynamics	partially (two profiles)
Holland 1976	Morphodynamics	partially (three profiles)
Holland 1953	Morphodynamics	no

**Table 1.2:** Overview of the tests in this report.



## 2 Laboratory experiments: hydrodynamics

The hydrodynamics form the basis for the morphodynamic behaviour. In this chapter the hydrodynamic results of XBeach are presented. All tests are run without the morphological module and the analysis is focused on the wave propagation and transformation computed by XBeach.

First, two analytical solutions are reproduced by XBeach. Subsequently, laboratory experiments of a barred beach and gentle sloping beach are presented. For the latter, the short-wave height, infragravity-wave height and setup are compared to the measurements.

The observed wave height is computed on the basis of the energy density spectrum in the frequency range of  $f_p/2$  until the Nyquist frequency,

$$H_{m0,HF} = 4\sqrt{m_{0,f>f_p/2}} \quad (2.1)$$

Where  $m_{0,f>f_p}$  is the zero-moment of the energy density spectrum where the frequency is larger than the cutoff-frequency ( $f_p/2$ ). In XBeach, the short wave height is computed as,

$$H_{m0,HF} = \text{rms}(H)\sqrt{2} \quad (2.2)$$

where  $H$  is the computed instantaneous short-wave height, which is computed in XBeach as we do not directly simulate the wave height. The infragravity-wave height in both the observations and the computations is defined as,

$$H_{m0,HF} = 4\sqrt{m_{0,f_p/20<f<f_p/2}} \quad (2.3)$$

where  $m_{0,f_p/20<f<f_p/2}$  is zero-moment of the energy density spectrum for energy in the infragravity region. Since XBeach also resolves the infragravity waves, the same definition is applied to compute the infragravity wave height from the XBeach results.

Similar as the infragravity wave height, both the observed and computed mean water level (setup) can be computed with the same formulation,

$$\text{setup} = \text{mean}(\eta) \quad (2.4)$$

where  $\eta$  is the surface elevation signal.

### 2.1 Long wave propagation

The purpose of the this test is to check whether the NSWE numerical scheme is not too dissipative and that it does not create large errors in propagation speed.

A long wave with a small amplitude of 0.01 m and period of 80 s is sent into a domain with a length of 1 km, a depth of 5 m and a grid size of 5 m. Since only long waves are modelled a grid size of 5 m can be applied (more than 100 points per wave length). At the end, a fully reflecting wall is imposed. The wave length in this case should be  $\sqrt{g \cdot d} \cdot T = \sqrt{9.81 \cdot 5} \cdot 80 = 560m$ . The velocity amplitude should be  $\sqrt{g/h} \cdot A = \sqrt{9.81/5} \cdot 0.01 = 0.014m$ , because the these waves are shallow water waves. After the wave has reached the wall, a standing wave with double amplitude should be created.

The computed surface elevation and velocity snapshots before the waves reach the end of the domain is shown in [Figure 2.1](#). The surface elevation and velocity snapshots with the standing wave pattern are shown in [Figure 2.2](#). The computed and analytical wave amplitudes and wave lengths are shown in [Table 2.1](#). Note that the maximum velocity and surface elevation amplitude is found at the wall.

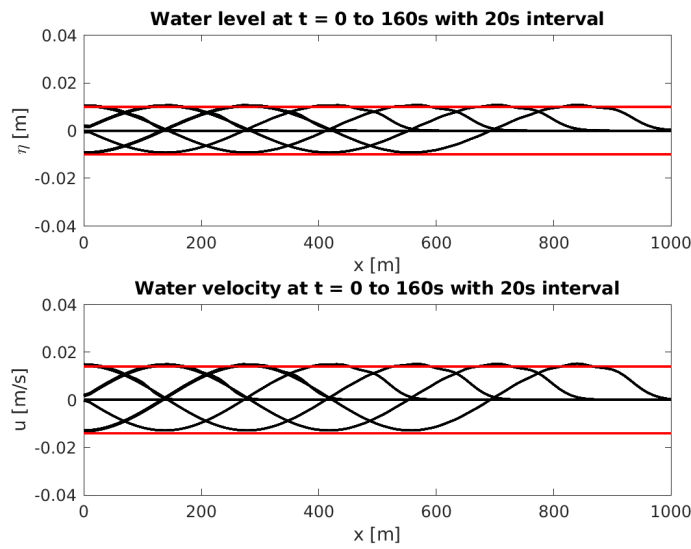


**Figure 2.1:** Water levels and velocities from the start of the experiment until the wave just reaches the end of the flume. The amplitude of the analytical solution is shown with a red line.

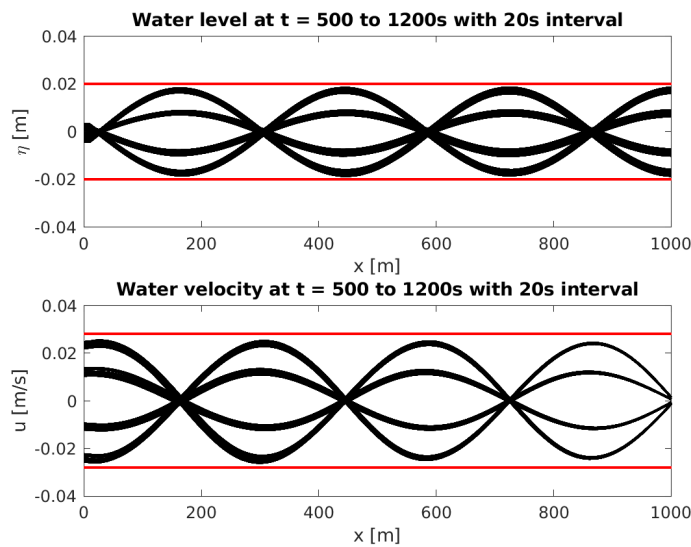


**Figure 2.2:** Snapshots of water levels and velocities showing a standing wave pattern. The amplitude of the analytical solution is shown with a red line.

**Table 2.1:** The XBeach and analytical wave heights and wave lengths. The amplitude without reflection is computed for the period  $t=0$  to  $t=600s$ . The amplitude for the standing wave pattern is computed for the period  $t=500$  to  $t=1200$ . The amplitude is defined as the maximum water level/velocity in the domain for the given time period.

	Amplitude [m]	Amplitude (Stand- ing wav) [m]	velocitie ampli- tude [m/s]	Velocitie ampli- tude (Stand- ing wave) [m/s]	Wave length [m]
XBeach	0.011	0.020	0.015	0.028	560.000
Analytical solution	0.010	0.020	0.014	0.028	560.000

## 2.2 1D wave runup (analytical solution)

The purpose of this test is to check the ability of the model to represent runup and rundown of non-breaking long waves. To that end, a comparison was made with the analytical solution of the non-linear shallow water equation (NSWE) by Carrier and Greenspan (1958), which describes the motion of harmonic, non-breaking long waves on a plane sloping beach without friction.

A free long wave with a wave period of 32 seconds and wave amplitude of half the wave breaking amplitude ( $a_{in} = 0.5 \cdot a_{br}$ ) propagates over a beach with constant slope equal to 1:25. The wave breaking amplitude is computed as  $a_{br} = 1/\sqrt{128} \cdot \pi^3 \cdot s^{2.5} \cdot T^{2.5} \cdot g^{1.25} \cdot h_0^{-0.25} = 0.0307m$ , where  $s$  is the beach slope,  $T$  is the wave period and  $h_0$  is the still water depth at the seaward boundary. The grid is non uniform and consists of 160 grid points. The grid size  $\Delta x$  is decreasing in shoreward direction and is proportional to the (free) long wave celerity ( $\sqrt{g \cdot h}$ ). The minimum grid size in shallow water was set at  $\Delta x = 0.1m$ .

A comparison of surface elevation and velocity snapshots is shown in Figure 2.3. The maximum and minimum values of the analytical solution and the XBeach computations are shown in Table 2.2

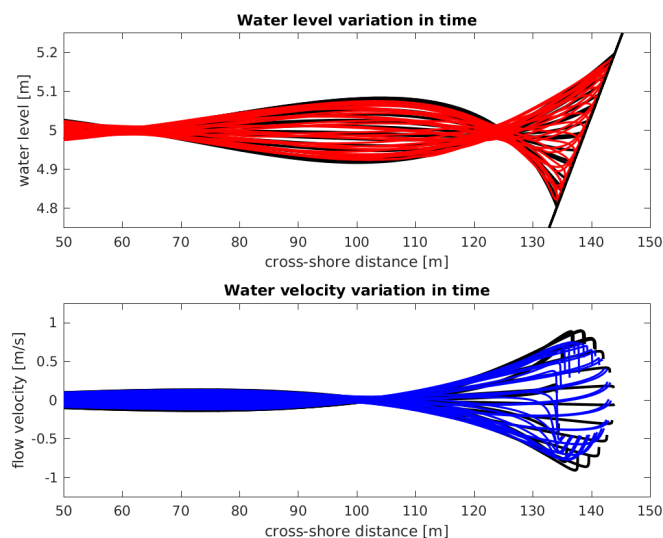


**Figure 2.3:** Snapshots of water level and velocity

**Table 2.2:** The maximum and minimum surface elevation and velocities in the runup.

	max( $\eta$ ) [m]	min( $\eta$ ) [m]	max( $u$ ) [m/s]	min( $u$ ) [m/s]
XBeach	5.20	4.80	0.90	-0.91
Analytical solution	5.19	4.82	0.75	-0.77

### 2.3 High- and low-frequency wave transformation over a barred beach

#### Experiment description

Boers (1996) performed experiments with irregular waves in the physical wave flume at Delft University of Technology. The flume has a length of 40 meters and a width of 0.8 m. The fixed concrete beach profile represents the beach profile of the LIP 11D-experiment 1B (excluding mega-ripples), on a scale of 1:28 with respect to prototype. This profile has a breaker bar and a surf zone trough. The still water level during the experiments is  $z = 0.75$  m above the bottom of the wave flume. The flume is equipped with a hydraulically driven, piston type wave generator with second-order wave generation and Active Reflection Compensation. Measurements were taken at 20 Hz. Three irregular wave conditions were studied (See Table 2.3). The surface elevation was measured at 70 locations shown in Figure 2.4. It is important to note that the waves are breaking from the start in Tests 1A and 1B. In addition, not a complete jonswap spectrum could be imposed at the boundary due to restrictions with the waveboard. Therefore, the XBeach model is forced with measured timeseries, rather than with a jonswap spectrum.

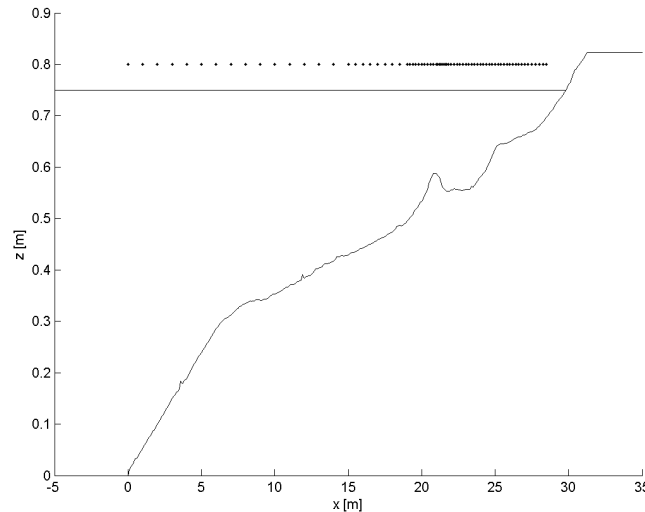


**Figure 2.4:** Locations of surface elevation measurements

Test	$H_{m0}$ [m]	$T_p$ [s]
1A	0.157	2.1
1B	0.206	2.1
1C	0.103	3.4

**Table 2.3:** The Boers (1996) wave conditions.

## Results

The comparison between the model and the observations for the wave height transformation of the short waves, the infragravity waves and the setup is shown in Figure 2.5, Figure 2.6 and Figure 2.7. The short-wave height and infragravity wave height are shown in the upper panel. The setup is shown in the second panel and the bathymetry is shown in the last panel. The XBeach boundary is located at the 9th wave gauge since this location contains velocity and surface elevation measurements and the model is forced with the incoming measured wave signal. Note that the setup for these small-scale tests is very small (maximum of several millimetres), which causes the scatter in the observations.

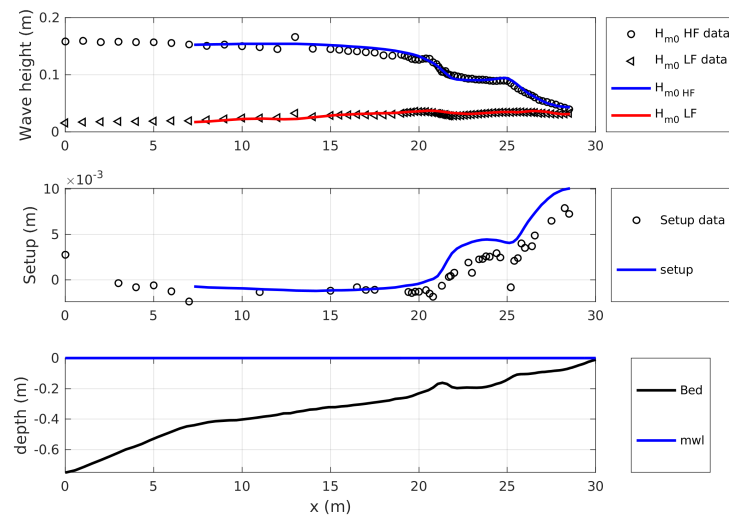


**Figure 2.5:** Wave hydrodynamics during experiment 1A. The observed short-wave height (dots) and observed infragravity wave height (triangles) are compared to the XBeach results (blue and red line) in the upper panel. The observed setup (dots) is compared to the setup computed with XBeach (blue line) in the second panel and the bathymetry is shown in the third panel.

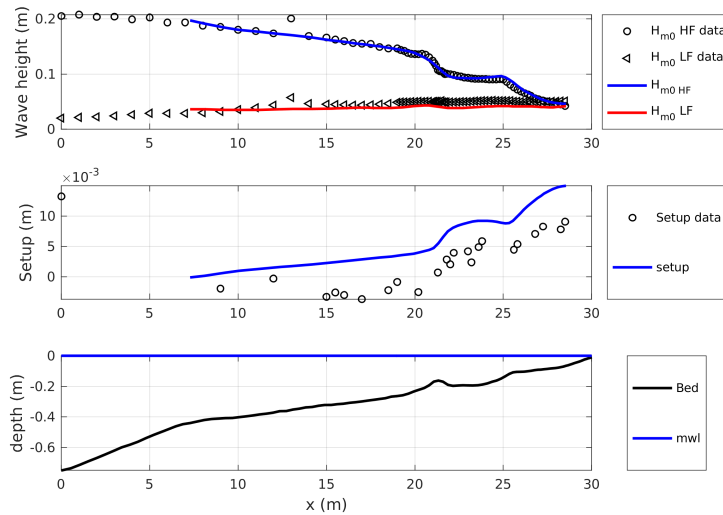


**Figure 2.6:** Wave hydrodynamics during experiment 1B. The observed short-wave height (dots) and observed infragravity wave height (triangles) are compared to the XBeach results (blue and red line) in the upper panel. The observed setup (dots) is compared to the setup computed with XBeach (blue line) in the second panel and the bathymetry is shown in the third panel.

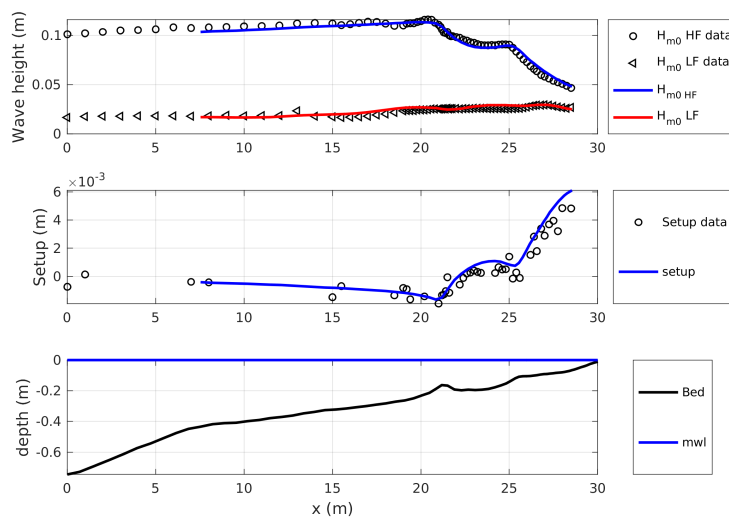


**Figure 2.7:** Wave hydrodynamics during experiment 1C. The observed short-wave height (dots) and observed infragravity wave height (triangles) are compared to the XBeach results (blue and red line) in the upper panel. The observed setup (dots) is compared to the setup computed with XBeach (blue line) in the second panel and the bathymetry is shown in the third panel.

### Overview

An overview of the skill scores is shown in Figure 2.8 and Table 2.4, where the relative bias and scatter index of the short-wave height, infragravity-wave height and setup are shown for the different Boers experiments.

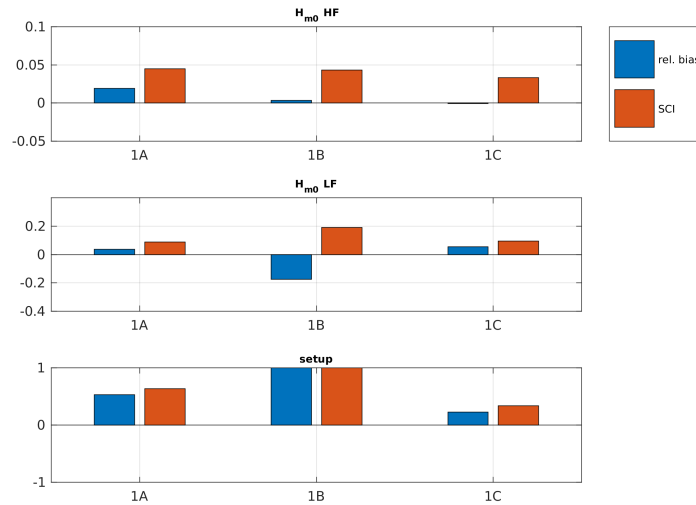


**Figure 2.8:** Overview of the statistical scores of the Boers experiments. The relative error and scatter index for the short-wave height (upper panel), infragravity wave height (second panel) and setup (third panel) are shown for the different Boers experiments.

**Table 2.4:** The statistical scores for the Boers experiments. The scatter index (SCI) and relative bias (rel. bias) are shown for the short-wave height, infragravity wave height and setup.

	1A	1B	1C
$H_{m0,HF}$ Rel. bias	0.02	0.00	-0.00
$H_{m0,HF}$ SCI	0.04	0.04	0.03
$H_{m0,LF}$ Rel. bias	0.04	-0.18	0.05
$H_{m0,LF}$ SCI	0.09	0.19	0.10
setup Rel. bias	0.53	1.06	0.22
setup SCI	0.63	1.10	0.33

## 2.4 High- and low-frequency wave transformation over a gentle sloping beach

### Experiment description

The laboratory data set was obtained during the GLOBEX project (Ruessink *et al.*, 2013). The experiments were performed in the Scheldegoet in Delft, The Netherlands, in April 2012. The flume is 110 m long, 1 m wide and 1.2 m high and has a piston-type wave maker equipped with an Active Reflection Compensation (ARC) to absorb waves coming from the flume and hence prevent their re-reflection from the wave maker. A fixed, mild-sloping (1:80) concrete beach was constructed over almost the entire length of the flume (with a fixed sandy upper layer), except for the first 16.6 m that were horizontal and where the mean water level was 0.85 m (Fig. 2.9). At the cross-shore position  $x = 16.6$  m ( $x = 0$  m is the wave-maker position at rest), the sloping bed started and intersected with the mean water level at  $x \approx 84.6$  m. The profile, and the conditions were on a 1:20 scale with respect to prototype. As detailed in Ruessink *et al.* (2013), the experimental program comprised 8 wave conditions. Here we will focus on the 3 irregular-wave cases: an intermediate energy sea-wave condition (A1;  $H_s = 0.1$  m,  $T_p = 1.58$  s), a high-energy sea-wave condition (A2;  $H_s = 0.2$  m,  $T_p = 2.25$  s), and a narrow-banded swell condition (A3;  $H_s = 0.1$  m,  $T_p = 2.25$  s). All wave-paddle steering

signals included second-order wave generation, and were based on a JONSWAP spectrum with a peak enhancement factor  $\gamma$  of 3.3 for  $A1$  and  $A2$ , and 20 for  $A3$ . Each condition had a duration of 75 minutes with 21 wave gauges and 5 flow meters sampling at 128 Hz, followed by a rest period of about 15 minutes. After all wave conditions were completed, most instruments were repositioned and the conditions were repeated with the same wave paddle signal. Altogether, the conditions were each repeated 10 times, resulting in a total of 190 positions with water level ( $\eta$ ) data and 43 positions with cross-shore flow-velocity ( $u$ ) data, with an instrument spacing varying from 2.2 m offshore, to 0.55 m in the middle section and 0.37 m inshore, see Figure 2.9. See Ruessink *et al.* (2013) for further details and initial data processing.

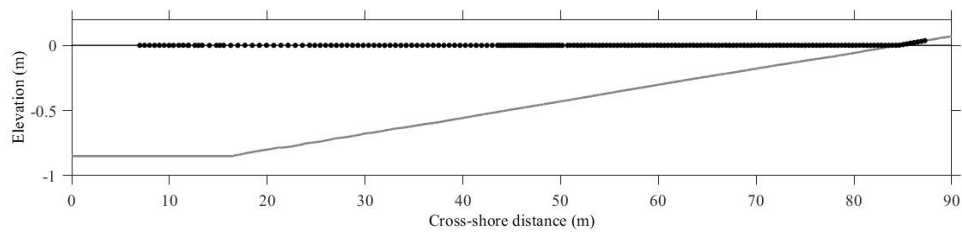


**Figure 2.9:** Elevation  $z$  versus cross-shore distance  $x$  in the Scheldegoot during the GLOBEX project. Here,  $x = 0$  is the location of the wave-maker at rest, and  $z = 0$  corresponds to the still water level. At  $x = 84.6$  m the still water level intersected with the bed. The 190 dots are the positions of the wave gauges.

## Results

The comparison between the model and the observations for the wave height transformation of the short waves, the infragravity waves and the setup is shown in Figure 2.10, Figure 2.11 and Figure 2.12.

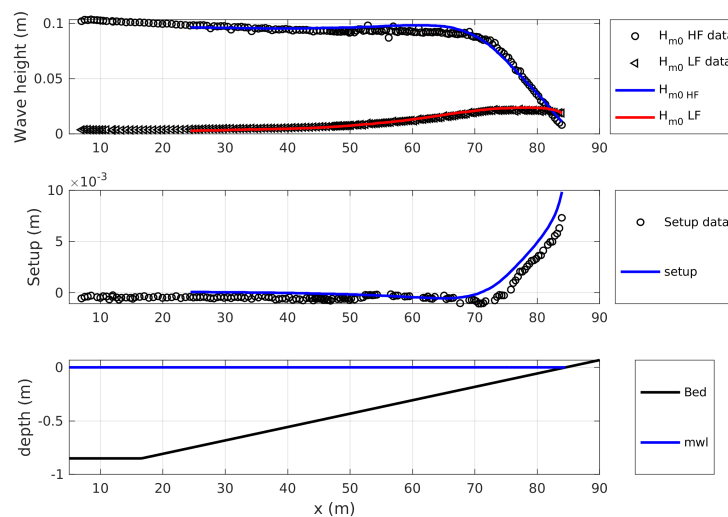


**Figure 2.10:** Wave hydrodynamics during experiment A1. The observed short-wave height (dots) and observed infragravity wave height (triangles) are compared to the XBeach results (blue and red line) in the upper panel. The observed setup (dots) is compared to the setup computed with XBeach (blue line) in the second panel and the bathymetry is shown in the third panel.

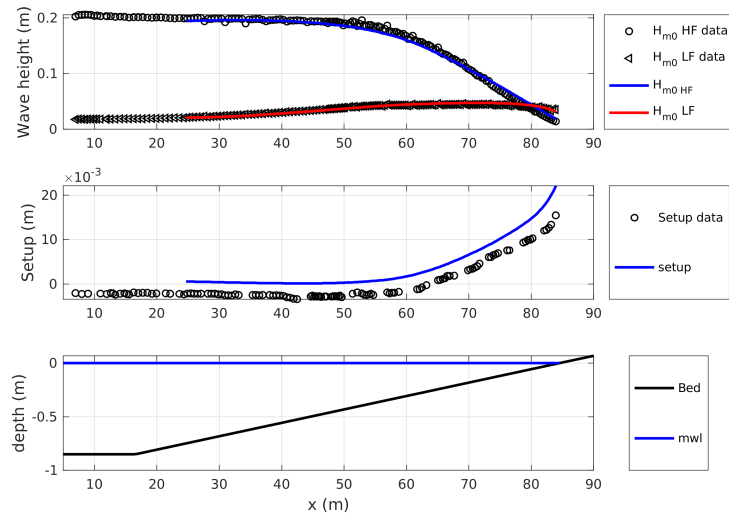


**Figure 2.11:** Wave hydrodynamics during experiment A2. The observed short-wave height (dots) and observed infragravity wave height (triangles) are compared to the XBeach results (blue and red line) in the upper panel. The observed setup (dots) is compared to the setup computed with XBeach (blue line) in the second panel and the bathymetry is shown in the third panel.

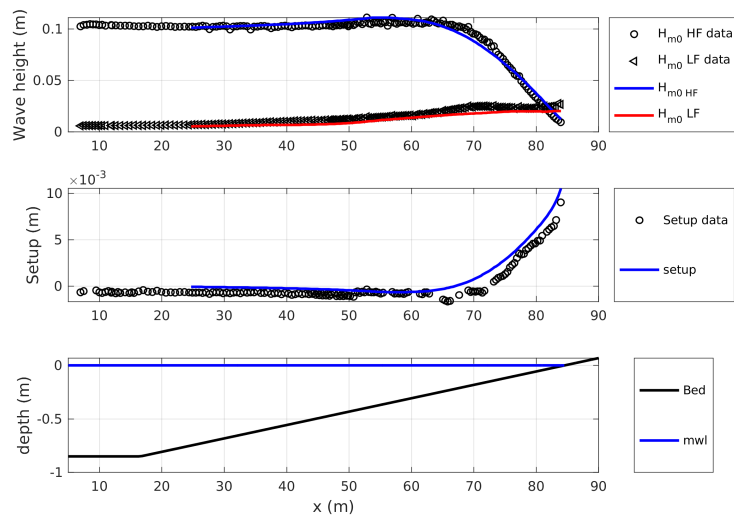


**Figure 2.12:** Wave hydrodynamics during experiment A3. The observed short-wave height (dots) and observed infragravity wave height (triangles) are compared to the XBeach results (blue and red line) in the upper panel. The observed setup (dots) is compared to the setup computed with XBeach (blue line) in the second panel and the bathymetry is shown in the third panel.

### Overview

An overview of the statistical scores is shown in Figure 2.13 and Table 2.5, where the relative bias and scatter index of the short-wave height, infragravity wave height and setup are shown for the different GLOBEX experiments.

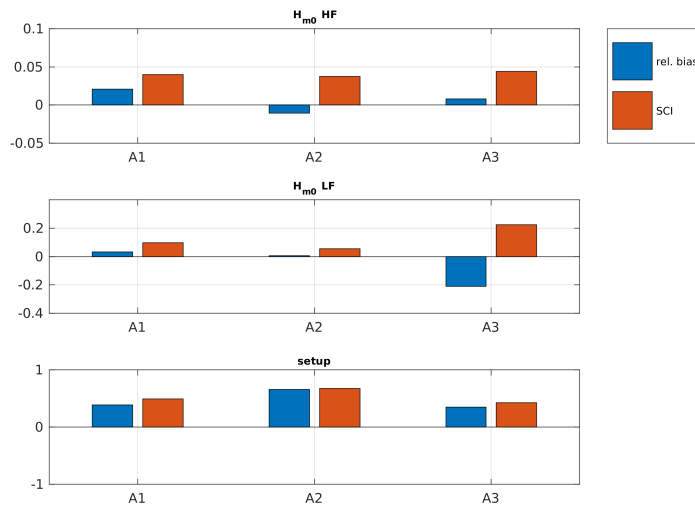


**Figure 2.13:** Overview of the statistical scores of the GLOBEX experiments. The relative error and scatter index for the short-wave height (upper panel), infragravity wave height (second panel) and setup (third panel) are shown for the different GLOBEX experiments.

**Table 2.5:** The statistical scores for the GLOBEX experiments. The scatter index (SCI) and relative bias (rel. bias) are shown for the short-wave height, infragravity wave height and setup.

	A1	A2	A3
$H_{m0, HF}$ Rel. bias	0.02	-0.01	0.01
$H_{m0, HF}$ SCI	0.04	0.04	0.04
$H_{m0, LF}$ Rel. bias	0.03	0.01	-0.21
$H_{m0, LF}$ SCI	0.10	0.06	0.22
setup Rel. bias	0.38	0.65	0.35
setup SCI	0.49	0.68	0.42

### 3 Laboratory experiments: morphodynamics

In this chapter, the performance of XBeach is compared to results obtained from physical model tests performed in a variety of experiments (this report) and field measurements (to be added in Fase 1 of the BOI Zandige Keringen project). Many of those tests are part of fundamental research to dune erosion and other morphological processes. Research took place at different laboratory scales, mainly depending on the size of the facility used. Since large-scale experiments show a more realistic dune erosion profile, only large scale physical experiments are shown.

The accuracy of XBeach is quantitatively verified for three indicators of the morphology (see ?). Based on the profiles on several moments in time ( $t$ ), the berm slope indicator, dune retreat indicator and erosion volume are compared to the observed indicator (See Figure B.2, Figure B.1 and Figure B.3). The definition of these indicators is given in Appendix B. The relative error of these indicators is computed for every moment in time where observations are available,

$$V_{rel} = (V_{xb,t} - V_{data,t})/V_{data,t_{end}} \quad (3.1)$$

$$S_{rel} = (slope_{xb,t} - slope_{data,t})/slope_{data,t} \quad (3.2)$$

$$dx_{rel} = (dx_{xb,t} - dx_{data,t})/dx_{data,t_{end}} \quad (3.3)$$

where  $V$  is the erosion volume above maximum still water level,  $slope$  the berm slope and  $dx$  the dune retreat. The quantities computed with XBeach are indicated with  $xb$  and the observed quantities are indicated with  $data$ . Next to the relative error with respect to the last timestep for the erosion volumes and dune retreat, the relative errors with the corresponding time is also computed:

$$V_{rel,t} = (V_{xb,t} - V_{data,t})/V_{data,t} \quad (3.4)$$

$$dx_{rel,t} = (dx_{xb,t} - dx_{data,t})/dx_{data,t} \quad (3.5)$$

The root-mean-squared value of these series of relative errors is used to obtain a single error measure per indicator for all moments in time (except for the data points in the first hour of an experiment). The relative errors in the first hour are ignored since this relative error can be large compared to the other moments in time and the fact that these initial errors are not important for the dune assessment (similar as described in ?).

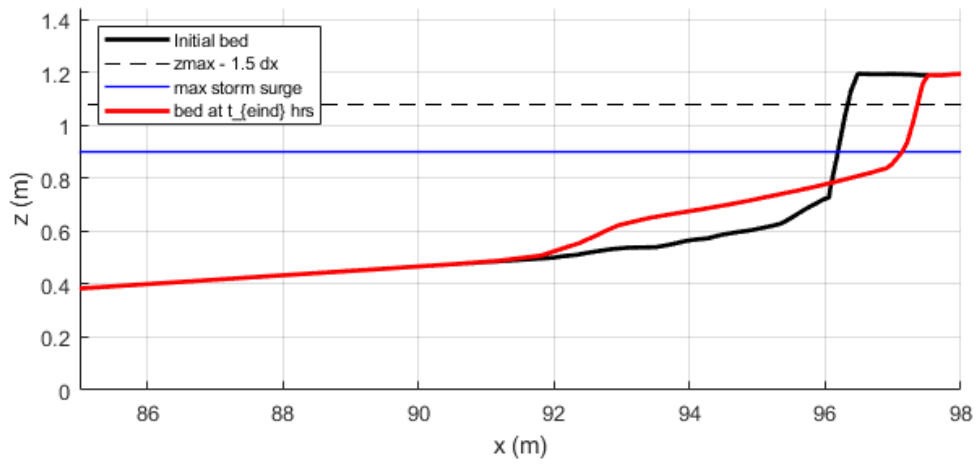


**Figure 3.1:** Dune retreat indicator. See the Appendix for the definition of this indicator.

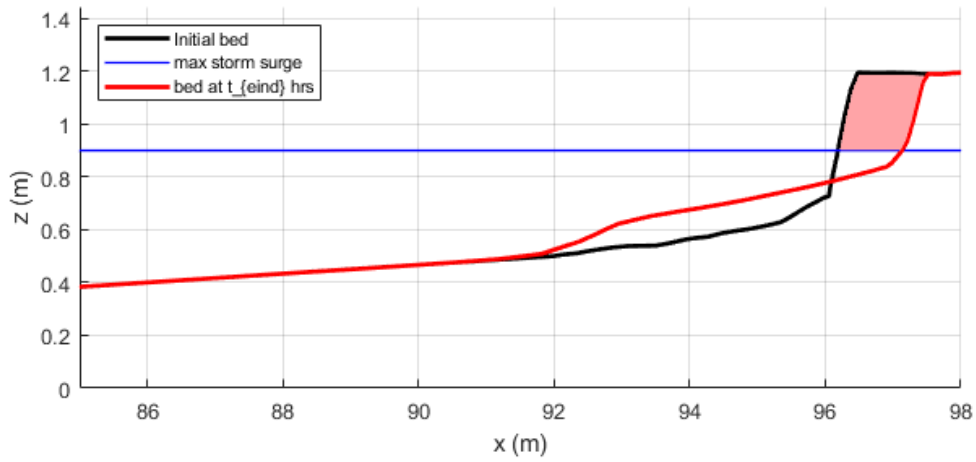


**Figure 3.2:** Definition of erosion volume. See the Appendix for the definition of this indicator.

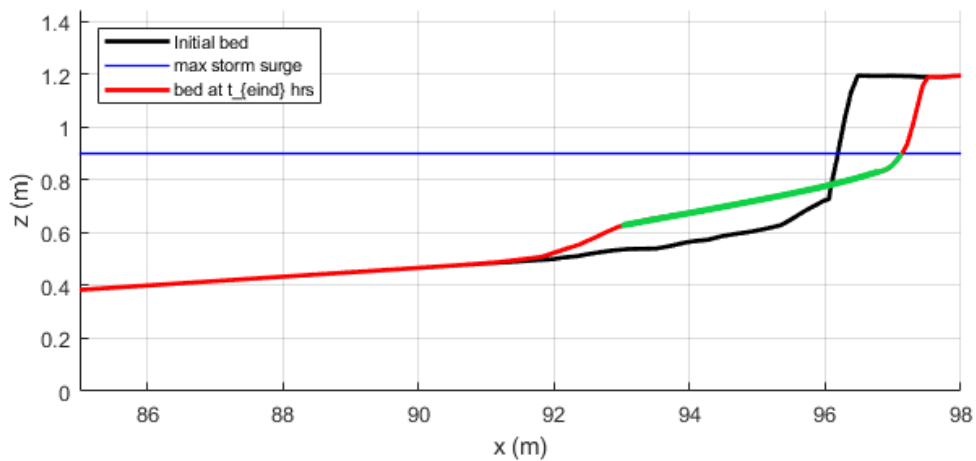


**Figure 3.3:** Berm slope indicator. See the Appendix for the definition of this indicator.

### 3.1 H4357: Delta Flume 2006

#### Experiment description

Van Gent *et al.* (2008) and Van Thiel de Vries *et al.* (2008) describe large-scale laboratory experiments that have been performed to study the influence of the wave period on the dune erosion process. They concluded that not only short waves, but also (wave group generated) long waves are important in the dune erosion process. Initially, about 30% of the dune erosion is due to long-wave energy, but this amount increases throughout the storm, with the development of an erosion profile. Moreover, an increase of the wave period was seen to increase the resulting dune erosion volumes.

These experiments have been performed in the Deltaflume of Delft Hydraulics, currently known as Deltares, using the reference profile for the Holland coast on a scale of 1:6. This is a schematized profile that is considered representative for the Holland coast. Furthermore, a significant wave height 1.50 m (corresponding to 9 m on proto-type scale) and a water depth of 4.50 m is used. The test programme is given in Table 3.1. During Test T01, T02 and T03 a single dune has been tested, whereas during test T08, the storm impact on a profile with a double dune row was analysed.

**Table 3.1:** Overview of experiments

Experiment	$T_p$	$T_{m-1,0}$	Spectrum
T01	4.90	4.45	Pierson-Moskowitz
T02	6.12	5.56	Pierson-Moskowitz
T03	7.35	6.68	Pierson-Moskowitz
T08	7.35	6.68	Pierson-Moskowitz

#### Results

The comparison between the observed and numerically predicted beach profiles with the BOI parameter settings is shown in Figure 3.4, Figure 3.6, Figure 3.8 and Figure 3.10. The observed profiles are represented by a dashed line and the computed profiles through a solid line. The line color indicates the moment in time. Table 3.2 to Table 3.5 show the results for the different indicators. In Figure 3.5, Figure 3.7, Figure 3.9 and Figure 3.11, the relative error is plotted as a function of time. Besides a comparison of the observed and predicted beach profiles, also a detailed hydrodynamic and morphodynamic analysis is performed, which is presented in Appendix C.1.

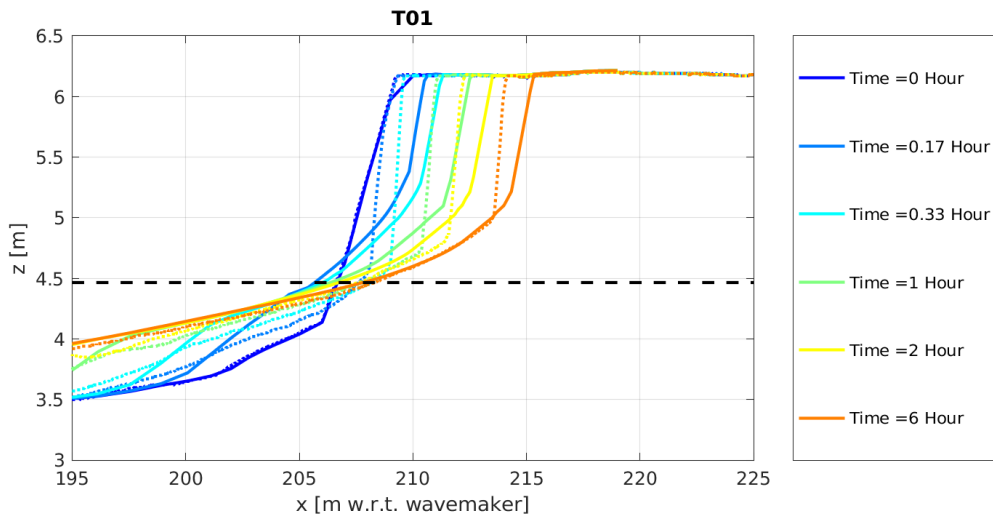


**Figure 3.4:** Comparisons of profiles from experiment T01 for different moments in time. Observed profiles are shown with a dashed line and the XBeach profiles with a solid line. The storm surge level is shown with a black dashed line.

**Table 3.2:** The computed and observed volume ( $V$ ) and berm slopes ( $S$ ) for T01. Volumes ( $V$ ) are given in  $m^3/m$ . The relative error is expressed in a percentage. Both the relative error in terms of the same time ( $rel, t$ ) and the final time are shown ( $rel$ ).

Time[hour]	$V_{xb}$ [ $m^3/m$ ]	$V_{data}$ [ $m^3/m$ ]	$V_{rel}$ [%]	$V_{rel,t}$ [%]	$S_{xb}$ [-]	$S_{data}$ [-]	$S_{rel}$ [%]	$dx_{xb}$ [m]	$dx_{data}$ [m]	$dx_{rel}$ [%]	$dx_{rel,t}$ [%]
0.17	1.88	0.96	11	97	0.12	0.09	37	1.50	0.00	30	Inf
0.33	2.91	2.21	8	32	0.08	0.07	18	2.17	0.50	33	333
1	5.01	4.29	8	17	0.06	0.06	-1	3.33	2.00	27	67
2	6.55	5.94	7	10	0.05	0.05	6	4.33	3.17	23	37
6	9.49	8.68	9	9	0.04	0.04	-4	6.17	5.00	23	23

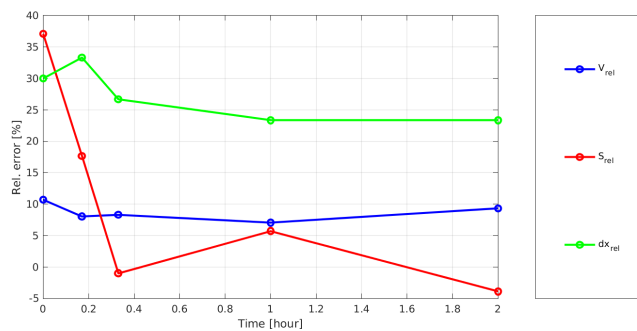


**Figure 3.5:** Temporal development of the relative error for the three indicators.

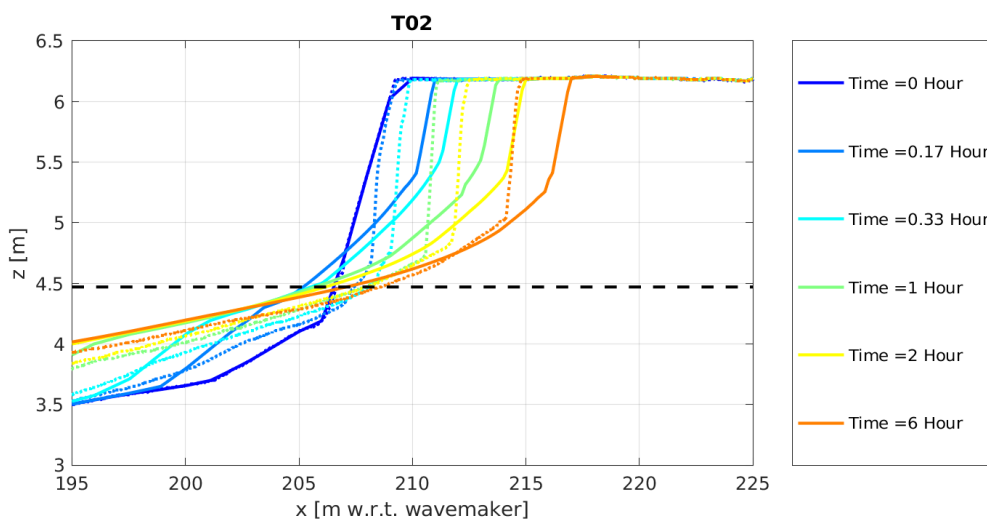


**Figure 3.6:** Comparisons of profiles from experiment T02 for different moments in time. Observed profiles are shown with a dashed line and the XBeach profiles with a solid line. The storm surge level is shown with a black dashed line.

**Table 3.3:** The computed and observed volume ( $V$ ) and berm slopes ( $S$ ) for T02. Volumes ( $V$ ) are given in  $m^3/m$ . The relative error is expressed in a percentage. Both the relative error in terms of the same time ( $rel, t$ ) and the final time are shown ( $rel$ ).

Time[hour]	$V_{xb}$ [ $m^3/m$ ]	$V_{data}$ [ $m^3/m$ ]	$V_{rel}$ [%]	$V_{rel,t}$ [%]	$S_{xb}$ [-]	$S_{data}$ [-]	$S_{rel}$ [%]	$dx_{xb}$ [m]	$dx_{data}$ [m]	$dx_{rel}$ [%]	$dx_{rel,t}$ [%]
0.17	2.22	1.04	12	113	0.12	0.09	45	1.83	0.17	29	1000
0.33	3.45	2.34	12	48	0.08	0.07	24	2.83	0.83	35	240
1	6.23	4.63	17	35	0.06	0.05	1	4.50	2.00	44	125
2	8.14	6.37	18	28	0.05	0.05	1	5.83	3.33	44	75
6	11.57	9.63	20	20	0.04	0.04	-8	7.83	5.67	38	38

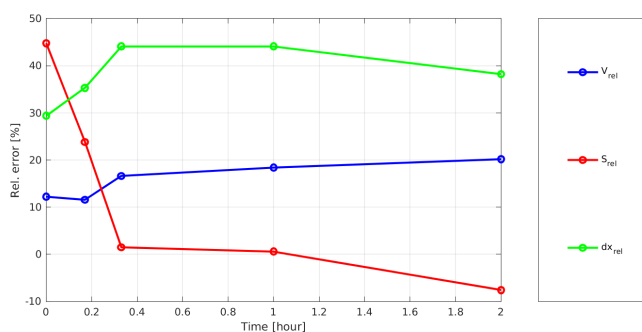


**Figure 3.7:** Temporal development of the relative error for the three indicators.

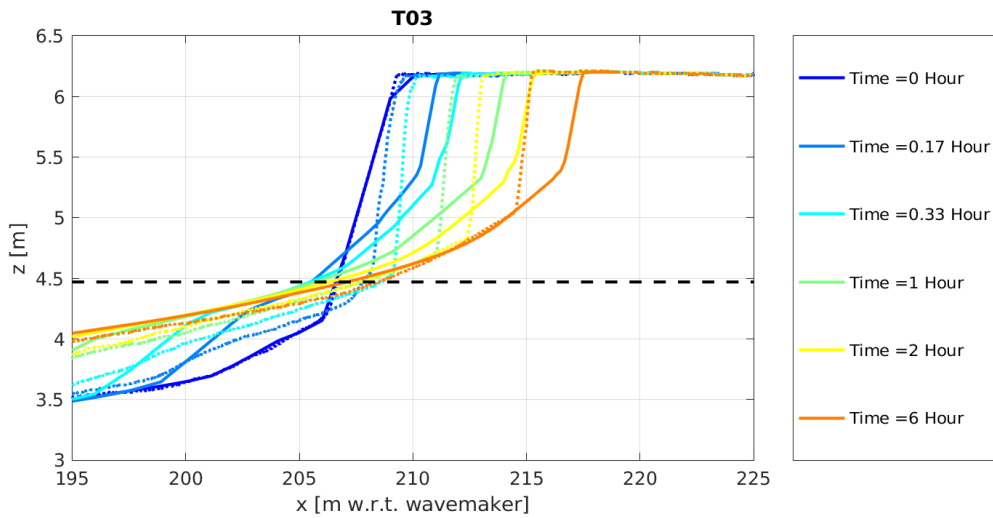


**Figure 3.8:** Comparisons of profiles from experiment T03 for different moments in time. Observed profiles are shown with a dashed line and the XBeach profiles with a solid line. The storm surge level is shown with a black dashed line.

**Table 3.4:** The computed and observed volume ( $V$ ) and berm slopes ( $S$ ) for T03. Volumes ( $V$ ) are given in  $m^3/m$ . The relative error is expressed in a percentage. Both the relative error in terms of the same time ( $rel, t$ ) and the final time are shown ( $rel$ ).

Time[hour]	$V_{xb}$ [ $m^3/m$ ]	$V_{data}$ [ $m^3/m$ ]	$V_{rel}$ [%]	$V_{rel,t}$ [%]	$S_{xb}$ [-]	$S_{data}$ [-]	$S_{rel}$ [%]	$dx_{xb}$ [m]	$dx_{data}$ [m]	$dx_{rel}$ [%]	$dx_{rel,t}$ [%]
0.17	2.32	1.22	11	91	0.11	0.08	34	2.00	0.33	27	500
0.33	3.73	2.60	11	43	0.08	0.06	26	3.00	0.83	35	260
1	6.52	5.41	11	20	0.06	0.05	10	4.83	2.83	32	71
2	8.48	7.21	13	18	0.05	0.05	4	6.17	4.00	35	54
6	11.76	9.96	18	18	0.04	0.04	11	8.33	6.17	35	35

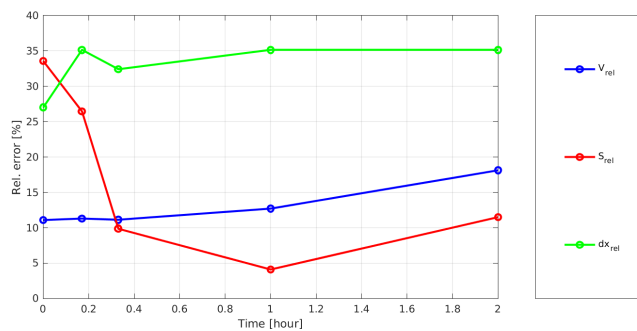


**Figure 3.9:** Temporal development of the relative error for the three indicators.

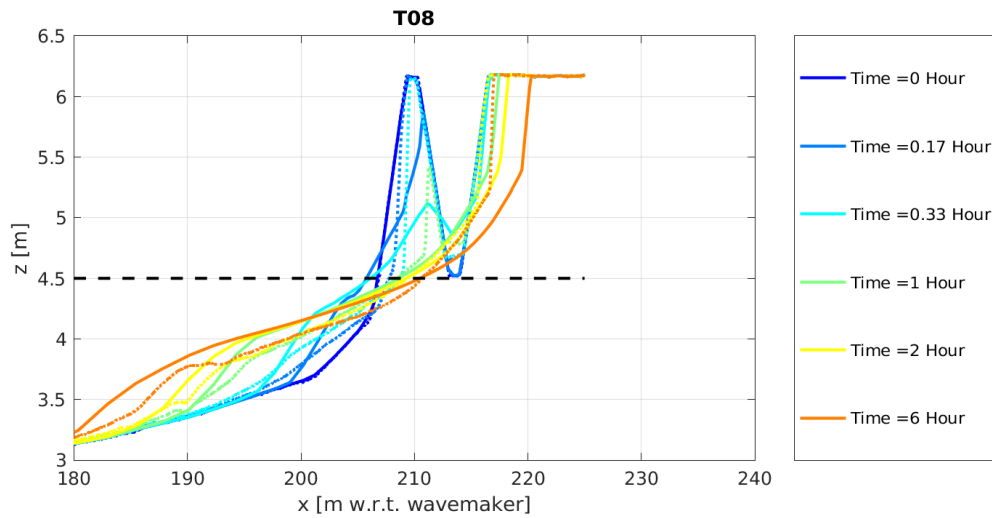


**Figure 3.10:** Comparisons of profiles from experiment T08 for different moments in time. Observed profiles are shown with a dashed line and the XBeach profiles with a solid line. The storm surge level is shown with a black dashed line.

**Table 3.5:** The computed and observed volume ( $V$ ) and berm slopes ( $S$ ) for T08. Volumes ( $V$ ) are given in  $m^3/m$ . The relative error is expressed in a percentage. Both the relative error in terms of the same time ( $rel, t$ ) and the final time are shown ( $rel$ ).

Time[hour]	$V_{xb}$ [ $m^3/m$ ]	$V_{data}$ [ $m^3/m$ ]	$V_{rel}$ [%]	$V_{rel,t}$ [%]	$S_{xb}$ [-]	$S_{data}$ [-]	$S_{rel}$ [%]	$dx_{xb}$ [m]	$dx_{data}$ [m]	$dx_{rel}$ [%]	$dx_{rel,t}$ [%]
0.17	2.09	1.19	13	76	0.12	0.09	39	7.17	0.17	88	4200
0.33	4.19	2.29	27	83	0.08	0.07	25	7.33	0.67	83	1000
1	6.50	4.84	24	34	0.04	0.06	-22	8.17	7.33	10	11
2	7.71	5.88	26	31	0.04	0.05	-6	9.00	7.33	21	23
6	10.62	7.03	51	51	0.04	0.04	-1	11.00	8.00	38	38

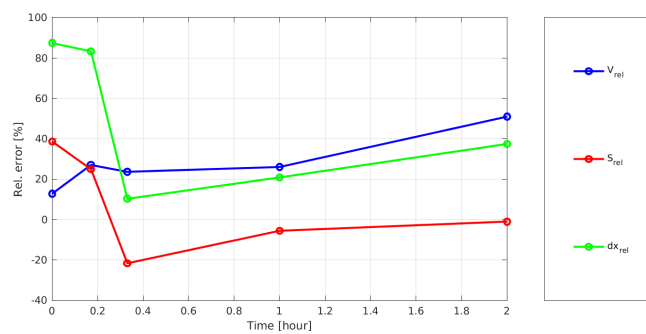


**Figure 3.11:** Temporal development of the relative error for the three indicators.

## Overview

An overview of the statistical scores is shown in Figure 3.12 and Table 3.6.

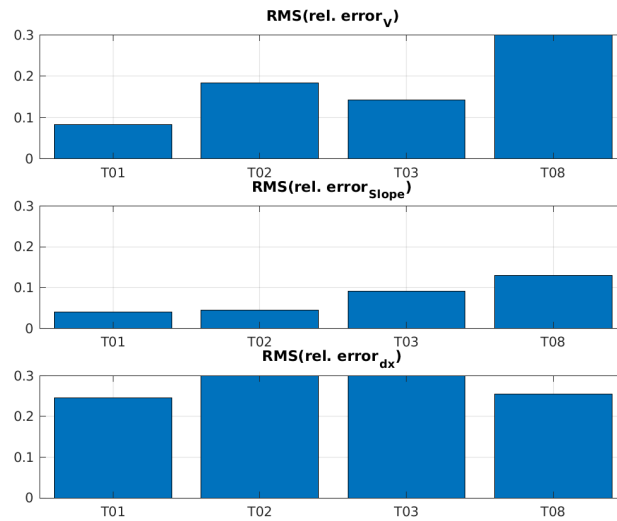


**Figure 3.12:** Overview of statistical scores for the Deltagoot 2006 experiments.

**Table 3.6:** Deltagoot 2006 statistical scores.

	T01	T02	T03	T08
$RMS(rel.volume)$	0.08	0.18	0.14	0.36
$RMS(rel.slope)$	0.04	0.04	0.09	0.13
$RMS(rel.retreat)$	0.24	0.42	0.34	0.25

### 3.2 M1797: Delta Flume 1981

In 1981, Delta Flume experiments were performed to gain insight in the effect of a dune revetment on the morphological behaviour of the dune, however, experiments were also carried out without a dune revetment. The profile in question is based on a stretch of coast called the Noorderstrand at Schouwen, the Netherlands (Vellinga, 1981). Two large scale experiments (depth scale of 2) were performed, one with and one without dune revetment. The latter is depicted in Figure 3.13. Table 3.7 shows the results for the indicators at different moments in time.

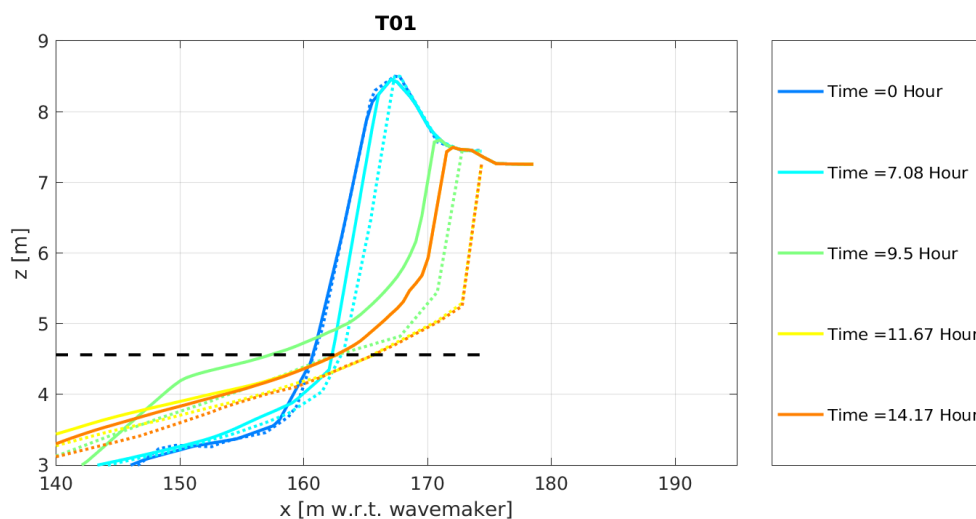


**Figure 3.13:** Comparison of profile during experiment T01. Observed profiles are shown with a dashed line and the XBeach profiles with a solid line. The storm surge level is shown with a black dashed line.

**Table 3.7:** The computed and observed volume ( $V$ ) and berm slopes ( $S$ ) for T01. Volumes ( $V$ ) are given in  $m^3/m$ . The relative error is expressed in a percentage. Both the relative error in terms of the same time ( $rel, t$ ) and the final time are shown ( $rel$ ).

Time[hour]	$V_{xb}$ [ $m^3/m$ ]	$V_{data}$ [ $m^3/m$ ]	$V_{rel}$ [%]	$V_{rel,t}$ [%]	$S_{xb}$ [-]	$S_{data}$ [-]	$S_{rel}$ [%]	$dx_{xb}$ [m]	$dx_{data}$ [m]	$dx_{rel}$ [%]	$dx_{rel,t}$ [%]
7.08	3.43	7.24	-11	-53	0.05	0.06	-22	0.50	2.00	-18	-75
9.5	17.48	28.28	-32	-38	0.09	0.06	38	5.00	7.00	-24	-29
11.67	22.70	33.04	-31	-31	0.05	0.06	-15	6.00	8.50	-29	-29
14.17	22.70	33.23	-32	-32	0.05	0.05	4	6.00	8.50	-29	-29

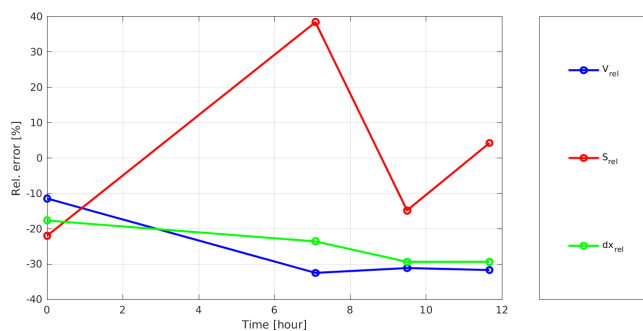


**Figure 3.14:** Temporal development of the relative error for the three indicators.

### 3.3 M1263 III: Delta Flume 1980-1981

#### Experiment description

The purpose of research programme M1263-3 was to verify the scale relations and the reliability of the deterministic dune erosion method according to Vellinga (1986), (Vellinga, 1984). In total 5 tests were performed in the Delta Flume of WL | Delft Hydraulics in the period of November 1980 till May 1981. Test 1 and Test 2 were performed at a depth scale of 5 and with a constant water level. In Test 1 the Dutch reference profile (see Figure 1.1) was used as initial profile with a geometric contraction of  $S_0 = 3$ , while in Test 2 a geometric contraction of  $S_0 = 2$  was applied. Test 3 was performed at the same depth scale as Test 2 and with the same initial profile, but with a varying water level. In Test 4 the storm surge of 1953 in The Netherlands was reproduced at a depth scale 3.27. Test 5 can be considered as a full-scale replica 1:1 of a moderate storm in nature; the reference profile was used with a steepness factor of  $S_0 = 2.47$ . The Delta Flume is approximately 230 m long, 5 m wide and 7 to 9 m deep. At the time these tests were performed the wave board in the Delta flume was not yet equipped with active reflection compensation (ARC) nor with second-order wave steering.

The five experiments are presented in Table 3.8. Tests 1, 2 and 5 had a constant surge level, while tests 3 and 4 had a variable surge level with a course depicted in Figure 3.15 and Figure 3.16 respectively.

**Table 3.8:** Overview of experiments

Experiment	Depth-scale	Profile contraction	Sediment diameter	Water depth	Wave height	Wave period
1	5	1.91	225	4.2	1.50	5.4
2	5	1.27	225	4.2	1.50	5.4
3	5	1.27	225	4.2	1.50	5.4
4	3.27	1.91	225	4.2	1.85	5.0
5	1	1	225	5.0	2.00	7.6

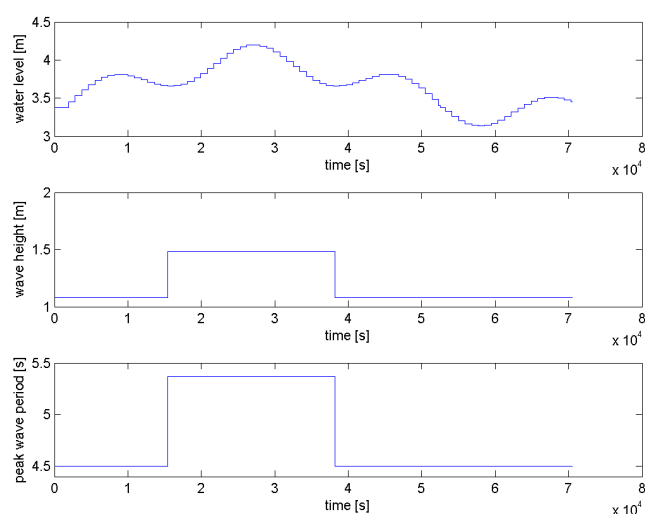


**Figure 3.15:** Boundary conditions for test 3. The storm development is shown for the water level (upper panel), the wave height (second panel) and the peak period (lower panel) as a function of time.

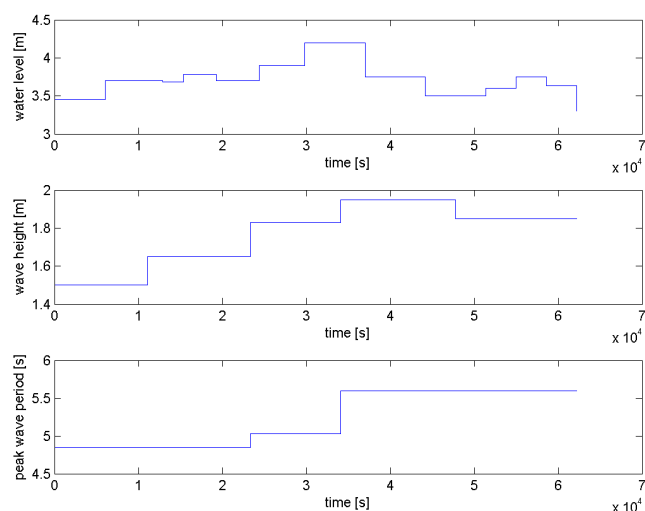


**Figure 3.16:** Boundary conditions for test 4. The storm development is shown for the water level (upper panel), the wave height (second panel) and the peak period (lower panel) as a function of time.

## Results

The profile developments are shown in Figure 3.17 to Figure 3.25. In Table 3.9 to Table 3.13, the indicators for different moments in time are shown. Next to the profiles, the relative errors as a function of time are shown in Figure 3.18, Figure 3.20, Figure 3.22, Figure 3.24 and Figure 3.26. Note that the depth-scale factor is relatively small for Test-4 and Test-5. This means that the grid resolution is also relatively large compared to the others tests, which affects the dune retreat indicator since the dune retreat is defined as the 1.5 grid cell below the maximum dune height. Therefore, the dune retreat indicator is not shown for these two tests since it does not represent correctly dune retreat.

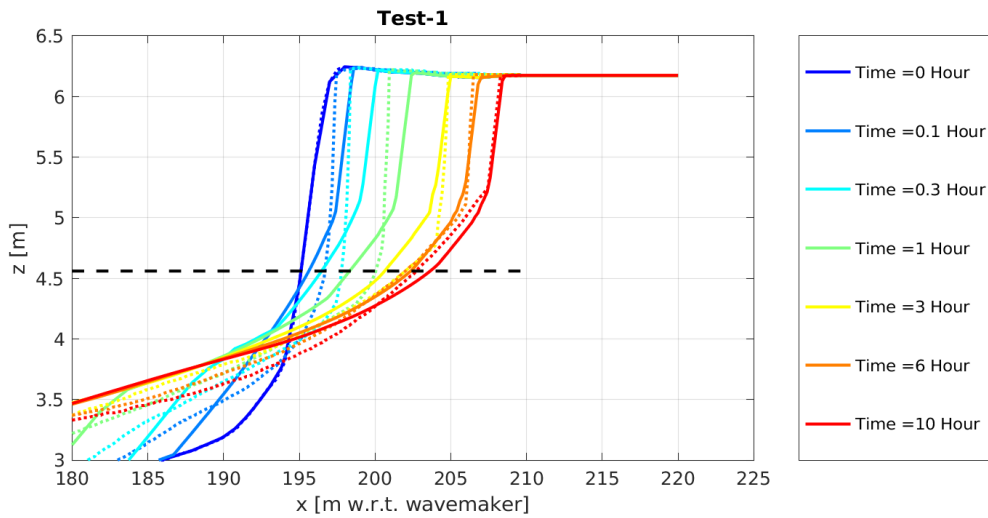


**Figure 3.17:** Comparisons of profiles from experiment Test-1 for different moments in time. Observed profiles are shown with a dashed line and the XBeach profiles with a solid line. The storm surge level is shown with a black dashed line.

**Table 3.9:** The computed and observed volume ( $V$ ) and berm slopes ( $S$ ) for Test-1. Volumes ( $V$ ) are given in  $m^3/m$ . The relative error is expressed in a percentage. Both the relative error in terms of the same time ( $rel, t$ ) and the final time are shown ( $rel$ ).

Time[hour]	$V_{xb}$ [ $m^3/m$ ]	$V_{data}$ [ $m^3/m$ ]	$V_{rel}$ [%]	$V_{rel,t}$ [%]	$S_{xb}$ [-]	$S_{data}$ [-]	$S_{rel}$ [%]	$dx_{xb}$ [m]	$dx_{data}$ [m]	$dx_{rel}$ [%]	$dx_{rel,t}$ [%]
0.1	2.50	1.85	4	35	0.18	0.12	52	1.60	0.60	9	167
0.3	4.90	3.52	8	39	0.11	0.08	34	3.20	1.60	14	100
1	8.62	7.70	5	12	0.08	0.07	13	5.40	4.20	11	29
3	12.64	13.67	-6	-7	0.06	0.05	6	8.00	8.00	0	0
6	15.65	15.66	-0	-0	0.05	0.05	-3	9.80	9.60	2	2
10	18.08	17.69	2	2	0.04	0.04	-3	11.40	11.40	0	0

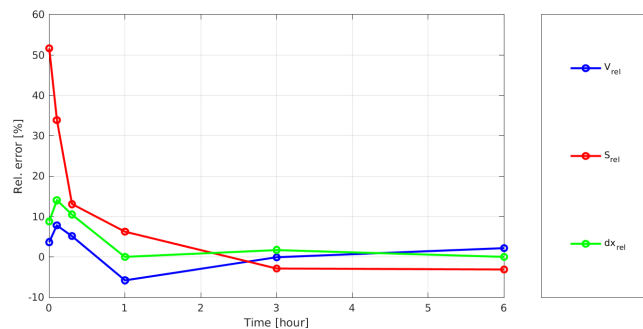


**Figure 3.18:** Temporal development of the relative error for the three indicators.

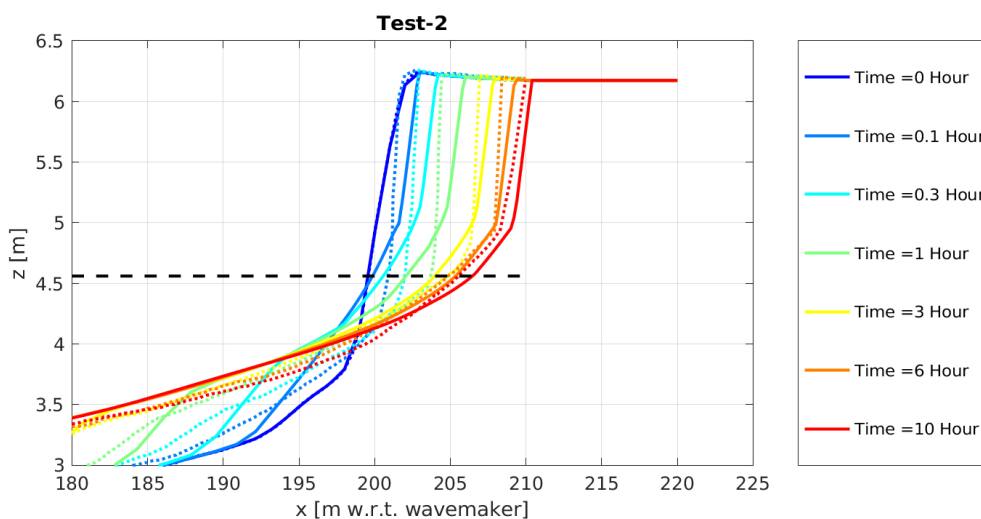


**Figure 3.19:** Comparisons of profiles from experiment Test-2 for different moments in time. Observed profiles are shown with a dashed line and the XBeach profiles with a solid line. The storm surge level is shown with a black dashed line.

**Table 3.10:** The computed and observed volume ( $V$ ) and berm slopes ( $S$ ) for Test-2. Volumes ( $V$ ) are given in  $m^3/m$ . The relative error is expressed in a percentage. Both the relative error in terms of the same time ( $rel, t$ ) and the final time are shown ( $rel$ ).

Time[hour]	$V_{xb}$ [ $m^3/m$ ]	$V_{data}$ [ $m^3/m$ ]	$V_{rel}$ [%]	$V_{rel,t}$ [%]	$S_{xb}$ [-]	$S_{data}$ [-]	$S_{rel}$ [%]	$dx_{xb}$ [m]	$dx_{data}$ [m]	$dx_{rel}$ [%]	$dx_{rel,t}$ [%]
0.1	1.85	1.00	6	86	0.17	0.11	57	1.00	0.00	12	Inf
0.3	3.77	2.92	6	29	0.11	0.08	36	2.20	1.40	10	57
1	6.70	5.64	8	19	0.07	0.06	13	4.00	2.80	15	43
3	9.91	9.55	3	4	0.06	0.05	6	5.80	5.40	5	7
6	12.23	11.61	5	5	0.05	0.05	-9	7.20	6.80	5	6
10	14.08	13.26	6	6	0.04	0.04	-1	8.40	8.00	5	5

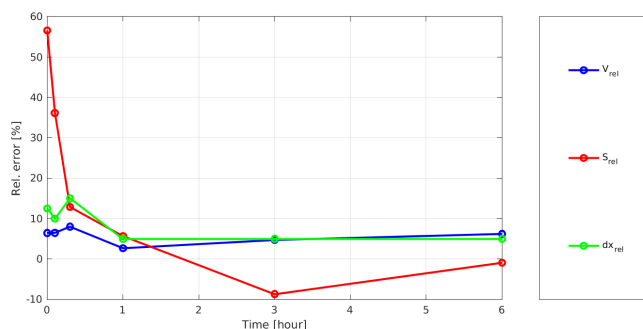


**Figure 3.20:** Temporal development of the relative error for the three indicators.

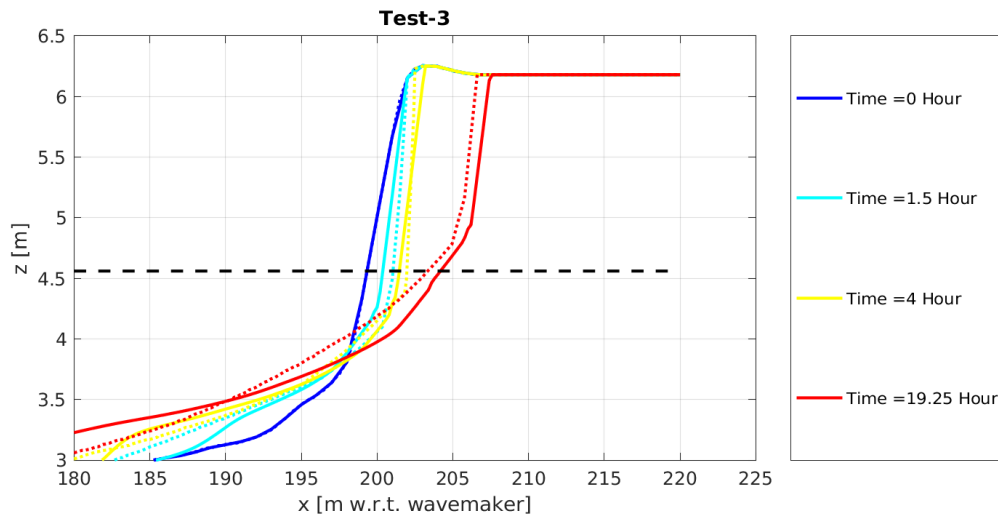


**Figure 3.21:** Comparisons of profiles from experiment Test-3 for different moments in time. Observed profiles are shown with a dashed line and the XBeach profiles with a solid line. The storm surge level is shown with a black dashed line.

**Table 3.11:** The computed and observed volume ( $V$ ) and berm slopes ( $S$ ) for Test-3. Volumes ( $V$ ) are given in  $m^3/m$ . The relative error is expressed in a percentage. Both the relative error in terms of the same time ( $rel, t$ ) and the final time are shown ( $rel$ ).

Time[hour]	$V_{xb}$ [ $m^3/m$ ]	$V_{data}$ [ $m^3/m$ ]	$V_{rel}$ [%]	$V_{rel,t}$ [%]	$S_{xb}$ [-]	$S_{data}$ [-]	$S_{rel}$ [%]	$dx_{xb}$ [m]	$dx_{data}$ [m]	$dx_{rel}$ [%]	$dx_{rel,t}$ [%]
1.5	0.96	1.58	-7	-39	0.11	0.09	24	0.20	0.40	-4	-50
4	2.76	2.62	2	5	0.07	0.06	19	1.40	1.00	8	40
19.25	9.69	8.67	12	12	0.04	0.05	-11	5.60	4.80	17	17

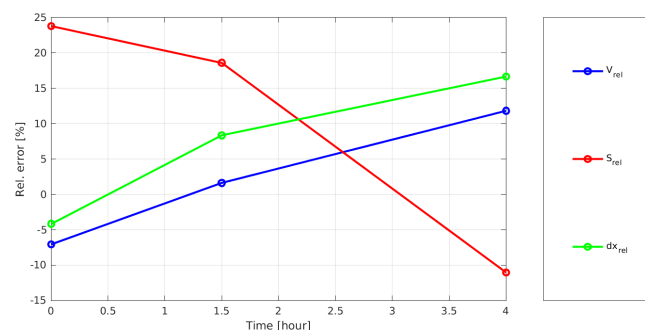


**Figure 3.22:** Temporal development of the relative error for the three indicators.

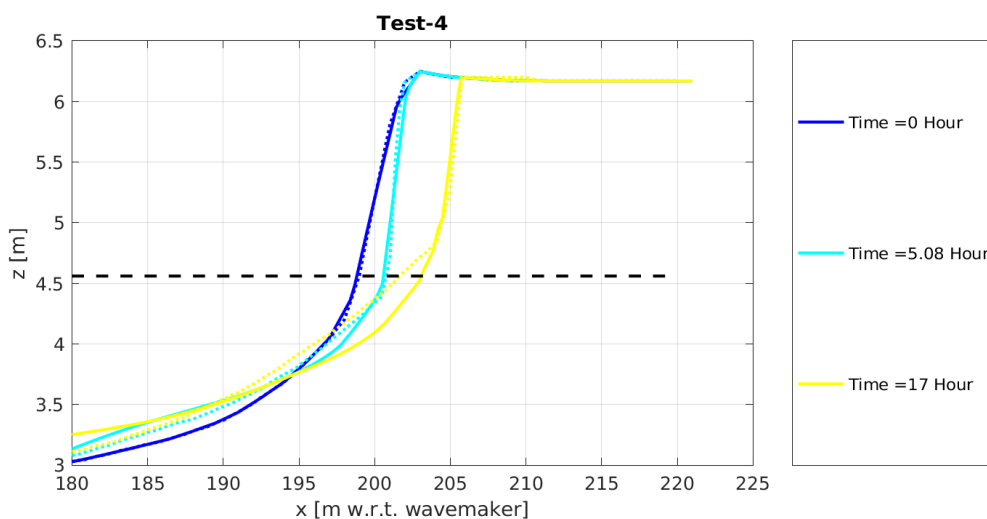


**Figure 3.23:** Comparisons of profiles from experiment Test-4 for different moments in time. Observed profiles are shown with a dashed line and the XBeach profiles with a solid line. The storm surge level is shown with a black dashed line.

**Table 3.12:** The computed and observed volume ( $V$ ) and berm slopes ( $S$ ) for Test-4. Volumes ( $V$ ) are given in  $m^3/m$ . The relative error is expressed in a percentage. Both the relative error in terms of the same time ( $rel, t$ ) and the final time are shown ( $rel$ ).

Time[hour]	$V_{xb}$ [ $m^3/m$ ]	$V_{data}$ [ $m^3/m$ ]	$V_{rel}$ [%]	$V_{rel,t}$ [%]	$S_{xb}$ [-]	$S_{data}$ [-]	$S_{rel}$ [%]
5.08	1.66	1.57	1	5	0.07	0.05	40
17	7.12	7.52	-5	-5	0.04	0.04	-3

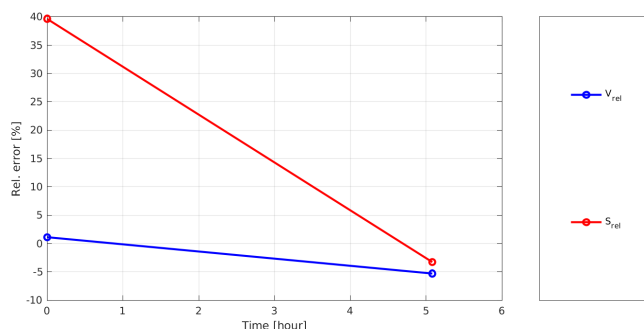


**Figure 3.24:** Temporal development of the relative error for the three indicators.

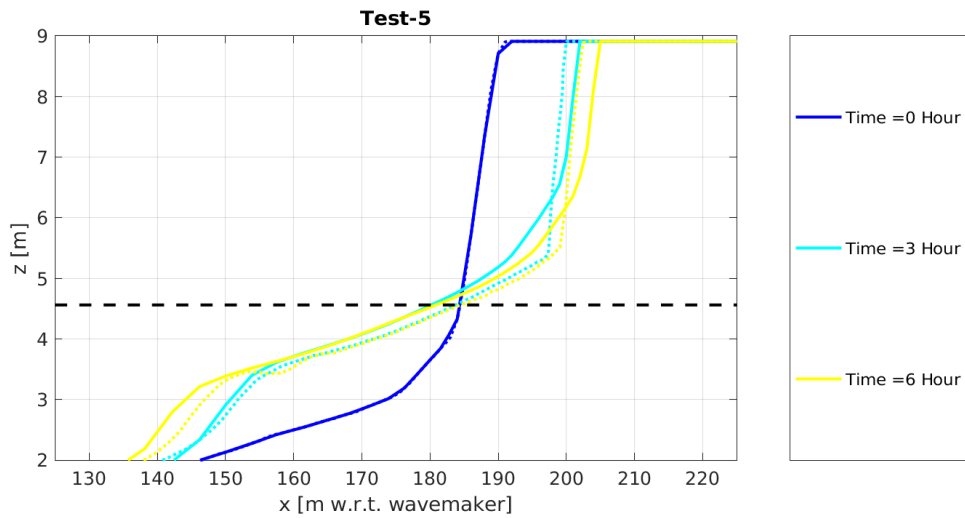


**Figure 3.25:** Comparisons of profiles from experiment Test-5 for different moments in time. Observed profiles are shown with a dashed line and the XBeach profiles with a solid line. The storm surge level is shown with a black dashed line.

**Table 3.13:** The computed and observed volume ( $V$ ) and berm slopes ( $S$ ) for Test-5. Volumes ( $V$ ) are given in  $m^3/m$ . The relative error is expressed in a percentage. Both the relative error in terms of the same time ( $rel, t$ ) and the final time are shown ( $rel$ ).

Time[hour]	$V_{xb}$ [ $m^3/m$ ]	$V_{data}$ [ $m^3/m$ ]	$V_{rel}$ [%]	$V_{rel,t}$ [%]	$S_{xb}$ [-]	$S_{data}$ [-]	$S_{rel}$ [%]
3	41.46	42.13	-1	-2	0.05	0.05	1
6	52.72	50.99	3	3	0.05	0.04	6

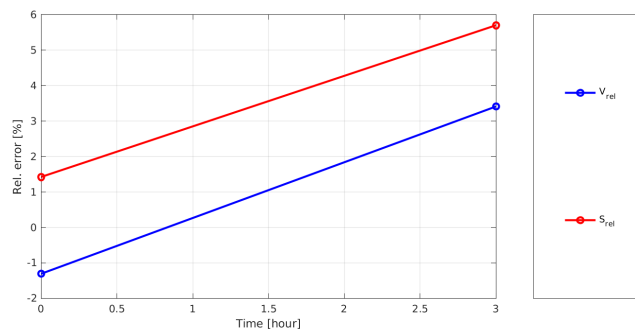


**Figure 3.26:** Temporal development of the relative error for the three indicators.

### Overview

The statistical scores for all experiments are shown Figure 3.27 in Table 3.14.

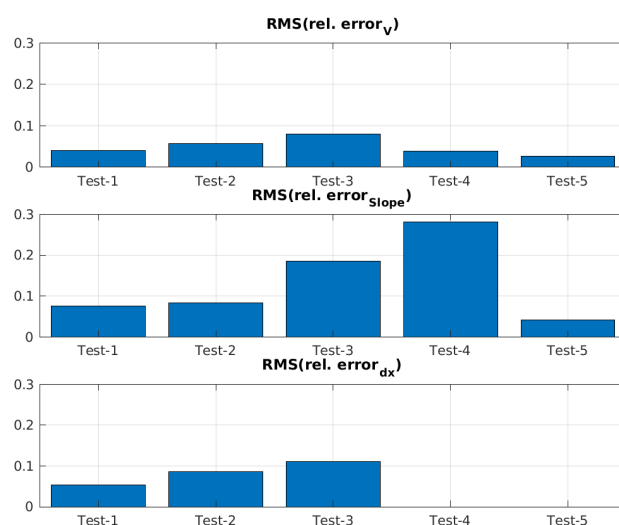


**Figure 3.27:** Overview of the statistical scores for M1263 experiments.

**Table 3.14:** M1263 III statistical scores.

	Test-1	Test-2	Test-3	Test-4	Test-5
$RMS(rel.volume)$	0.04	0.06	0.08	0.04	0.03
$RMS(rel.slope)$	0.08	0.08	0.19	0.28	0.04
$RMS(rel.retreat)$	0.05	0.09	0.11	NaN	NaN

### 3.4 LIP11D: Delta Flume 1994

The purpose of research programme LIP 11D was the generation of high quality and high resolution data on hydrodynamics and sediment transport dynamics on a natural 2DV beach under equilibrium, erosive and accretive conditions. In total 7 tests were performed in the Delta Flume of WL | Delft Hydraulics in the period of April 1993 till June 1993. Test 2E is incorporated in the skillbed, because the profiles and hydraulic conditions in this test correspond rather well to the Dutch situation. Since there is no direct agreement with the reference profile, scale factors or steepness factors cannot be determined in a similar way as in the research programmes in the 1980's. We assume a scale factor of 1:5. The wave board in the Delta Flume was equipped with active reflection compensation (ARC) at the time these tests were performed, and it is assumed that no second-order wave steering was applied. Waves were measured at a location 20 m from the wave board where the bed level was still horizontal. The sand had a diameter of  $D_{50} = 220 \mu\text{m}$ .

The model test 2E, also described in [Arcilla et al. \(1994\)](#), concerns extreme conditions with a raised water level at 4.6 m above the flume bottom, a significant wave height,  $H_{m0}$ , of 1.4 m (corresponding to some 7 m on prototype scale) and peak period,  $T_p$ , of 5 s (corresponds to 11 s on prototype scale). During the test substantial dune erosion took place.

Based on the integral wave parameters  $H_{m0}$  and  $T_p$  and a standard Jonswap spectral shape, time series of wave energy were generated and imposed as boundary condition. Since the flume tests were carried out with first-order wave generation (no imposed super-harmonics and sub-harmonics), the hindcast runs were carried out with the incoming, bound long waves set to zero as well. Active wave reflection compensation (ARC) was applied in the physi-

cal model, which has a result similar to the weakly reflective boundary condition in XBeach, namely to prevent re-reflecting of outgoing waves at the wave paddle (offshore boundary).

The comparison between the observed profiles and computed profiles is shown in Figure 3.28 and the results for the indicators are shown in Table 3.15. The relative errors from Table 3.15 are also shown in Figure 3.29.

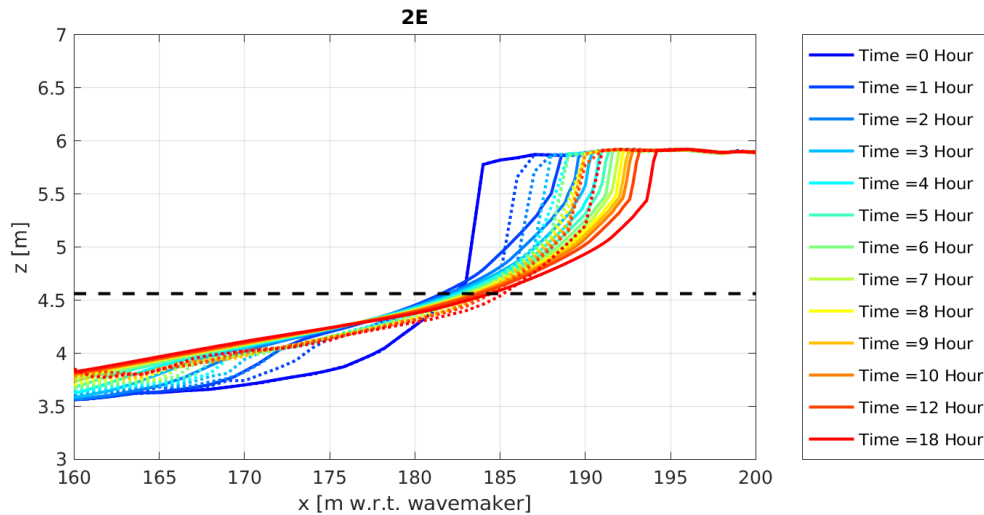


**Figure 3.28:** Comparisons of profiles from experiment LIP 2E for different moments in time. Observed profiles are shown with a dashed line and the XBeach profiles with a solid line. The storm surge level is shown with a black dashed line.

**Table 3.15:** The computed and observed volume ( $V$ ) and berm slopes ( $S$ ) for 2E. Volumes ( $V$ ) are given in  $m^3/m$ . The relative error is expressed in a percentage. Both the relative error in terms of the same time ( $rel, t$ ) and the final time are shown ( $rel$ ).

Time[hour]	$V_{xb}$ [ $m^3/m$ ]	$V_{data}$ [ $m^3/m$ ]	$V_{rel}$ [%]	$V_{rel,t}$ [%]	$S_{xb}$ [-]	$S_{data}$ [-]	$S_{rel}$ [%]	$dx_{xb}$ [m]	$dx_{data}$ [m]	$dx_{rel}$ [%]	$dx_{rel,t}$ [%]
1	3.51	2.50	14	40	0.05	0.06	-11	4.20	2.00	33	110
2	4.73	3.50	17	35	0.05	0.06	-12	5.40	3.00	36	80
3	5.56	4.16	19	34	0.04	0.05	-19	6.20	3.80	36	63
4	6.20	4.73	20	31	0.04	0.03	34	6.60	4.60	30	43
5	6.72	4.99	23	35	0.04	0.03	27	7.20	4.80	36	50
6	7.18	5.15	27	39	0.04	0.03	23	7.40	4.80	39	54
7	7.57	5.61	27	35	0.03	0.03	21	7.80	5.60	33	39
8	7.92	5.80	29	37	0.03	0.03	20	8.00	5.60	36	43
9	8.24	5.92	31	39	0.03	0.03	18	8.20	5.80	36	41
10	8.54	6.15	32	39	0.03	0.03	17	8.60	5.80	42	48
12	9.07	6.38	36	42	0.03	0.03	23	9.00	5.80	48	55
18	10.32	7.39	40	40	0.03	0.03	17	10.00	6.60	52	52

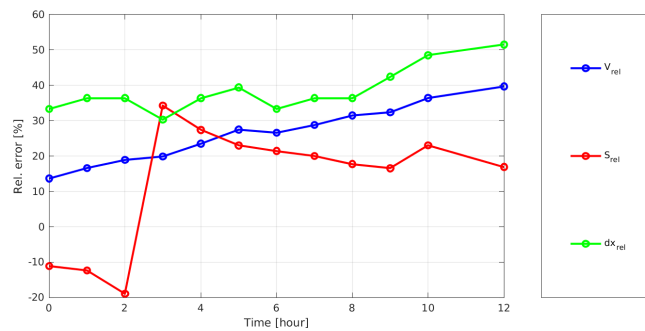


Figure 3.29: Temporal development of the relative error for the three indicators.

### 3.5 Deltaflume H4731

In the H4731 Delta flume experiments, it was studied how a collapsed dune revetment affects dune erosion (Van Gent and Coeveld, 2007). Four large-scale experiments were performed in the Delta flume with a depth scale of  $n_d$  equals 6. A wave height of 9 m (prototype) and peak period of 12 s (prototype) were forced at the wave maker. The test without a revetment (T14) is modelled with XBeach (Figure 3.30). The results for the indicators for different moments in time are shown in Table 3.16. Note that the observed dune retreat is zero since the dune front does not erode in the observed profiles. This means that the relative error in dune retreat cannot be computed.

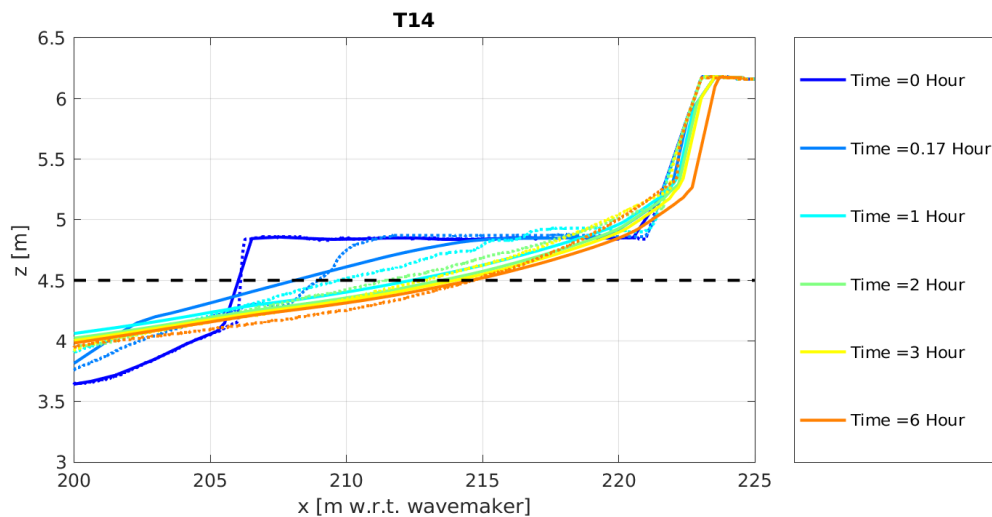
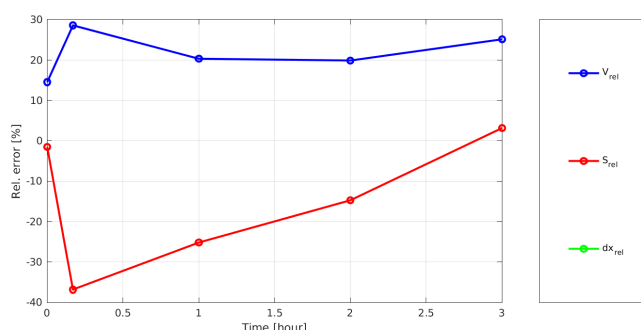


Figure 3.30: Comparison of profile during experiment T14. Observed profiles are shown with a dashed line and the XBeach profiles with a solid line. The storm surge level is shown with a black dashed line.

**Table 3.16:** The computed and observed volume ( $V$ ) and berm slopes ( $S$ ) for T14. Volumes ( $V$ ) are given in  $m^3/m$ . The relative error is expressed in a percentage. Both the relative error in terms of the same time ( $rel,t$ ) and the final time are shown ( $rel$ ).

Time[hour]	$V_{xb}$ [ $m^3/m$ ]	$V_{data}$ [ $m^3/m$ ]	$V_{rel}$ [%]	$V_{rel,t}$ [%]	$S_{xb}$ [-]	$S_{data}$ [-]	$S_{rel}$ [%]	$dx_{xb}$ [m]	$dx_{data}$ [m]	$dx_{rel}$ [%]	$dx_{rel,t}$ [%]
0.17	1.83	1.28	15	43	0.08	0.08	-2	0.00	0.00	NaN	NaN
1	3.44	2.36	29	46	0.04	0.07	-37	0.00	0.00	NaN	NaN
2	3.81	3.04	20	25	0.04	0.05	-25	0.00	0.00	NaN	NaN
3	4.07	3.32	20	23	0.04	0.04	-15	0.17	0.00	Inf	Inf
6	4.75	3.79	25	25	0.04	0.04	3	0.50	0.00	Inf	Inf



**Figure 3.31:** Temporal development of the relative error for the three indicators.

### 3.6 Grosse Wellen Kanal 1998

#### Experiment description

The purpose of research programme GWK98 was to improve the methods of design and performance assessment of beach nourishments. In total 24 tests were performed in the wave flume in Hannover (Grosse Wellen Kanal) in the period of November 1996 till August 1997.

These tests were not carried out with an initial profile similar to the Dutch reference profile, nor with hydraulic conditions characteristic for the Dutch coast. Scale factors or steepness factors can therefore not be determined in a similar way as in the research programmes in The Netherlands in the 1980's. We assumed wave-height scaling with respect to super-storm conditions for the Dutch coast (wave-height of 9 m), which resulted in a scale of 1:8. In total 8 series of tests were performed with different initial profiles with and without supporting structures. Imposed wave heights for all tests was 1.16 m (estimated as 9 m on prototype scale), with a wave period of 6.4 s (corresponding to 18 s on prototype scale). In total 5 tests without structures are incorporated in the skillbed, which have a dune-type cross-shore profile and hydraulic conditions large enough to cause significant erosion. First order wave steering was applied, and ARC compensation was present.

#### Results

The profile development is shown in Figure 3.32 to Figure 3.40. The results for the indicators for different moments in time are shown in Table 3.17 to Table 3.21. Note that the profile measurements do not show a clear dune retreat. Therefore, the dune retreat is not included in shown tables.

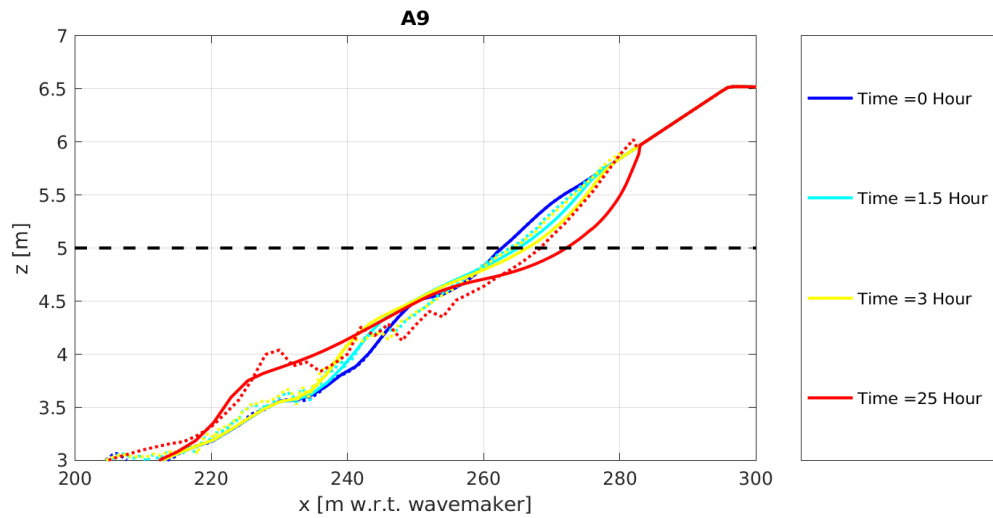


**Figure 3.32:** Comparisons of profiles from experiment A9 for different moments in time. Observed profiles are shown with a dashed line and the XBeach profiles with a solid line. The storm surge level is shown with a black dashed line.

**Table 3.17:** The computed and observed volume ( $V$ ) and berm slopes ( $S$ ) for A9. Volumes ( $V$ ) are given in  $m^3/m$ . The relative error is expressed in a percentage. Both the relative error in terms of the same time ( $rel, t$ ) and the final time are shown ( $rel$ ).

Time[hour]	$V_{xb}$ [ $m^3/m$ ]	$V_{data}$ [ $m^3/m$ ]	$V_{rel}$ [%]	$V_{rel,t}$ [%]	$S_{xb}$ [-]	$S_{data}$ [-]	$S_{rel}$ [%]
1.5	1.70	0.90	26	90	0.04	0.04	12
3	2.58	1.15	46	124	0.04	0.04	-12
25	6.91	3.12	121	121	0.03	0.03	-5

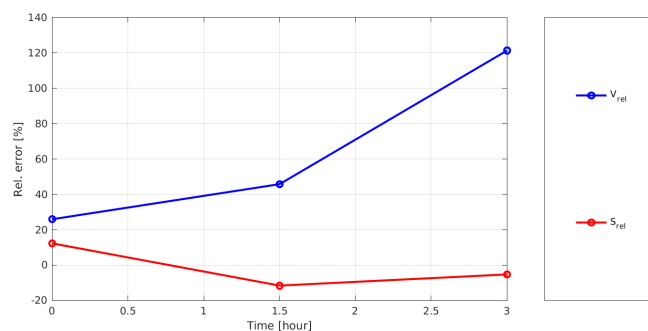


**Figure 3.33:** Temporal development of the relative error for the three indicators.

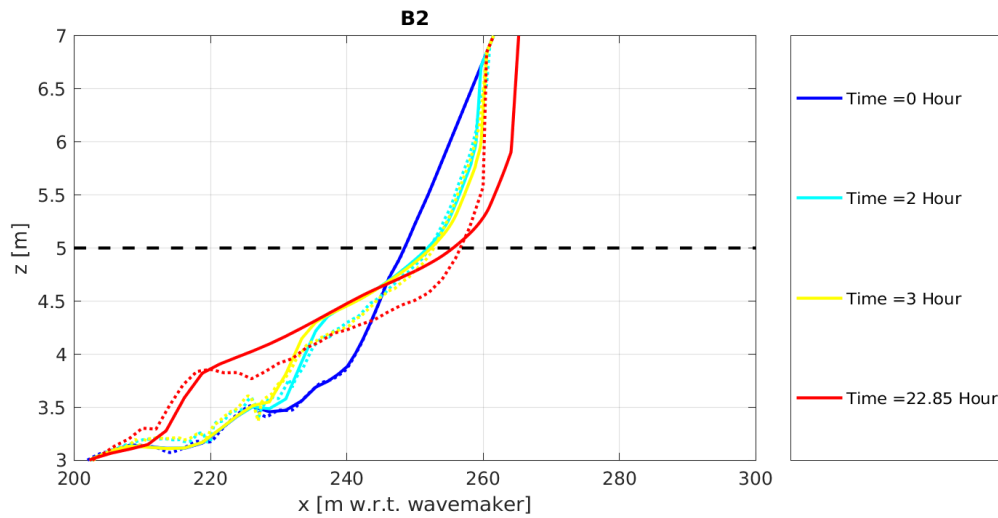


**Figure 3.34:** Comparisons of profiles from experiment B2 for different moments in time. Observed profiles are shown with a dashed line and the XBeach profiles with a solid line. The storm surge level is shown with a black dashed line.

**Table 3.18:** The computed and observed volume ( $V$ ) and berm slopes ( $S$ ) for B2. Volumes ( $V$ ) are given in  $m^3/m$ . The relative error is expressed in a percentage. Both the relative error in terms of the same time ( $rel, t$ ) and the final time are shown ( $rel$ ).

Time[hour]	$V_{xb}$ [ $m^3/m$ ]	$V_{data}$ [ $m^3/m$ ]	$V_{rel}$ [%]	$V_{rel,t}$ [%]	$S_{xb}$ [-]	$S_{data}$ [-]	$S_{rel}$ [%]
2	5.75	5.56	2	3	0.06	0.06	-6
3	7.04	5.98	11	18	0.06	0.06	-0
22.85	17.02	9.40	81	81	0.04	0.04	1

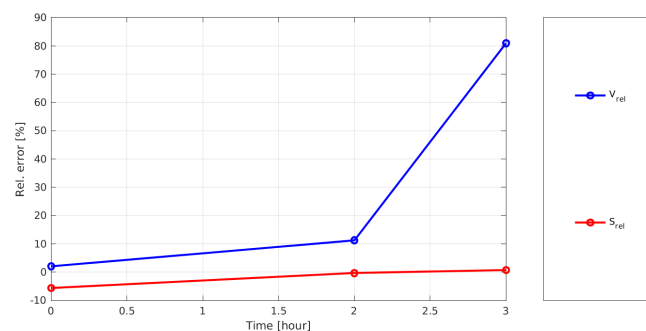


**Figure 3.35:** Temporal development of the relative error for the three indicators.

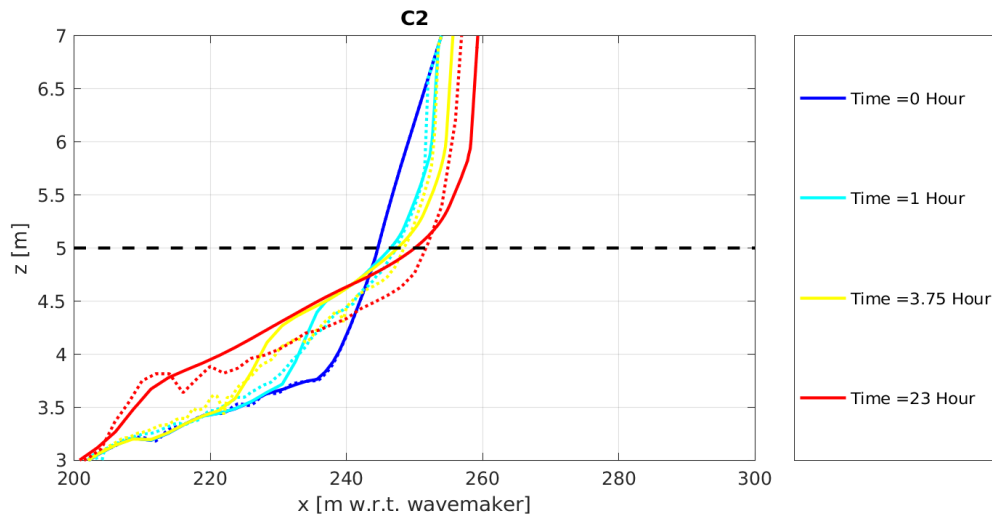


**Figure 3.36:** Comparisons of profiles from experiment C2 for different moments in time. Observed profiles are shown with a dashed line and the XBeach profiles with a solid line. The storm surge level is shown with a black dashed line.

**Table 3.19:** The computed and observed volume ( $V$ ) and berm slopes ( $S$ ) for C2. Volumes ( $V$ ) are given in  $m^3/m$ . The relative error is expressed in a percentage. Both the relative error in terms of the same time ( $rel, t$ ) and the final time are shown ( $rel$ ).

Time[hour]	$V_{xb}$ [ $m^3/m$ ]	$V_{data}$ [ $m^3/m$ ]	$V_{rel}$ [%]	$V_{rel,t}$ [%]	$S_{xb}$ [-]	$S_{data}$ [-]	$S_{rel}$ [%]
1	4.98	4.19	6	19	0.07	0.07	-4
3.75	9.33	6.13	24	52	0.05	0.05	-13
23	19.59	13.40	46	46	0.03	0.03	7

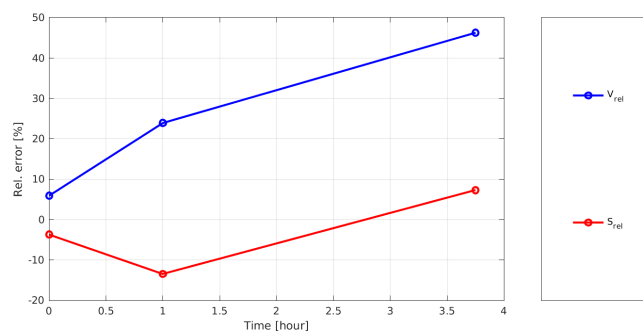


**Figure 3.37:** Temporal development of the relative error for the three indicators.

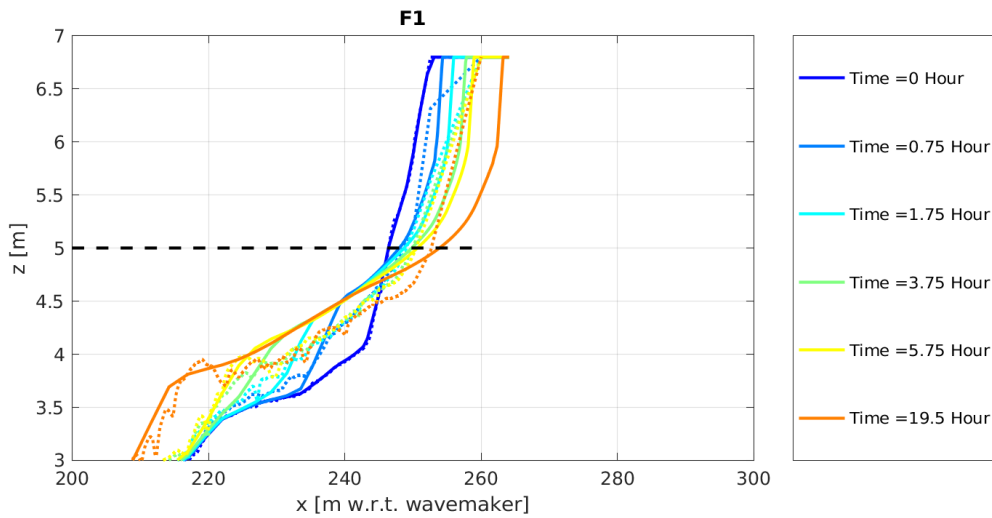


**Figure 3.38:** Comparisons of profiles from experiment F1 for different moments in time. Observed profiles are shown with a dashed line and the XBeach profiles with a solid line. The storm surge level is shown with a black dashed line.

**Table 3.20:** The computed and observed volume ( $V$ ) and berm slopes ( $S$ ) for F1. Volumes ( $V$ ) are given in  $m^3/m$ . The relative error is expressed in a percentage. Both the relative error in terms of the same time ( $rel, t$ ) and the final time are shown ( $rel$ ).

Time[hour]	$V_{xb}$ [ $m^3/m$ ]	$V_{data}$ [ $m^3/m$ ]	$V_{rel}$ [%]	$V_{rel,t}$ [%]	$S_{xb}$ [-]	$S_{data}$ [-]	$S_{rel}$ [%]
0.75	4.84	6.88	-12	-30	0.08	0.08	-3
1.75	7.53	12.12	-26	-38	0.06	0.06	-4
3.75	10.60	13.79	-18	-23	0.05	0.05	-5
5.75	12.63	14.75	-12	-14	0.04	0.04	8
19.5	19.91	17.43	14	14	0.04	0.04	-1

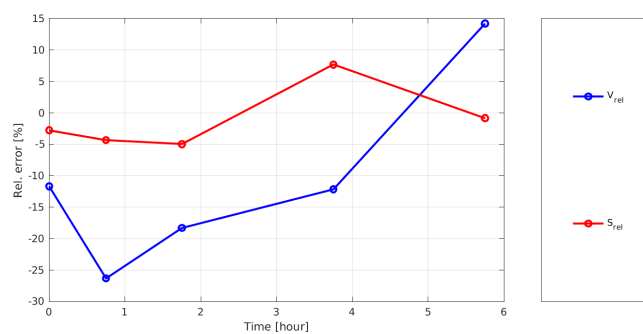


**Figure 3.39:** Temporal development of the relative error for the three indicators.

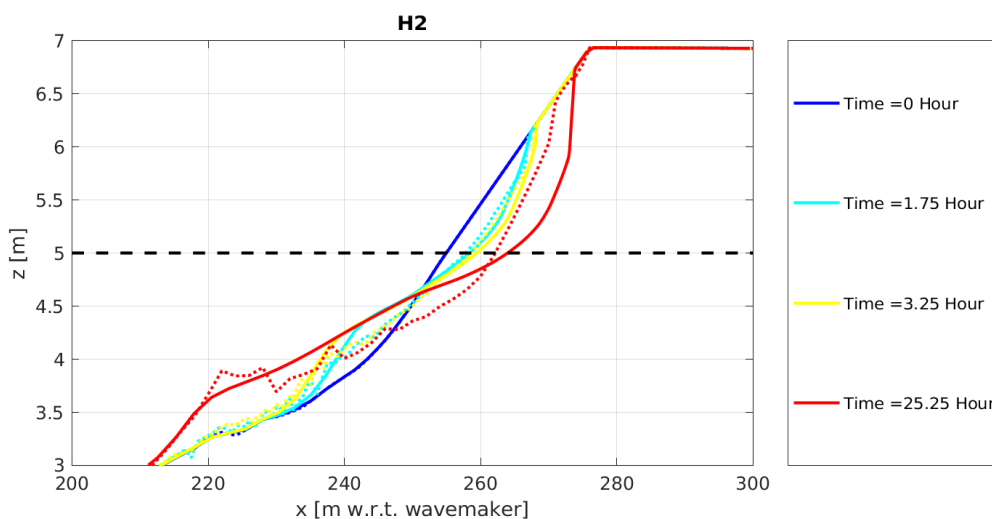


**Figure 3.40:** Comparisons of profiles from experiment H2 for different moments in time. Observed profiles are shown with a dashed line and the XBeach profiles with a solid line. The storm surge level is shown with a black dashed line.

**Table 3.21:** The computed and observed volume ( $V$ ) and berm slopes ( $S$ ) for H2. Volumes ( $V$ ) are given in  $m^3/m$ . The relative error is expressed in a percentage. Both the relative error in terms of the same time ( $rel, t$ ) and the final time are shown ( $rel$ ).

Time[hour]	$V_{xb}$ [ $m^3/m$ ]	$V_{data}$ [ $m^3/m$ ]	$V_{rel}$ [%]	$V_{rel,t}$ [%]	$S_{xb}$ [-]	$S_{data}$ [-]	$S_{rel}$ [%]
1.75	3.31	2.80	7	18	0.05	0.05	-8
3.25	4.62	3.68	13	25	0.05	0.05	-8
25.25	12.27	6.95	77	77	0.03	0.03	-5

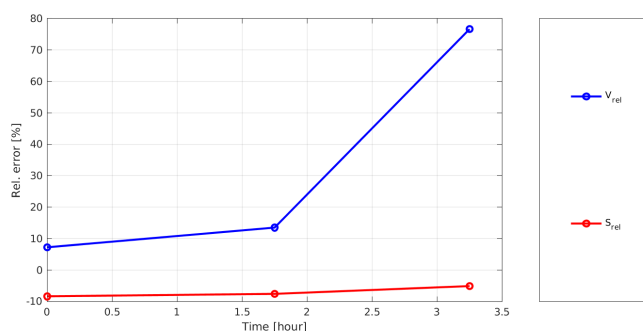


**Figure 3.41:** Temporal development of the relative error for the three indicators.

**Overview**

An overview of the statistical scores is shown in Figure 3.42 and Table 3.22. Note that dune retreat is not shown and that only the errors in dune erosion volume and berm slope are shown.

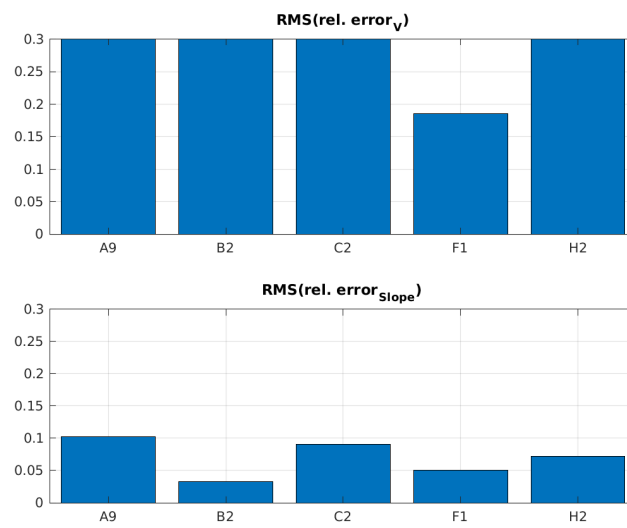


**Figure 3.42:** GWK overview

**Table 3.22:** Statistical scores for the Grosse Wellen Kanal experiments.

	A9	B2	C2	F1	H2
$RMS(rel.volume)$	0.76	0.47	0.30	0.19	0.45
$RMS(rel.slope)$	0.10	0.03	0.09	0.05	0.07

## 4 Field validation

In total, nine field datasets, comprising 69 cross-shore profiles, are available with data on either hydro- or morphodynamics of a storm. In total, two profiles are available purely for the hydrodynamic validation and 60 for the morphodynamics validation. In addition, seven transects (Egmond aan Zee) are used for both hydrodynamic and morphodynamic validation. [Table 4.1](#) provides an overview of these cases. The cases cover a variety of wave and water level conditions, profiles shapes and grain sizes, as explained below. This variation is strongly related to the variation in geographical location of the cases studies: most locations are at several locations along the North Sea coast, but Case 2 is along the French Atlantic coast and Case 5 along the East coast of the USA. Each case comprises 1 to 30 cross-shore profiles for which validation data are available and a 1D BOI-XBeach simulation is set up. As far as possible, the chosen profiles are at a more-or-less alongshore uniform location to limit processes in the alongshore direction that affect the 1D validation results. For the morphodynamic validation, Case 9 ('Holland 1953') could only be used for a general validation (focus on the order of magnitude of dune erosion) due to limitations in available data, but this is still valuable since this storm resulted in the largest recorded dune erosion volumes along the Dutch coast. In the following sections of this report, each individual field case is described in more detail. This comprises a case description and a comparison of the latest XBeach model results with the measurements.

### 4.1 Schiermonnikoog

#### Experiment description

Hydrodynamic data were obtained along a cross-shore transect at the tail of the Dutch barrier island 'Schiermonnikoog' in the Wadden Sea during a measurement campaign of the department Physical Geography of Utrecht University (UU) in the winter of 2014-2015. The campaign was part of the PhD research of Anita Engelstad and Daan Wesselman. The measurements are used for the validation of the hydrodynamics in the BOI-version of the dune erosion model XBeach, with a focus on the validation of simulated infragravity waves.

The location of the measurements is indicated in [Figure 4.1](#). The beach and nearshore morphology near the transect is alongshore almost uniform. The cross-shore profile is a typical Wadden Sea profile, with a mildly sloping foreshore (about 1:100) and three offshore bars. In the intertidal zone, two to three bars are present, which is also visible in the aerial photograph ([Figure 4.1](#)). The highest point along the transect – the beach crest – is at less than 1.8 m +NAP: no dunes are present at the tail and the tail is completely inundated several times per year. At the landward side of the beach crest, the profile gently slopes towards the Wadden Sea. The elevation along the intertidal and subtidal part of the transect has been measured with a RTK-GPS system at the beginning and the end of the field campaign. For the subtidal part, open-source yearly Jarkus transects and 'Vaklodingen' data of RWS are available.

**Table 4.1:** Overview of the validation case studies and characteristics.

Nr.	Case Name	Nr. of Profiles	Type	Profile shape characteristics	Remarks
1	Schiermonnikoog (NL)	1	Hydro	Long gentle Wadden profile with bars	No dunes; overwash conditions
2	Saint Trojan (France)	1	Hydro	Long. Average beach slope, $\sim 1:180$ to long, gentle shelf	Very long swell waves; high infragravity waves
3	Egmond (NL)	7	Hydro / Morpho	Short. Average beach slope with bars	Limited erosion.
4	Flemish Coast (Belgium)	15	Morpho	Short. Average beach slope, steeper slope ( $\sim 1:45 - 1:65$ ) to very shallow flat shelf.	High surge level, but minor dune erosion
5	Fire Island, NY (USA)	6	Morpho	Long, steep and with bar, low dunes (2-6 m)	Extreme wave conditions leading to dune erosion, overwash and dune breaching.
6	Vedersoe (Denmark)	2	Morpho	Steepest beach, nearshore slope of Holland coast. Short.	Two profiles with different erosion volume, of which one the largest example of erosion in this validation study.
7	Langeoog (Germany)	6	Morpho	Gentle Wadden profile	Profiles with and without beach nourishment. Little dune erosion.
8	Holland (NL)	1976 30	Morpho	Long Holland profile	Profile shape varies due to bars and channels
9	Holland (NL)	1953 1	Morpho	Holland reference profile	Indicative due to limited data. Significant dune erosion.

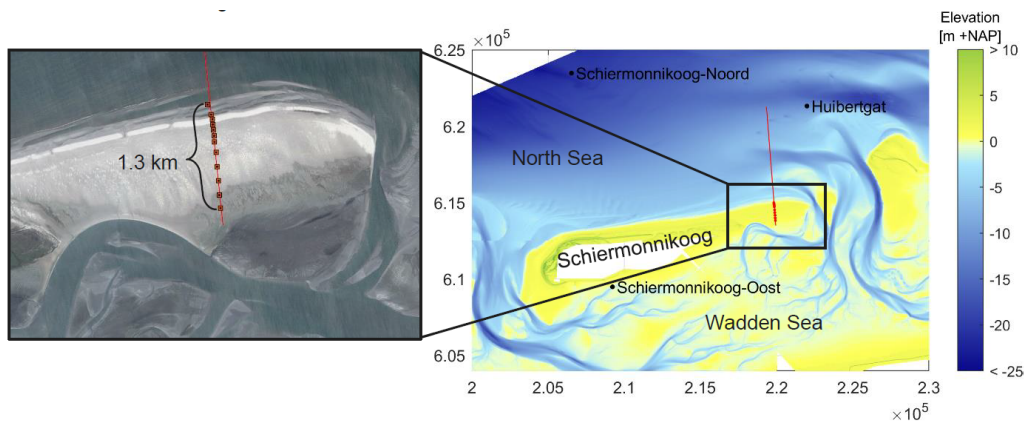


**Figure 4.1:** Overview of the Schiermonnikoog study area. Right: elevation at and surrounding Schiermonnikoog (mosaic of the ‘Vaklodingen’ of 2012-2015) and the location of the (offshore) hydraulic stations of RWS (black dots) and the transect (red line) with measurement equipment locations (red dots). Left: aerial photograph of the tail of Schiermonnikoog at 04-20-2014 (Google Earth). The coordinates are in meter (RD-new projection).

The conditions at the case site are mesotidal, mixed-energy and tide-dominated. Generally, the offshore high water levels are about 0.7 m +NAP during neap tide and 1.2 m +NAP during spring tide, while the highest storm surge level in the last 25 years reached 3.5 m +NAP (Wesselman *et al.*, 2018). The mean offshore significant wave height ranges from 0.5 - 1 m in summer to 1 - 2 m in winter, and can increase to 8 - 11 m during (northwestern) storm events. The highest recorded storm setup at this location is approximately 3.5-4 m (Engelstad *et al.*, 2017).

During the observation period, the island tail was flooded 11 times during high water due to storm setup. The highest water levels and wave heights were observed during the storm at 10 and 11-01-2015, with local wind speeds of about 19 m/s from the west and waves from the northwest. This storm is used for the XBeach simulation with BOI-settings for the hydrodynamic validation. The offshore conditions are based on RWS data shared by the UU: offshore water level data at the North Sea (‘Huibertgat’ station) and in the Wadden Sea (‘Schiermonnikoog-Oost’ station), and wave height, period and directional spreading at the North Sea (‘Schiermonnikoog-Noord’ wave buoy) with a 10-min data interval.

The storm peak is defined as the moment with highest water levels (WL = 2.7 m +NAP at the North Sea at Huibertgat and 2.9 m +NAP in the Wadden Sea at Schiermonnikoog-Oost) and coincides with high tide. At this moment, the  $H_s$  was about 6.0 m and  $T_s$  12 s. The highest offshore significant wave height ( $H_s$ ) at the station Schiermonnikoog-Noord was 7.1 m, and occurred during the low tide (about -0.3 m NAP) in advance of the storm peak. The corresponding significant wave period ( $T_s$  or  $T_{1/3}$ ) was 13 s. The wave heights remained higher than 5 m for a full day. During the storm, the waves were more focused: the directional wave spreading decreased from more than 35° to about 23° during the storm peak and about 29° afterwards. Based on the water level, the return period of this storm is about 10 years.

During the field campaign, measurements along the transect from the North Sea to the Wadden Sea (red dots in Figure 4.1) were performed using among others ten stand-alone pressure transducers (PT’s) from 04-11-2014 to 31-01-2015. The PT’s recorded the water level continuously at 10 Hz with an accuracy of 1 mbar (approximately 1 cm). Short and infragravity wave heights were determined for 15 min blocks by multiplying the standard deviation of the second-order detrended sea surface elevation with four, using a highpass filter (0.05-1 Hz) for

short waves and a lowpass filter (0.005-0.05 Hz) for infragravity waves. More information on the data can be found in [Wesselman et al. \(2018\)](#) and [Engelstad et al. \(2017\)](#). The processed data was made available by the UU in order to compare this with the XBeach model output.

## Results

Figure 4.2 shows the spatial patterns in the water depth and wave heights ( $H_{m0}$ ) along the cross-section during the storm peak. Figure 4.3 shows an example timeseries of the water depth and wave heights during the three tidal cycles just before and during the storm for the first measurement location at the beach (P1). The dots represent the measured values and the blue line the modelled values. Figure 4.4 shows the measured versus the modelled water depth and wave height of the short and infragravity waves for the entire model period and all locations. A quantitative comparison between the model results and the measurements is presented in Table 4.2 by means of goodness-of-fit indicators.

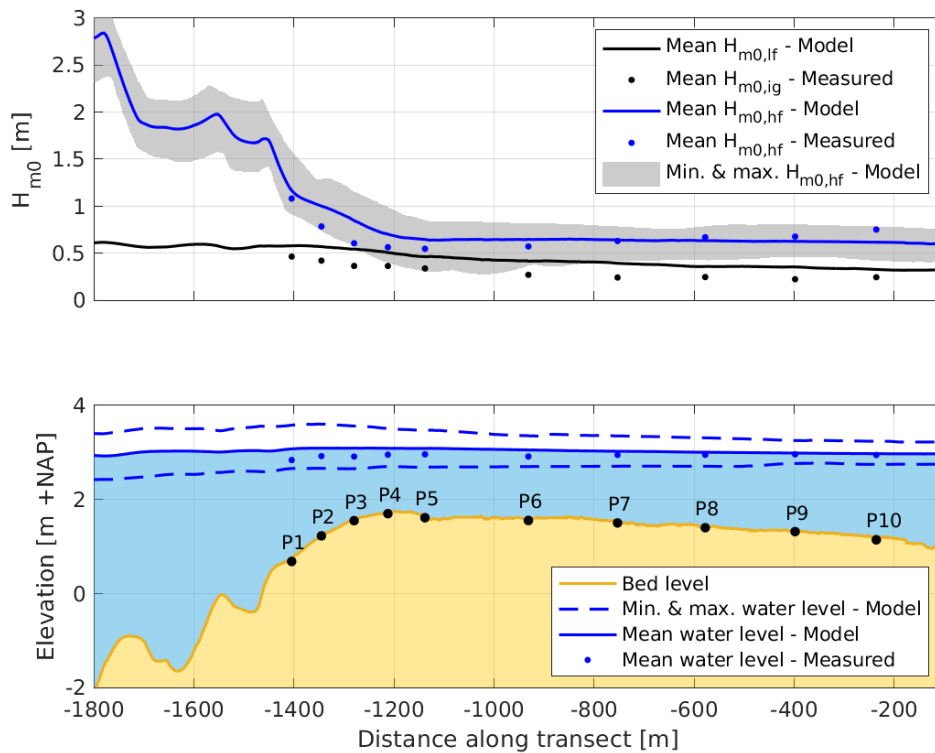


**Figure 4.2:** Cross-section with the modelled and measured water level and spectral significant wave height ( $H_{m0}$ ) of high and low frequency waves during the storm peak (11-01-2015 13:00-13:30). The grey zone around the modelled  $H_{m0,hf}$  indicates the minimum and maximum  $H_{m0,hf}$ . Note the difference between the modelled low frequency  $H_{m0}$  (no frequency domain filter) (black line) and the measured infragravity  $H_{m0}$  (0.005 and 0.05 Hz) at the point locations (grey-green dots).

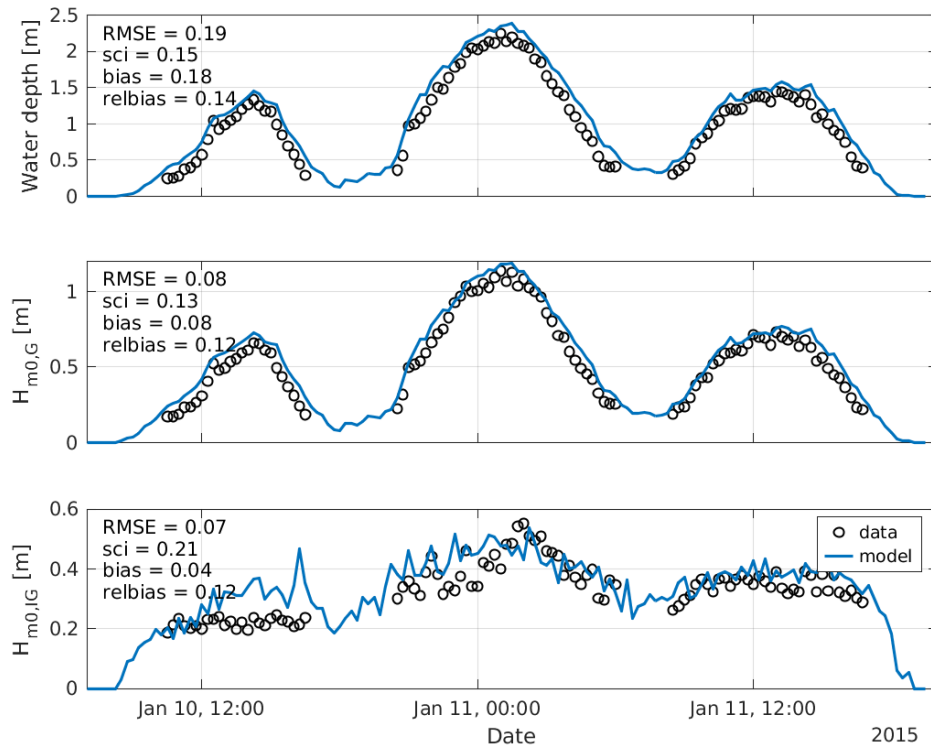


**Figure 4.3:** Timeseries of measured and modelled water depth, short and infragravity spectral significant wave height including goodness-of-fit indicators for measurement location P1.

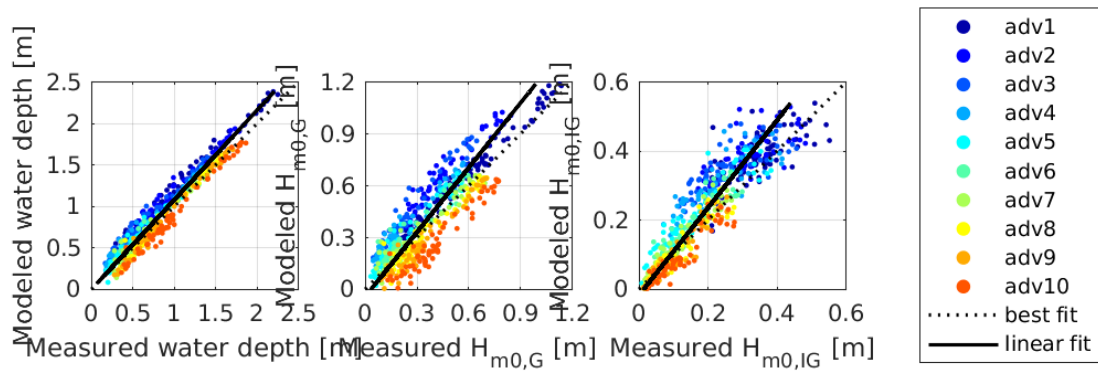


**Figure 4.4:** Scatter plot of the measured versus modelled water depth, spectral significant wave height ( $H_{m,0}$ ) of short waves (G) and infragravity waves (IG) for all measurement locations at Schiermonnikoog. The dashed line indicates a perfect fit, the continuous line represents a linear fit through the point cloud

**Table 4.2:** Erosion volume and dune retreat at 3m+NAP for the Egmond case

	$WL_{RMSE}$	$WL_{sci}$	$WL_{bias}$	$WL_{relbias}$	$HF_{RMSE}$	$HF_{sci}$	$HF_{bias}$	$HF_{relbias}$	$IG_{RMSE}$
P1	0.19	0.15	0.18	0.14	0.08	0.13	0.08	0.12	0.07
P2	0.19	0.18	0.18	0.17	0.21	0.43	0.20	0.41	0.09
P3	0.18	0.23	0.17	0.21	0.19	0.57	0.18	0.55	0.11
P4	0.12	0.17	0.10	0.15	0.13	0.42	0.12	0.40	0.09
P5	0.09	0.12	0.07	0.09	0.08	0.29	0.07	0.24	0.06
P6	0.07	0.08	0.04	0.05	0.08	0.24	0.07	0.19	0.05
P7	0.07	0.08	0.01	0.02	0.05	0.13	0.01	0.03	0.03
P8	0.06	0.07	-0.01	-0.01	0.06	0.15	-0.04	-0.10	0.03
P9	0.07	0.07	-0.03	-0.03	0.08	0.20	-0.07	-0.18	0.03
P10	0.12	0.11	-0.10	-0.09	0.15	0.33	-0.14	-0.31	0.03
Mean	0.13	0.14	0.07	0.07	0.12	0.28	0.05	0.11	0.07

## 4.2 Saint-Trojan

### Experiment description

The field dataset of Saint Trojan in France is used for hydrodynamic validation of the BOI-version of dune erosion model XBeach, in particular regarding the infragravity-wave behavior. The field campaign took place in February 2017 on the gently sloping Saint-Trojan Beach during an energetic storm. Bertin *et al.* (2020) compared observations to a 2DH XBeach model and presented detailed analysis on infragravity-wave behavior.

The field site is a dissipative sandy beach located in the central part of the French Atlantic coast (Figure 4.5), along the southwestern coast of Oléron Island. The continental shelf in front of the study area is about 150 km wide, with a very gently sloping shoreface, the 20 m isobath being some 10 km away from the shoreline. The beach slope typically ranges from about 0.0015 at the shoreface to 0.015 in the intertidal area, and the beach is mainly composed of fine and well-sorted sands ( $D_{50} = 0.18\text{--}0.22$  mm). The tidal regime in this region is semidiurnal and macrotidal, with a tidal range varying between about 1.5 m during neap tides and 5.5 m during spring tides. Tidal currents are weak at the studied beach, and the impact of tides on short waves remains mostly restricted to water level variations.

The storm Kurt generated very long swell waves that reached the coast between the 2nd and 3rd of February 2017. At the deep-water buoy of Biscay (Figure 4.5a), the mean wave period increased from 8.0 to 13.0 s, and  $H_s$  rapidly increased from 3.0 m to almost 10.0 m, which corresponds to a return period on the order of 1 year (Lerma *et al.*, 2015). The wave hindcast described in Guérin *et al.* (2018) suggests that the peak wave period  $T_p$  exceeded 20 s.

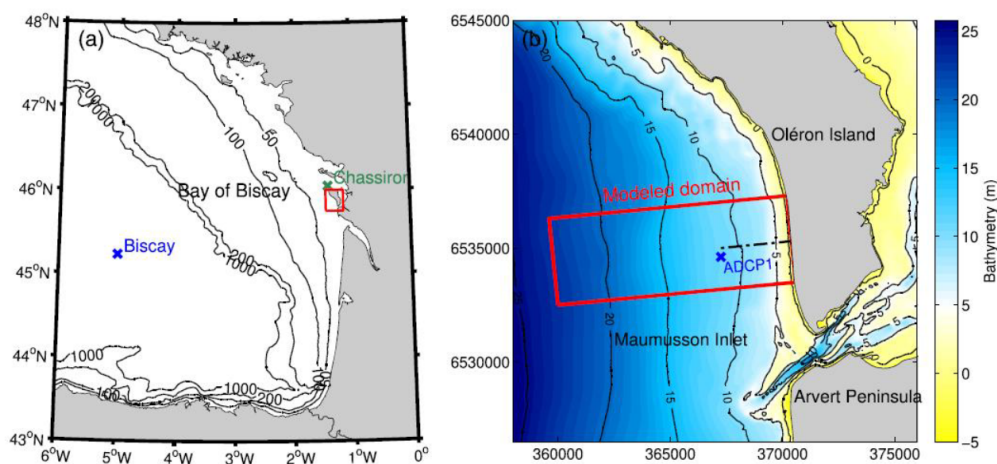


**Figure 4.5:** Location of the Saint Trojan study area in the Bay of Biscay, with the Biscay buoy (x) and Chassiron Meteorological station (x). (b) Detailed bathymetry of the study area (m relative to mean sea level), showing the location of the offshore ADCP1 (x) and the instrumented cross-shore profile (dashed line). The coordinates are in meter (Lambert-93 projection). Source: Bertin *et al.* (2020)

The measurement period of the field campaign encompassed four tidal cycles, from the 1st of February 2017 to the 3rd of February 2017, and is characterized by a tidal range of 3.5 to 4 m. An Acoustic Doppler Current Profiler (ADCP1) equipped with a pressure sensor was deployed about 3 km offshore (Figure 4.5b). In the intertidal zone, nine pressure transducers (PT) sampling at 4 Hz were deployed, as well as a second ADCP at the location of PT3. For each sensor, bottom pressure measurements were first corrected for sea level atmospheric pressure measured at the nearby meteorological station of Chassiron. The entire record was

then split into consecutive bursts of 30 min, and only the bursts in which the sensor was continuously submerged were considered. PT9 was never continuously submerged for more than 30 min and data from this PT was therefore discarded. Bottom pressure power density spectra  $E_p(f)$  were computed using Fast Fourier Transforms, with 10 Hanning windowed, 50% overlapping segments (20 degrees of freedom). These pressure spectra were subsequently converted into elevation spectra considering linear wave theory. The spectral significant wave height ( $H_{m,0}$ ) was computed as  $H_{m,0} = 4\sqrt{m_0}$  where the upper threshold frequency was set to 0.4 Hz. The threshold frequency between the high-frequency waves and the lower infragravity waves is time-varying and defined following Roelvink and Stive (1989) and Hamm and Peronnard (1997) as half the continuous peak frequency  $f_p$ . It is important to note that in processing of the observations the infragravity-wave frequency band was not delimited by a lower threshold, and therefore also covers the VLF (very low frequency) waves. For more information on the field campaign and data processing please refer to Bertin *et al.* (2020).

### Results

The observed and predicted water level, short- and long-wave heights during the peak of the storm are presented in Figure 4.6. The local timeseries of observed and modeled water level and wave-height variations of measurement locations PT3 and PT7 are depicted in Figure 4.7 and Figure 4.8 respectively. Goodness-of-fit indicators are presented in each subplot (per location), and additionally assembled for all locations in Table 4.3. An aggregated scatter plot of observed versus modelled water levels and wave heights is presented in Figure 4.9.

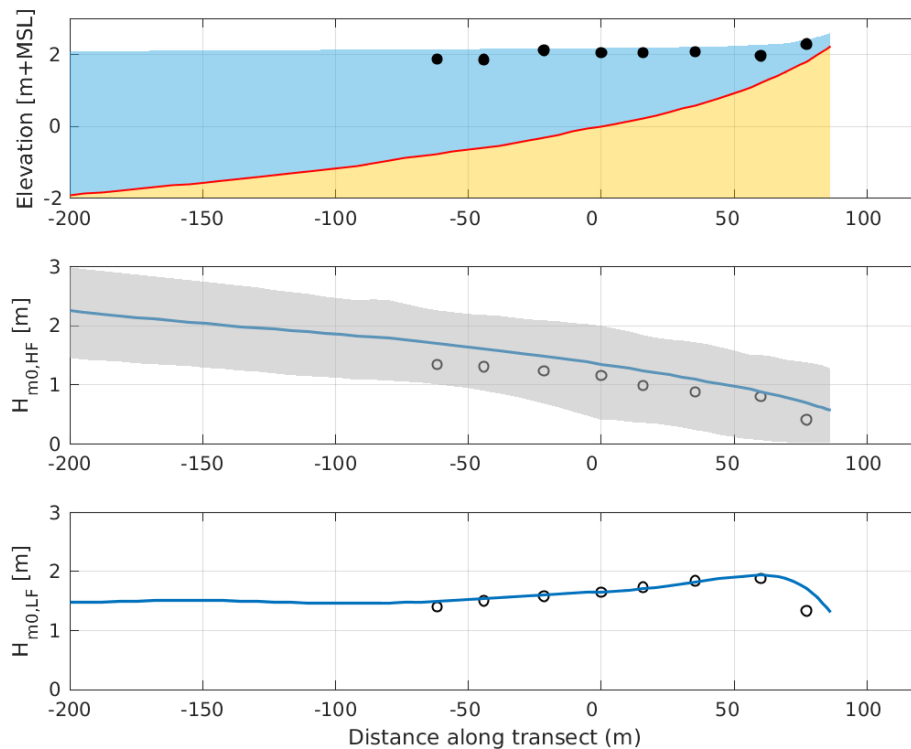


**Figure 4.6:** Cross-section at the transect location during storm peak (3rd of February 2017 at 8 AM) of the water level (upper panel), short-wave height (middle panel) and low-frequency (IG and VLF) wave height (middle panel). In blue the model results, and the observations are represented by circles. In grey the predicted minimum and maximum short-wave heights during the half hour around the peak of the storm.

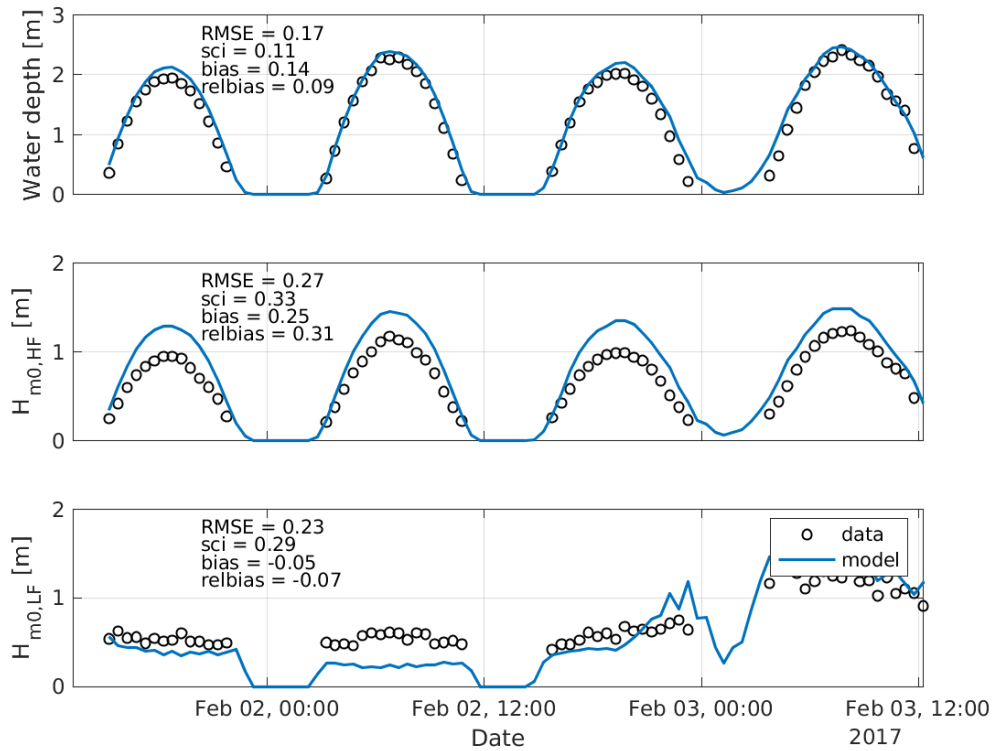


**Figure 4.7:** Modeled (blue line) against observed (circles) water depth (top), short-wave height (middle) and low-frequency wave height (bottom) at PT3.

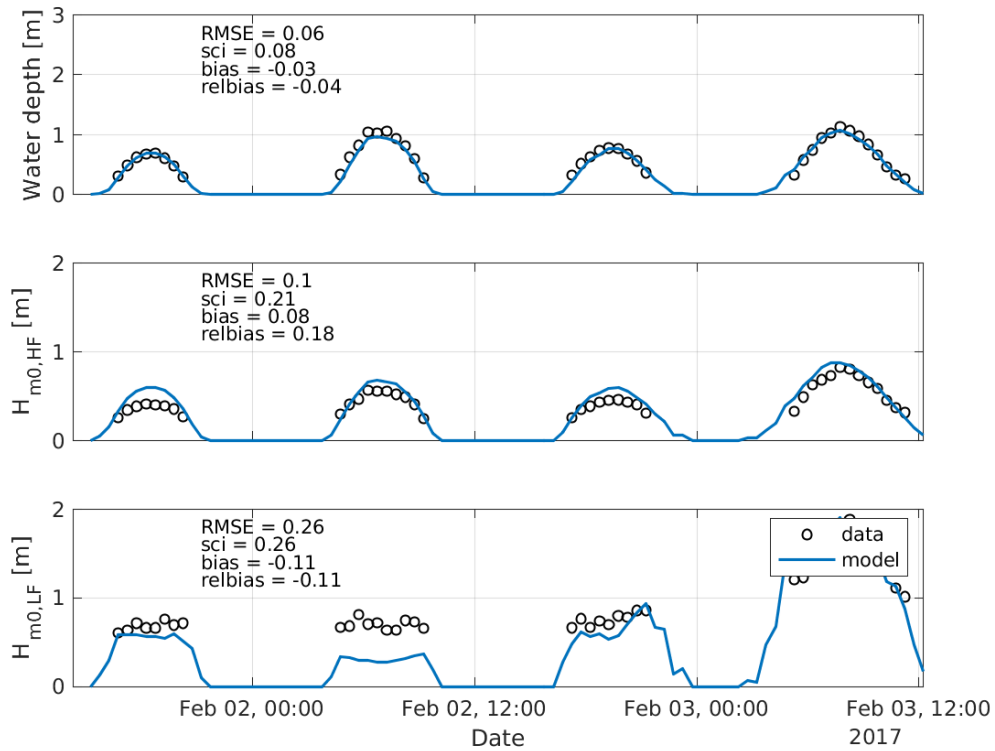


**Figure 4.8:** Modeled (blue line) against observed (circles) water depth (top), short-wave height (middle) and low-frequency wave height (bottom) at PT7.

**Table 4.3:** Erosion volume and dune retreat at 3m+NAP for the Egmond case

	$WL_{RMSE}$	$WL_{sci}$	$WL_{bias}$	$WL_{relbias}$	$HF_{RMSE}$	$HF_{sci}$	$HF_{bias}$	$HF_{relbias}$	$IG_{RMSE}$
ADCP1	NaN	NaN	NaN	NaN	NaN	NaN	NaN	NaN	NaN
PT1	0.12	0.06	0.07	0.04	0.21	0.21	0.19	0.19	0.23
PT2	0.25	0.14	0.23	0.13	0.34	0.41	0.32	0.39	0.22
PT3	0.17	0.11	0.14	0.09	0.27	0.33	0.25	0.31	0.23
PT4	0.10	0.07	0.04	0.03	0.23	0.32	0.21	0.29	0.22
PT5	0.21	0.17	0.18	0.14	0.28	0.45	0.27	0.43	0.23
PT6	0.21	0.22	0.20	0.20	0.19	0.32	0.18	0.30	0.27
PT7	0.06	0.08	-0.03	-0.04	0.10	0.21	0.08	0.18	0.26
PT8	0.15	0.33	-0.13	-0.30	0.18	0.73	0.16	0.64	0.27
PT9	0.14	0.42	-0.13	-0.39	0.13	0.72	0.12	0.68	0.43

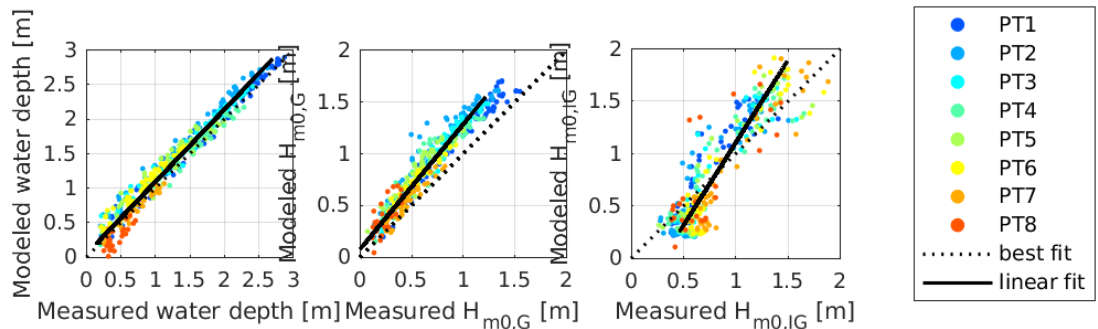


**Figure 4.9:** Observed versus predicted (left) water levels, (middle) short-wave height  $H_{m0,HF}$  and (right) low-frequency wave-height  $H_{m0,LF}$ .

### 4.3 Egmond

#### Experiment description

The field dataset collected at Egmond aan Zee in the Netherlands is used for both hydrodynamic and morphodynamic validation of the BOI-version of XBeach. Egmond aan Zee is located along the Dutch Holland coast [Figure 4.10](#), where tides are semi-diurnal, with a neap and spring tidal range of 1.4 and 1.8 m. Annual mean offshore wave height  $H_{m0} = 1.3$  m and wave period  $T_{m02} = 4.5$  s ([Wijnberg, 2002](#)). During northwesterly storms, significant wave heights can reach up to 7 m and storm surges can raise the water level by more than 1 m ([Ruessink \*et al.\*, 2019](#)). The coastal zone of the field site is characterized by 2-3 subtidal bars and an intertidal bar on a gently sloping intertidal (1:40) beach. The dune toe is located at 3 m + MSL and changes into a steep fore dune with a 1:2,5 slope. Around 14 to 17 m + MSL, the profile abruptly changes in slope and continues gently to the foredune crest at a height of 20 to 25 m + MSL. Alongshore variability in foredune shape and height is small. During multiple years without dune erosion, embryo dunes can develop at the toe of the foredune ([De Winter \*et al.\*, 2015](#)). The well-sorted quartz sand at the study site has a medium grain size of 250–300  $\mu\text{m}$ , with a tendency to decrease in the landward direction.

A 'quick reaction force' was set up to collect field data directly preceding, during and following storms. The dune erosion event on 8-9 January 2019 is selected for validation. The offshore water level at the study site reached 2 m + MSL and the maximum significant wave height ( $H_s$ )

was just below 5 m and maximum peak period ( $T_p$ ) was 15 s. The waves arrived obliquely incident, from west-southwest during the beginning of the storm and the direction changed to the northwest for the remainder of the storm.

During the winter of 2018/2019 7 pairs of pressure sensors were deployed spaced 250 - 750 m apart, along a 1.5 – 3 km stretch of beach south of Egmond aan Zee (Figure 4.10, right panel). The pairs consist of a seaward and a landward sensor (40m distance in cross-shore direction). The landward sensors were located above the high tide water level, each at different elevation levels (maximum 1 m difference). The surface elevations were collected at a frequency of 5 Hz and post-processed into consecutive bursts of 30 min, only the bursts in which the sensor was continuously submerged were considered, to calculate mean water levels and significant wave heights in the sea-swell (HS,SS) and infragravity (Hs,IG) frequency band.

Full bathymetric (sonar-equipped jetski) and topographic (mobile laser scanner) surveys provided pre and post the storm observations. Bathymetric data was collected on 23 November 2018 and 22 January 2019, while topographic survey was collected directly preceding (7 January 2019) and post (10 January 2019) the storm event. The bed level measurements show that the storm did not result in large erosion volumes, but erosion of the lower dune face did occur along the entire field site. Due to the northwesterly wave incidence during the largest storms, the outer crescentic bar mostly rotated clock-wise, leading to an alternation of onshore and offshore migration alongshore.

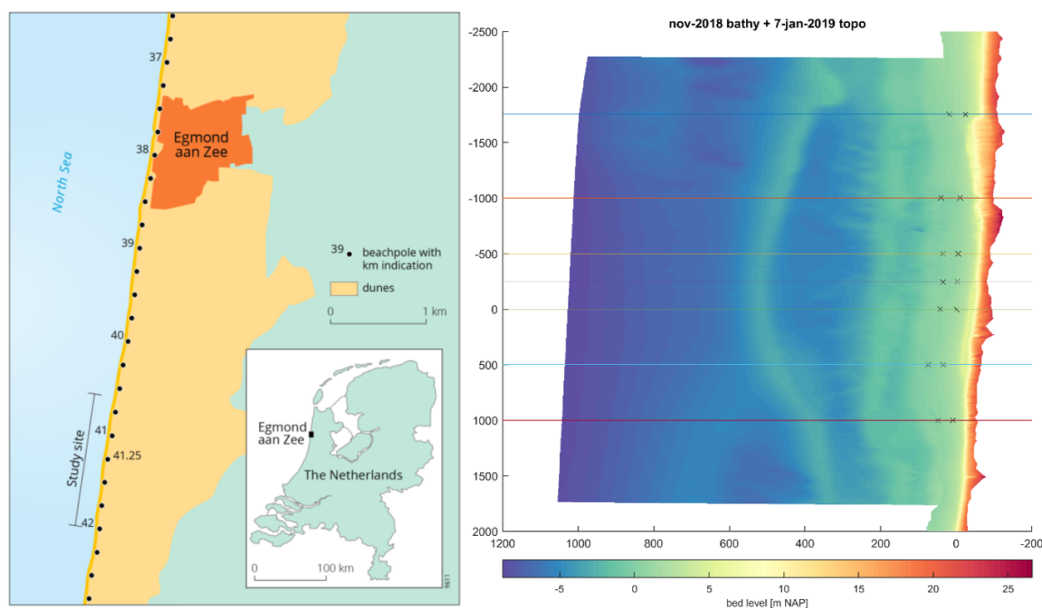


**Figure 4.10:** Location of study site (left panel). The beach poles form an alongshore reference line, with the km number referring to the distance to the zero point at the northern end of the Holland coast. The origin of the local coordinate system used (right panel) here is beach pole 41.25, with positive  $x$  and  $y$  in the seaward and southern direction, respectively. The crosses ('x') indicate the different pressure sensors.

## Results Hydrodynamics

The timeseries of observed and modeled water levels, high frequency and infragravity wave heights for all pressure sensors are presented in Figure 4.11, Figure 4.12 and Figure 4.13 respectively. Some of the sensors run dry during lower water elevations, especially the sensors closer to the beach (right column in the figures), explaining the gaps in the observations. The

modelled surface elevations are collected at a frequency of 10 Hz and post-processed into consecutive bursts of 30 min to calculate mean water levels and significant wave heights in the sea-swell (HS,SS) and infragravity (Hs,IG) frequency band. Only the bursts for which the sensor was continuously submerged are considered.

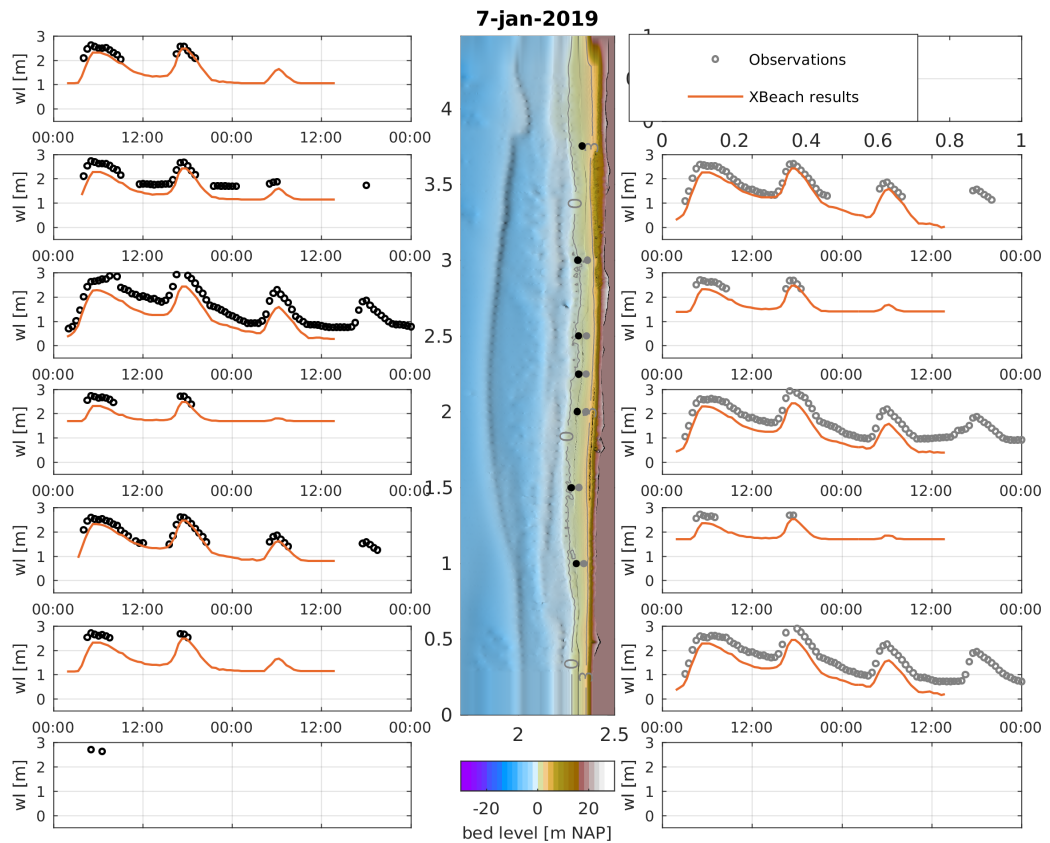


**Figure 4.11:** Observed water levels (black circles) against the modelled water levels (orange) for all pressure sensors. The panel in the middle shows the location of the pressure sensors, and the surrounding subpanels follow the order from North to South (top to bottom) and from sea (left) to the beach (right).

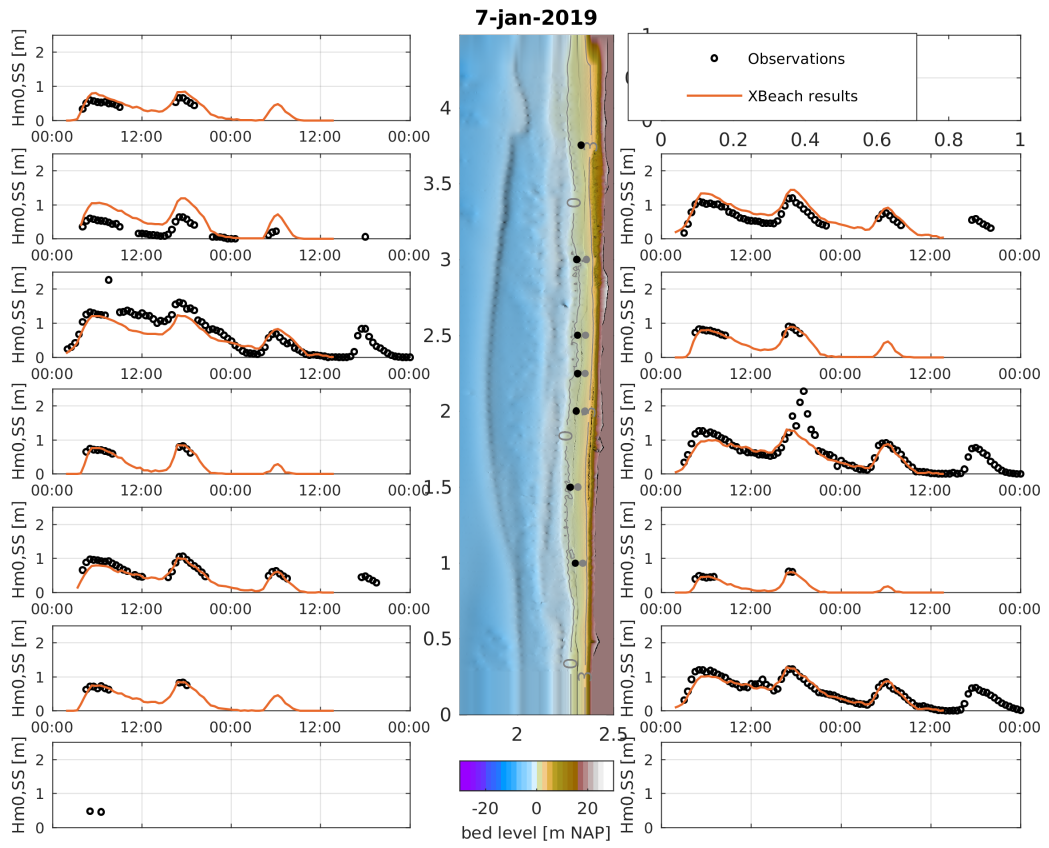


**Figure 4.12:** Observed short-wave heights (black circles) against the modelled short-wave heights (orange) for all pressure sensors. The panel in the middle shows the location of the pressure sensors, and the surrounding subpanels follow the order from North to South (top to bottom) and from sea (left) to the beach (right).

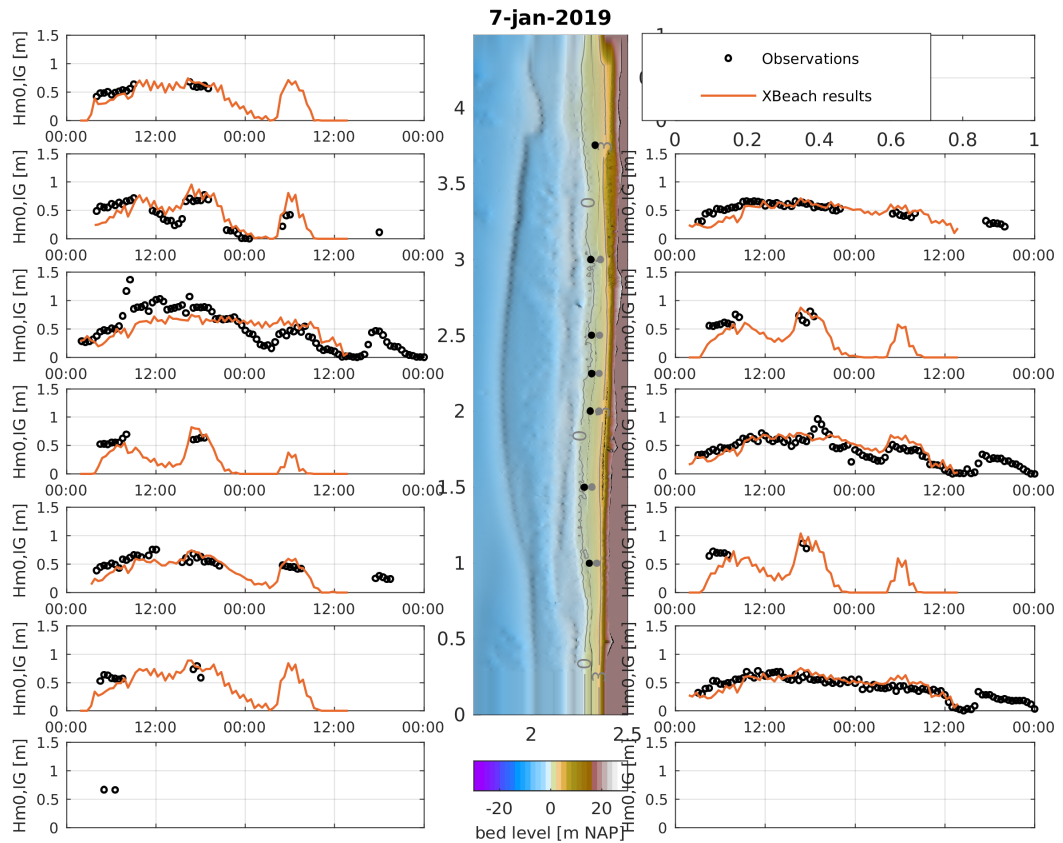


**Figure 4.13:** Observed infragravity wave heights (black circles) against the modelled infragravity wave heights (orange) for all pressure sensors. The panel in the middle shows the location of the pressure sensors, and the surrounding sub-panels follow the order from North to South (top to bottom) and from sea (left) to the beach (right).

### Results Morphodynamics

The morphological model results are validated using the topography measurements of the beach and dunes, collected on January 10th. The vertical reference level of maximum dune retreat is determined at NAP + 3 m, based on the observed pre- and post-storm topography. A quantitative comparison between observed and modelled erosion volumes and dune retreat is presented in Table 4.4. For transects T(y=0) and T(y=-1755), graphical comparisons are presented as well in Figure 4.14 and Figure 4.15.

**Table 4.4:** A quantitative comparison of modelled and observed erosion volumes [ $m^3/m$ ] and dune retreat [ $m$ ] at 3m + NAP for all 7 profiles.

	VeroXB	VeroMeas	retreatXB	retreatMeas
T -1001	12.90	1.38	5.38	1.70
T -1755	7.01	0.03	4.88	0.57
T -249	8.07	8.15	2.10	3.75
T -502	7.56	6.22	3.07	4.16
T 0	4.78	3.86	1.48	2.77
T 1001	8.45	5.88	2.60	4.01
T 499	7.08	3.99	3.11	2.63

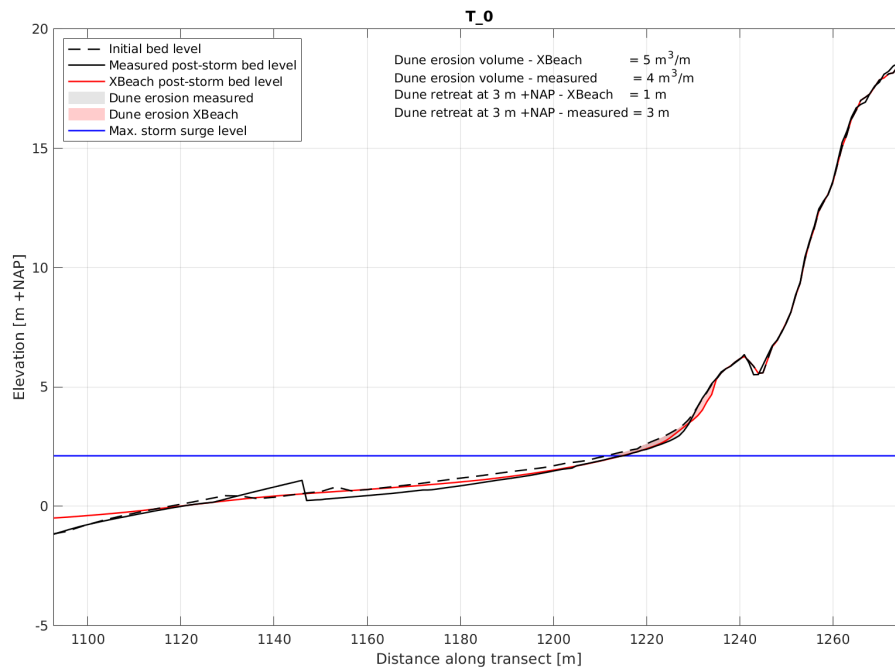


**Figure 4.14:** XBeach results for cross-shore transect 0 at Egmond aan Zee. Initial bed levels are depicted by the black dotted line, observed post-storm bed levels by the black solid line and XBeach model results are presented in red. The modelled dune erosion is shown by the red shaded area.

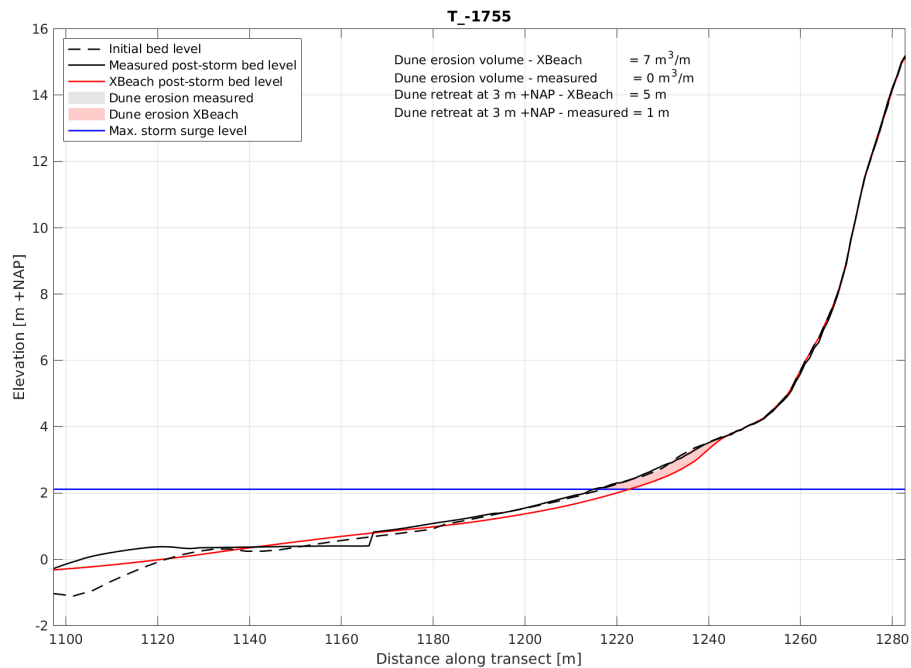


**Figure 4.15:** XBeach results for cross-shore transect -1755 at Egmond aan Zee. Initial bed levels are depicted by the black dotted line, observed post-storm bed levels by the black solid line and XBeach model results are presented in red. The modelled dune erosion is shown by the red shaded area.

#### 4.4 Vlaanderen

##### Experiment description

At 5-6 December 2013, the northwestern storm at the North Sea called ‘Storm Xaver’ or the ‘Sint Nicholas storm (Sinterklaasstorm)’ with relatively low wind speeds and a long fetch resulted in high surge levels in combination with moderately high waves (Trouw *et al.*, 2015). This resulted in beach and dune erosion along among others the Belgian coast on the order of 8 m<sup>3</sup>/m (Lanckriet *et al.*, 2015). The Coastal Division of the Flemish Government collected 122 cross-shore profiles of the beach and (first) dune row during a dGPS survey 2-4 days before this storm and based on an airborne lidar survey 4 days after this storm (Trouw *et al.*, 2015). A selection of these pre- and post-storm profiles (Figure 4.16) is being used for the validation of the morphodynamics in the BOI-version of the dune erosion model XBeach, focusing on dune erosion volumes and retreat distances.



**Figure 4.16:** Overview of the Belgian coastline with the location of the analyzed cross-shore profiles measured before and after the Sint Nicholas storm and the water level (WL) and wave measurement locations used for this case.

Based on the data of the Vlaamse Banken, the offshore storm surge levels reached up to 6.0 m +TAW1 (5 min average) during the Sint Nicholas storm at measurement pole 'A2' and 'Scheur Wielingen' in front of the Belgian coast (bottom depth respectively about -7 m LAT2 and -10 m LAT). This was the result of a combined high storm setup and spring tide. At the harbor of Ostend, storm surge levels reached 6.19 m TAW (Trouw *et al.*, 2015). The observed water levels were highest since 1953 and were estimated to have a return period of about 40 year in Belgium (IMDC, 2005). Besides, significant wave heights reached up to 3.8 m (20 min average) at the offshore wave buoy 'ZW-Akkaert' at -20 m LAT (Figure 6). The highest peak occurred during rising tide; at the peak water level, the wave height was already about 0.5 m lower. The peak wave period during the storm was about 8 s with a peak to 15 s at the end of the storm at the same location. This corresponds to a return period in the order of 1 year along the Belgian coast (IMDC, 2005). The waves approached approximately shore-normal from the northwest. After more than one day of high waves, the wave height gradually reduced, together with the storm surge.

The Belgian coast has gently sloping, dissipative beaches that are slightly steeper towards the east. They are mainly composed of fine to medium sand (Degraer *et al.*, 2003). The tidal regime along the Belgian coast is semidiurnal and macrotidal, with a of 3.7-3.9 m neap tidal range and 4.5-5 m spring tidal range which slightly decrease from west to east (Degraer *et al.*, 2003). To prevent the beaches from erosion by the strong tidal currents, a large part of the coastline is protected by groynes. Moreover, a concrete dike along the most of the coastline must protect the inland from flooding (Degraer *et al.*, 2003). In the areas with natural beach-dune transitions between Ostend and the Dutch-Belgian border, 15 profiles are selected for this case study (Figure 4.16). The beaches in the selected profiles have a slope of on average 1:45 to 1:65 from the dune toe to the relatively flat zone at -5 m TAW (westernmost profiles) to -7 m TAW (easternmost profiles). Just below mean sea level, 2-4 bars are present in all profiles except the easternmost profiles (117-121). The relatively flat plateau extends more than 10 km into the sea and contains some sand banks. Further offshore, seaward of the profiles, the bathymetry is characterized by large sand banks at intermediate to deep water.

## Results

The dune erosion volumes and retreat distances at 7m + TAW, based on the measured pre- and post-storm profiles and the XBeach simulations for all 15 profiles are tabulated in [Table 4.5](#). As an example, the pre- and post-storm profile for profile nr. 119 based on the measurements and on the XBeach simulation are presented in [Figure 4.17](#).

**Table 4.5:** Erosion volume and dune retreat at 3m+NAP for the Egmond case

	VeroXB	VeroMeas	retreatXB	retreatMeas
T <sub>1</sub> 17	11.35	13.53	5.55	5.88
T <sub>1</sub> 18	12.55	10.06	6.24	4.99
T <sub>1</sub> 19	7.66	8.09	3.90	4.12
T <sub>1</sub> 20	11.43	18.54	4.46	5.56
T <sub>1</sub> 21	4.26	8.47	2.50	3.46
T <sub>6</sub> 0	8.85	12.59	5.31	8.36
T <sub>6</sub> 1	6.54	7.21	3.89	4.85
T <sub>6</sub> 2	7.12	10.00	3.12	3.92
T <sub>6</sub> 3	7.88	10.27	3.94	4.42
T <sub>6</sub> 4	4.57	7.91	2.27	4.43
T <sub>6</sub> 9	9.54	15.22	4.02	5.35
T <sub>7</sub> 1	4.00	6.21	1.65	3.26
T <sub>7</sub> 9	4.58	10.06	2.29	2.89
T <sub>8</sub> 0	4.57	7.13	0.01	1.25
T <sub>8</sub> 3	3.15	3.88	1.95	1.63

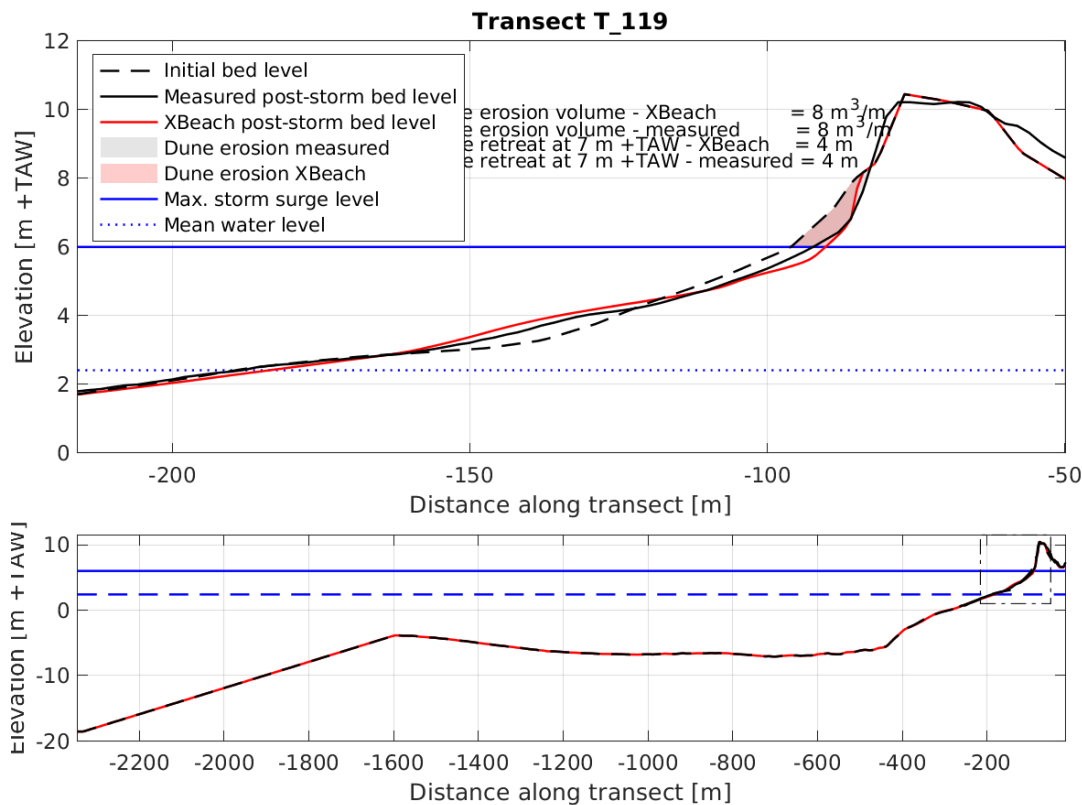


**Figure 4.17:** Cross-section profile nr. 119 before and after the Sint Nicholas storm based on the measurements and XBeach, including dune erosion volumes and retreat distances. Bottom: entire XBeach profile, top: zoom of beach and dune profile.

## 4.5 Vedersøe

### Experiment description

Vedersøe is located at the Danish North Sea coast. Coastal measurements along multiple transects were obtained before and after a severe storm in January 2005, and reported to the Danish Coastal Authority. The observed dune retreats and erosion volumes show a high variability in alongshore direction. A study by the Danish Coastal Authority (DCA), as a part of the larger EU-InterReg project Building with Nature, considered two 1D transects close to each other (< 500 m) for which the observed dune retreat ranges from 4 to 14 meter, see [Figure 4.18 \(Kystdirektoratet, 2021\)](#). Though the profiles show large similarity, the different erosive behavior is likely due to the presence of a berm (above storm surge level) which reduces the erosion for one of the profiles. The two transects at Vedersøe are used to validate the BOI-XBeach model and settings for morphological changes due to storm impact. Compared to the Dutch coast, the Danish profiles have a similar slope in the lower shoreface, but a steeper surfzone.

According to [Saye and Pye \(2006\)](#) the Danish Southwest coast has a strong alongshore variation in grain size, with grain sizes up to 0.4 mm. However, [Clemmensen et al. \(2006\)](#) show that dunes in the southwest of Denmark are mainly formed by aeolian transport of fine-grained sand with a  $D_{50}$  of around 0.2 mm. They also note that the ‘inland’ dunes are more coarse-grained than the coastal dunes. A  $D_{50}$  of 0.25 mm is used within the BOI project.

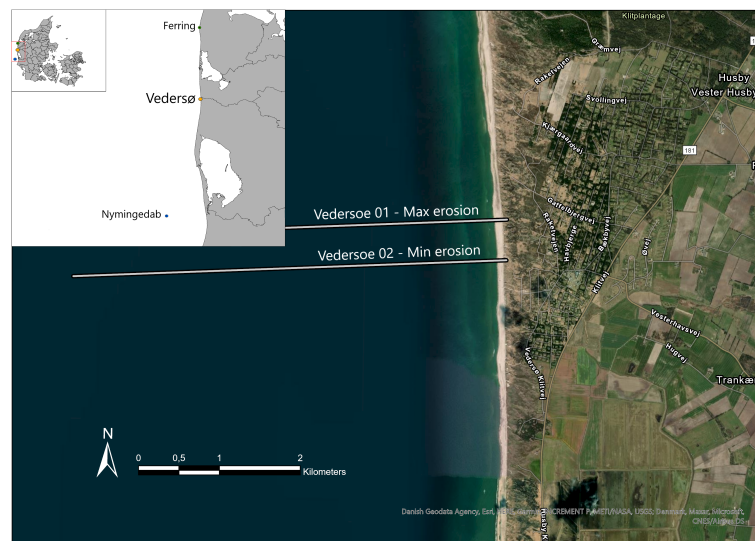


**Figure 4.18:** Location of the study area near Vedersø (Denmark). The two different transects considered in this study are located close to each other, but different morphological behaviour is observed. Source: *Kystdirektoratet (2021)*

The wave climate during the storm in 2005 is measured by wave buoys located outside Nymindegab ( 50 km southward of Vedersø at 17.5 m depth). At the deep-water wave buoy, the peak wave period  $T_p$  increased from 9.0 to 13.3 s, and  $H_s$  rapidly increased from 2.9 to 6.6 m. Water levels during the storm are obtained at a tidal gauge on one of the headlands of Ferring ( 30 km to the North from Vedersø), and reached up to 3 m +MSL during the 2005 storm.

### Results

Although the two transects are located within 500 m of each other and were exposed to the same hydrodynamic forcing, their morphological response differs significantly. The results for Vedersø 01 are presented in [Figure 4.19](#) and the results for Vedersø 02 are presented in [Figure 4.20](#). In addition, the dune erosion volumes and retreat distances at 5m + MSL, based on the measured pre- and post-storm profiles and the XBeach simulations are tabulated for both profiles in [Table 4.6](#).

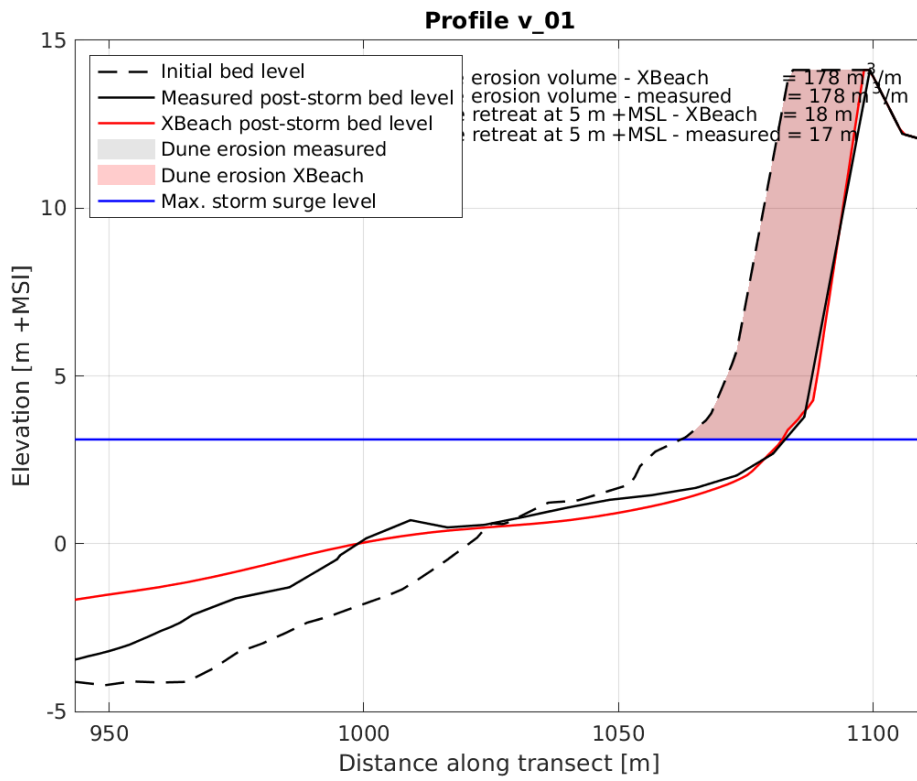


**Figure 4.19:** XBeach results for cross-shore transect Vedersoe 01 Initial bed levels are depicted by the black dashed line, observed post-storm bed levels by the black solid line and XBeach model results are presented in red. The modelled dune erosion is shown by the red shaded area, whereas the observed dune erosion is depicted with the grey shaded area.

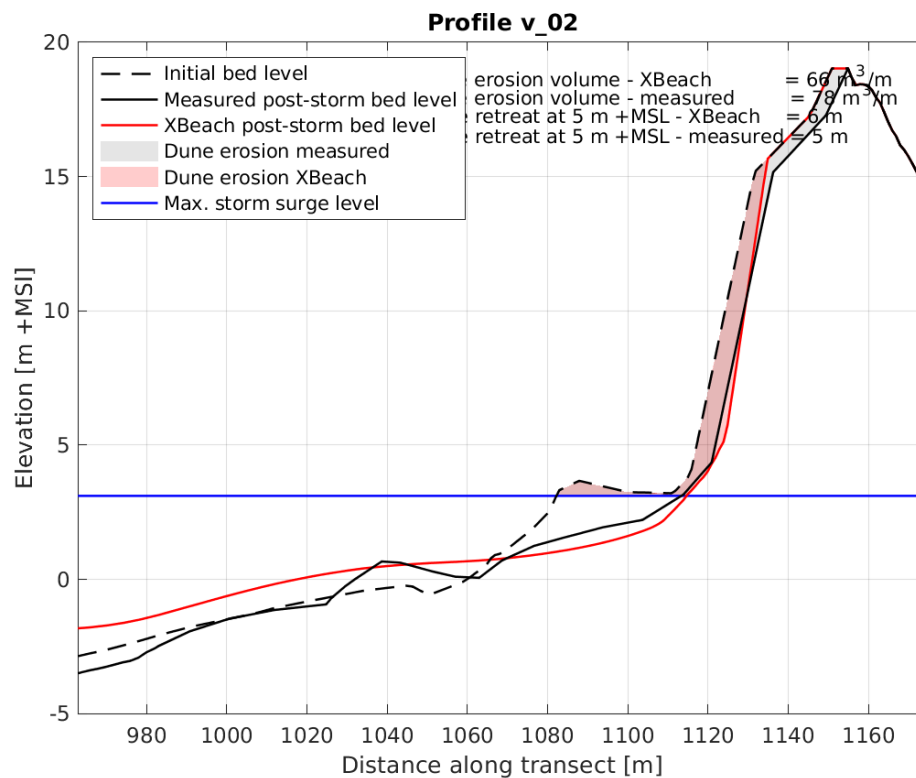


**Figure 4.20:** XBeach results for cross-shore transect Vedersoe 02. Initial bed levels are depicted by the black dashed line, observed post-storm bed levels by the black solid line and XBeach model results are presented in red. The modelled dune erosion is shown by the red shaded area, whereas the observed dune erosion is depicted with the grey shaded area.

**Table 4.6:** Erosion volume and dune retreat at 3m+NAP for the Egmond case

	VeroXB	VeroMeas	retreatXB	retreatMeas
$v_01$	177.79	178.12	17.72	16.69
$v_02$	66.01	78.05	6.26	4.67

## 4.6 Fire-Island

### Experiment description

Hurricane Sandy made landfall as a Category 1 post-tropical storm on the New Jersey Coast on October 29, 2012. The storm severely impacted the Fire Island barrier island off the Long Island, New York, coast, where profile volume loss along the entire barrier island varied from 25% to 75% (Hapke *et al.*, 2013). Off the coast of Bellport (NY, Figure 4.21), an uninhabited section of the barrier island Wilderness Area breached during Sandy. Dune crests were lowered, and large wash-over fans developed in the area around the breach. Prior to the storm, the area was covered by dune grass, wetland- and woody vegetation. The sea floor offshore of Fire Island shows shoreface-connected sand ridges in the western part and smaller, sorted bedforms along the eastern part of the island that includes the Wilderness area (Schwab *et al.*, 2013). The cross-shore profiles are characterized by a steeply sloped beach (1 in 20 slope), a pronounced alongshore-uniform breaker bar, and a foreshore slope that gradually becomes less steep (1 in 85 slope) up to the wide continental shelf at a depth of 25 m.

During Sandy, maximum water levels (surge and tide) ranged 1.8 m (Montauk) to 3.5 m NAVD881 (The Battery) along the barrier island and offshore significant wave heights reached 10 m with periods up to 14 s. LiDAR surveys of the island were flown pre-Sandy in May 2012 (Fredericks, 2016) and post-Sandy on November 5, 2012. A median grain size of 400 m was reported at Wilderness (Buster *et al.*, 2018) with a grading of D90/D50 = 1.5.

Comparison of pre- and post-storm observations of bed elevations (Figure 1) shows that the initial dune crest heights were ranging from only 2 to 6 m, much lower than generally found in the Netherlands. The observed cumulative erosion-sedimentation patterns show that the dune front eroded several meters along the entire stretch of coast. A breach developed between kilometer marks (KM) 1 and 1.2 where originally a high dune was located. Large overwash deposits were observed east of the breach (KM 1.2–2). West of the breach the dune crests were initially higher, and impact remained in the collision regime with little overwash deposits.

Van der Lugt *et al.* (2019) setup a 2DH morphodynamic XBeach model with hydrodynamic forcing extracted from a regional coupled D-Flow FM/SWAN model, and showed that the model predicted erosion volumes, dune-crest lowering and breach-formation well. The model bathymetry and boundary conditions of this 2DH model is used to set-up 1D transects and validate the BOI-XBeach settings for morphological storm impact.

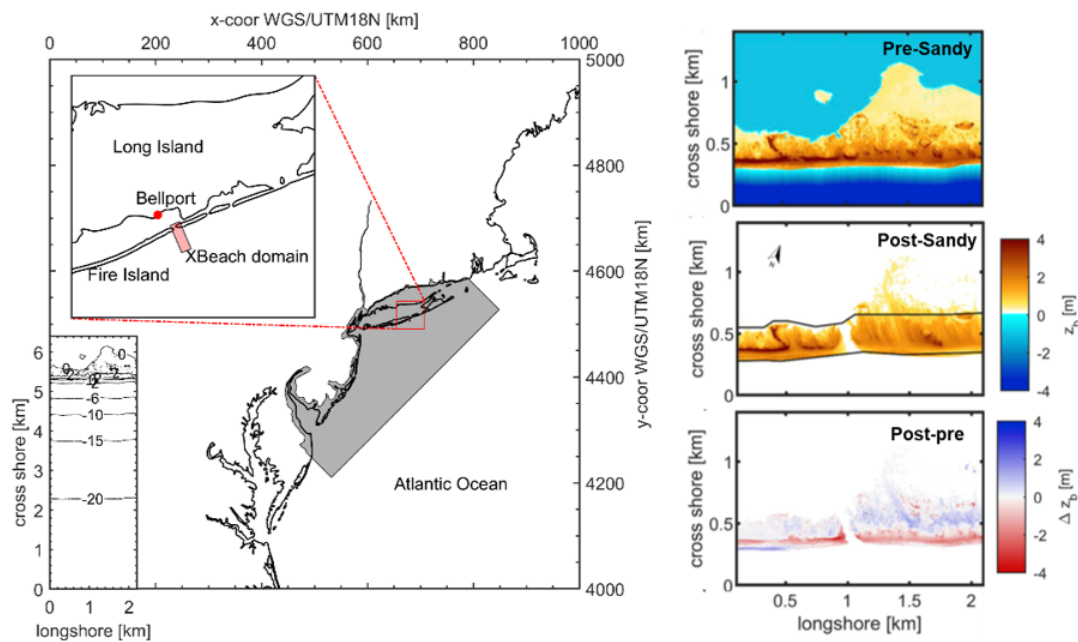


**Figure 4.21:** Left: Model domain extent of the nested regional D-Flow FM/SWAN model (in grey) and the XBeach model (in red): Wilderness breach. Right: observed pre- (top) and post- (middle) bathymetry and sedimentation/erosion (bottom).

## Results

The XBeach model results are validated using the post-Sandy LiDAR data obtained on November 5, 2012. The dune erosion volumes and retreat distances at 3 m +NAVD88, based on the measured pre- and post-storm profiles and the XBeach simulations for all 6 profiles are tabulated in Table 4.7. Furthermore, the pre- and post-storm profile for profiles 5, 305 and 405 based on the measurements and on the XBeach simulation are presented in Figure 4.22, Figure 4.23 and Figure 4.24 respectively.

**Table 4.7:** Erosion volume and dune retreat at 3m+NAP for the Egmond case

	VeroXB	VeroMeas	retreatXB	retreatMeas
005	51.29	51.29	NaN	NaN
105	54.20	44.73	NaN	NaN
205	75.33	75.29	NaN	NaN
305	71.00	68.17	NaN	28.61
365	27.78	24.86	5.27	5.85
405	32.93	55.81	13.52	23.08

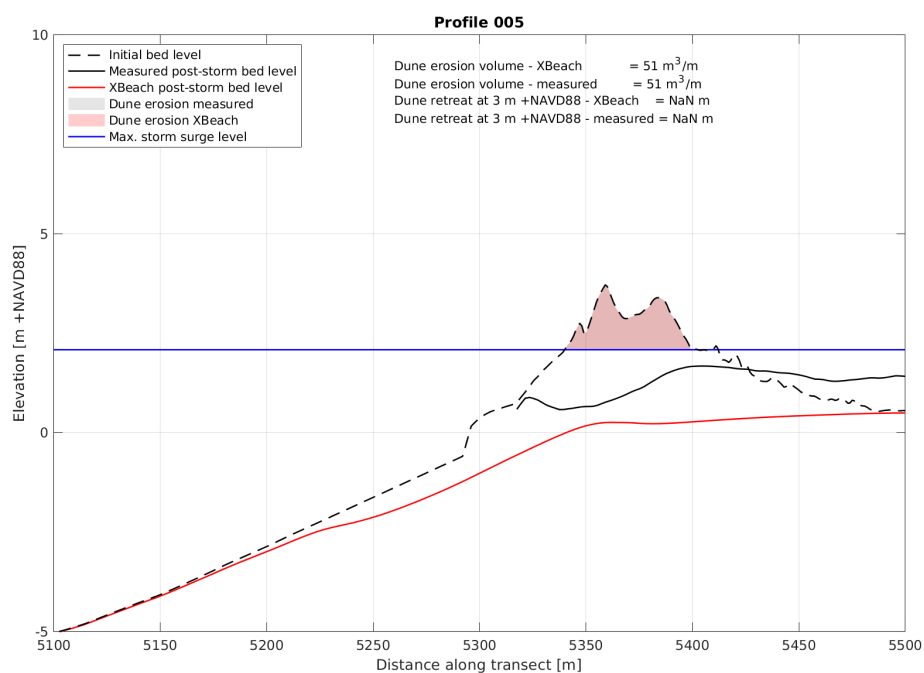


**Figure 4.22:** XBeach results for cross-shore transect 005 at Fire Island. Initial bed levels are depicted by the black dotted line, observed post-storm bed levels by the black solid line and XBeach model results are presented in red. The modelled dune erosion is shown by the red shaded area.

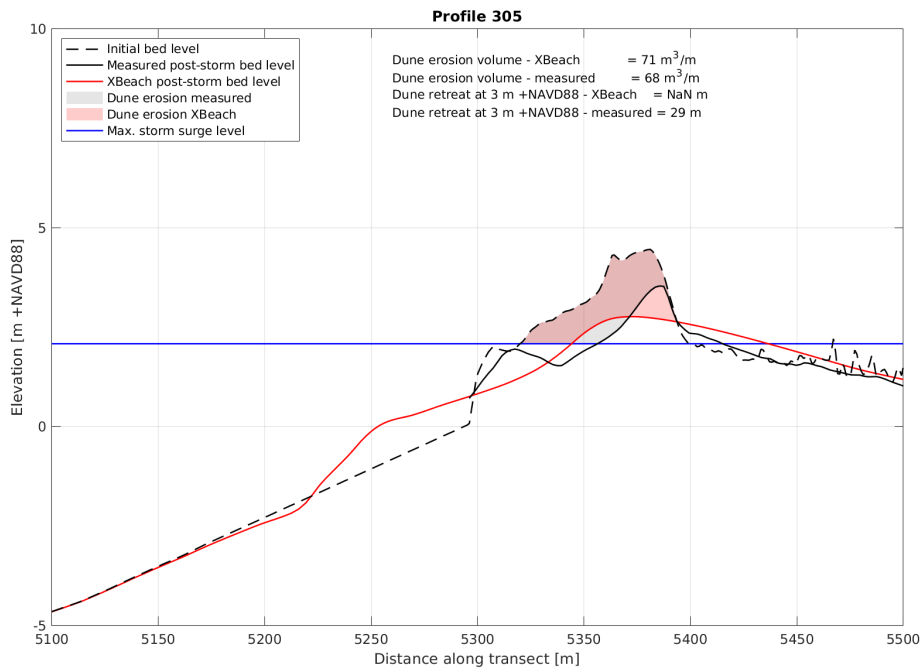


**Figure 4.23:** XBeach results for cross-shore transect 305 at Fire Island. Initial bed levels are depicted by the black dotted line, observed post-storm bed levels by the black solid line and XBeach model results are presented in red. The modelled dune erosion is shown by the red shaded area.

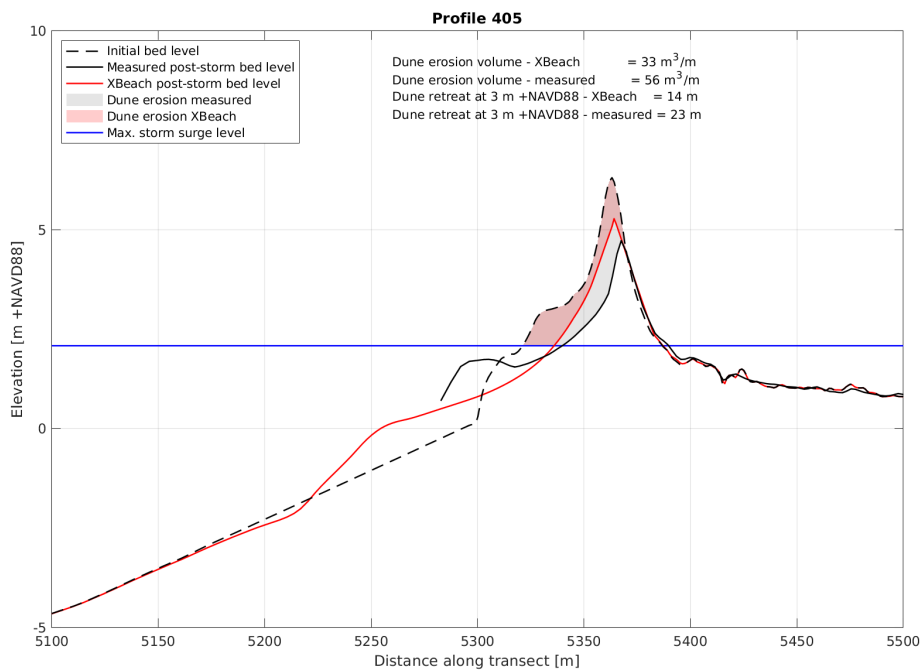


**Figure 4.24:** XBeach results for cross-shore transect 405 at Fire Island. Initial bed levels are depicted by the black dotted line, observed post-storm bed levels by the black solid line and XBeach model results are presented in red. The modelled dune erosion is shown by the red shaded area.

## 4.7 Langeoog

### Experiment description

The island of Langeoog is one of seven inhabited barrier islands situated along the East Frisian German North Sea coast (Figure 4.25). The shoreface of Langeoog can be characterized by migrating sand shoals through the ebb-tidal delta and a breaker bar system that migrates in eastern direction, comparable to the morphological configuration for the Dutch Wadden Sea Islands. The mildly sloping and shallow shoreface extends to deeper water with a slope of 1:300. On Langeoog approximately 3.9 million m<sup>3</sup> of sand have been nourished since 1971 to protect the inhabited areas landwards of the dunes. This coastal area can be classified as mesotidal with semidiurnal tides with a mean tidal range of about 2.7 m at the Langeoog gauge. The mean grain size (D50) for Langeoog northern beaches is in the order of 0.25 mm (Hillmann, 2021). The upper beach and dune foot area has a mean grain size of 0.20 mm, whereas in the surf zone it is in the order of 0.30 mm.

Storm Xaver passed Langeoog from 5 to 7 December 2013, in the Netherlands referred to as 'Sinterklaasstorm', and led to an extreme maximum storm surge level of NHN1 +3.95 m at Langeoog gauge station. Offshore of Langeoog a maximum wave height of  $H_s = 7$  m and period  $T_p = 15$  s was observed. The storm caused significant dune erosion at the Northern side of the island. Two months prior to the storm, October 2013, a beach nourishment was deployed on the North-Western part of the island (Figure 4.25). A large part of the beach nourishment was eroded due to the storm, and the observed dune erosion landwards of the nourishment was considerably less compared to the adjacent dunes.

Topographic measurements of the beach/dunes were collected after the beach nourishment placement, on October 18th, 2013, 2 months prior to Storm Xaver. Post-storm topography was collected on December 13th, 2013 for the area around the beach nourishment and April 30th, 2014 for the Eastern part of the island. Bathymetric data of the shoreface was collected in August 2013.

In the Interreg VB North Sea Region Building with Nature project a 2D XBeach model of Langeoog was set-up and validated for the 2013 storm (Hillmann and Frederiksen, 2021). The 2D model domain is 4km in longshore and 4.5km in cross-shore direction, and covers the area where the beach nourishment was located (Figure 4.25). The initial model bathymetry was constructed by combining the August 2013 shoreface measurements and October 18th, 2013 topographic measurements. From this 2D model bathymetry and accompanying forcing conditions, six transects were extracted to use for the morphological validation of the BOI-XBeach model and settings.

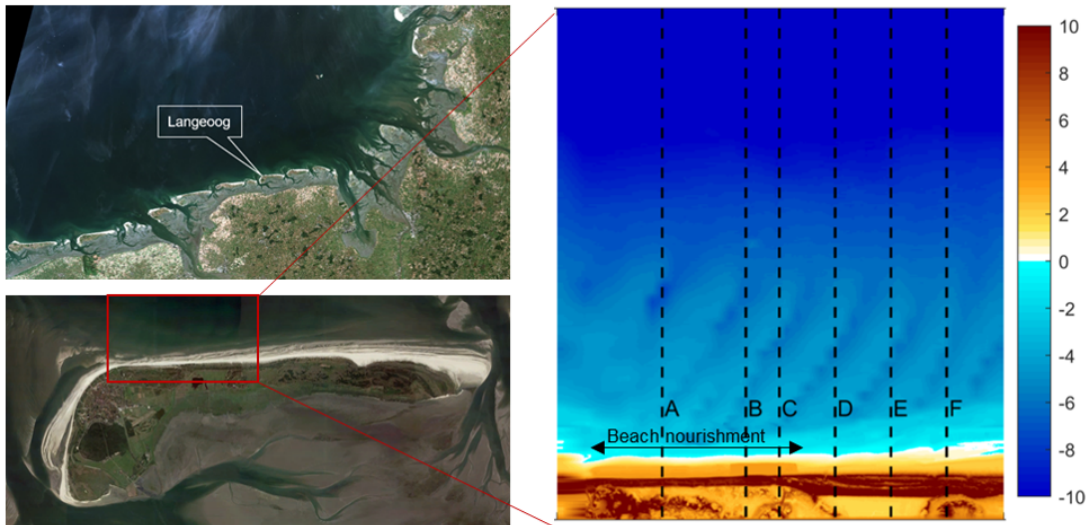


**Figure 4.25:** Location of the study site in Langeoog, Germany and location of the XBeach model. Model input bathymetry (right panel) with the location of the beach nourishment and the six transects A to F. Source: Hillmann and Frederiksen (2021)

## Results

The model results are validated using the topography measurements of the beach and dunes, collected on December 13th, 2013 for the area around the beach nourishment and April 30th, 2014 for the Eastern part of the island. The dune erosion volumes and retreat distances at 5 m +NHN, based on the measured pre- and post-storm profiles and the XBeach simulations for all 6 profiles are tabulated in Table 4.8. Furthermore, the pre- and post-storm profile for profiles A and D based on the measurements and on the XBeach simulation are presented in Figure 4.26 and Figure 4.27 respectively.

**Table 4.8:** Erosion volume and dune retreat at 3m+NAP for the Egmond case

	VeroXB	VeroMeas	retreatXB	retreatMeas
profile <sub>A</sub>	15.52	0.97	-2.83	0.52
profile <sub>B</sub>	14.47	12.76	-2.71	3.53
profile <sub>C</sub>	10.29	10.13	-1.77	4.01
profile <sub>D</sub>	31.07	17.97	4.76	6.49
profile <sub>E</sub>	28.46	13.85	5.72	7.03
profile <sub>F</sub>	26.25	10.81	7.02	4.52

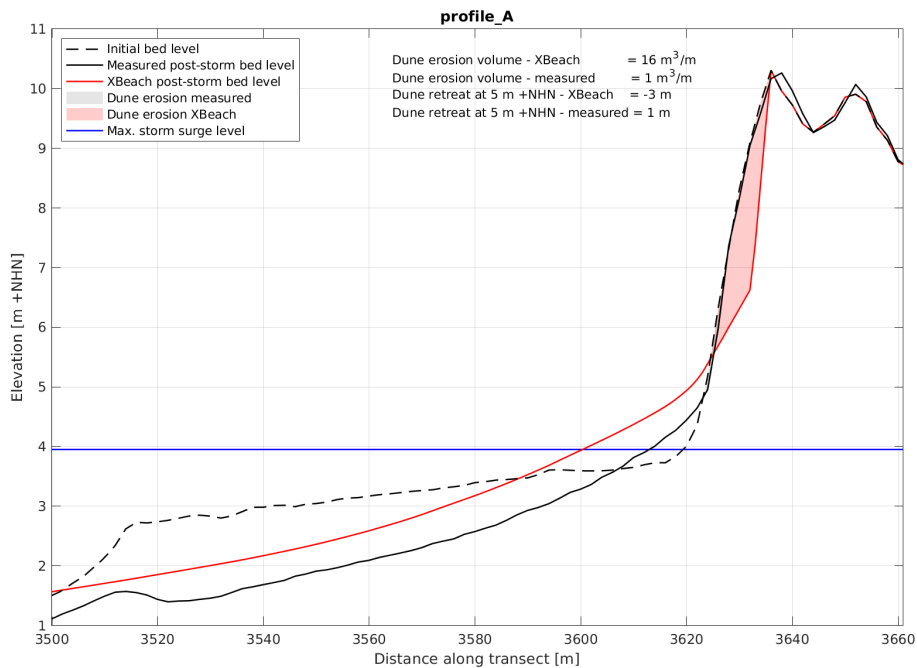


**Figure 4.26:** XBeach results for cross-shore transect A at Langeoog. Initial bed levels are depicted by the black dotted line, observed post-storm bed levels by the black solid line and XBeach model results are presented in red. The modelled dune erosion is shown by the red shaded area.

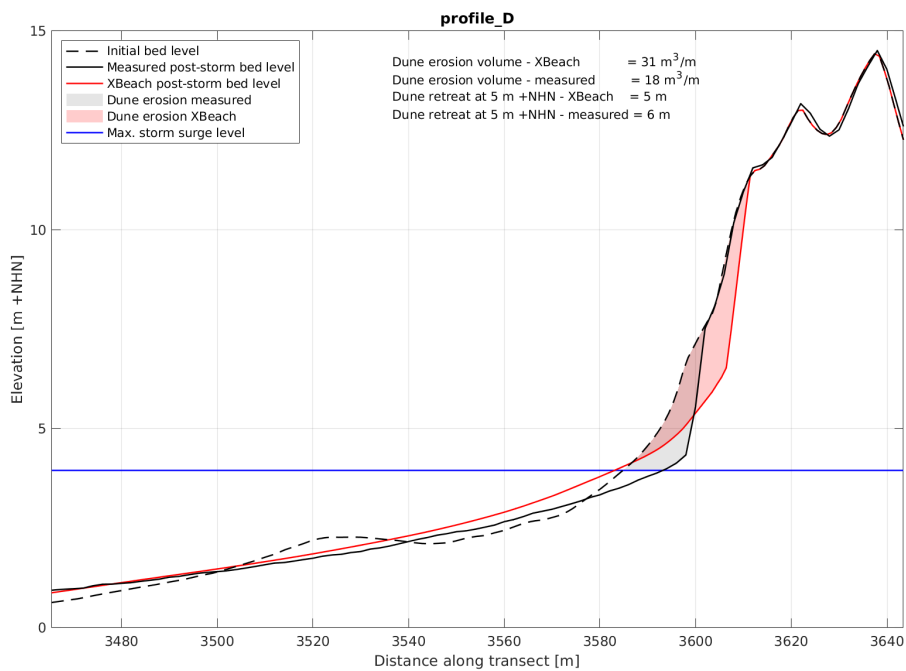


**Figure 4.27:** XBeach results for cross-shore transect D at Langeoog. Initial bed levels are depicted by the black dotted line, observed post-storm bed levels by the black solid line and XBeach model results are presented in red. The modelled dune erosion is shown by the red shaded area.

## 4.8 Holland 1976

### Experiment description

The storm that hit the Dutch coast in the night between the 2nd and 3rd of February 1976 is classified as a violent storm ('zeer zware storm'); 11 at the Beaufort scale. A storm event severity that is very rarely experienced in the Netherlands. While the storm surge and high waves impacted the entire Dutch coast, the Delta coast (Zeeland) was hit the hardest with a peak storm surge level of 4.1 m +NAP at Vlissingen: the highest water level since the 1953 storm surge (4.5 m +NAP). The Belgian coast was also impacted heavily, including major flooding in the province of Antwerp. This led to the initiation of the Sigmoplan, designed to better protect the Scheldt basin from flooding during storm surges.

For this validation case the impact of the 1976 storm surge on the northern part of the Dutch coast (the coastal section between Noordwijk and Den Helder) is compared to observations. For the hydraulic boundary conditions, the [Van der Werf \*et al.\* \(2011\)](#) study is used as a starting point. This validation case then focusses more on the morphodynamic comparison between simulated and observed dune erosion and dune retreat, which is available for a set of 30 profiles in the considered coastal section (between profile 568 in the north and profile 7100 in the south, as shown in [Figure 4.28](#)). Most profiles have a profile with high dunes, multiple bars up above -9 m NAP and slopes similar to the representative Holland coast profile.

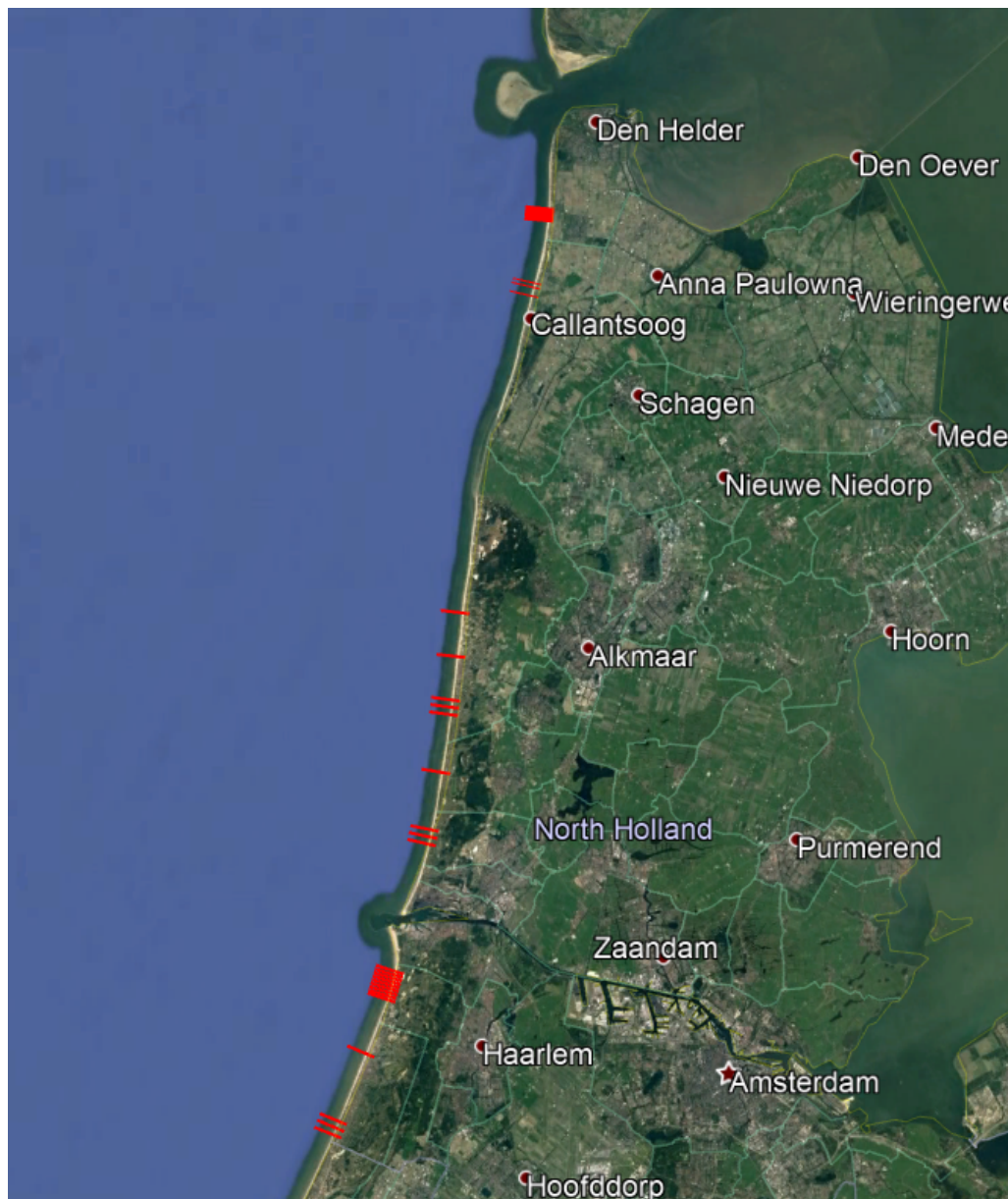


**Figure 4.28:** Indication of assessed coastal profiles in red, from 568 in the north to 7100 in the south.

The hydraulic boundary conditions are as follows:

- ◇ The peak surge level consisting of tide and storm surge is 2.99 m +NAP.
- ◇ The peak significant wave height  $H_s$  during the storm is 6.1 meters.
- ◇ The maximum wave peak period  $T_p$  is 10.8 seconds.

### Results

The dune erosion volumes and retreat distances at 4m + NAP, based on the measured pre- and post-storm profiles and the XBeach simulations for all 30 profiles are tabulated in [Table 4.9](#). To provide some more insight in the results, the pre- and post-storm profiles for profiles 648, 5000 and 7100 are presented in [Figure 4.29](#), [Figure 4.30](#) and [Figure 4.31](#).

**Table 4.9:** Erosion volume and dune retreat at 3m+NAP for the Egmond case

	VeroXB	VeroMeas	retreatXB	retreatMeas
Raai1085	31.08	3.87	4.98	2.33
Raai1115	37.94	9.77	5.64	4.17
Raai1175	39.30	13.03	8.43	6.93
Raai3400	0.00	19.35	0.00	8.98
Raai3700	12.57	7.07	2.14	2.15
Raai4000	51.19	13.61	7.74	5.82
Raai4050	17.39	21.04	6.44	9.69
Raai4100	38.10	13.16	5.09	5.70
Raai4500	34.94	5.93	5.18	2.92
Raai4900	37.31	9.68	4.90	4.69
Raai4950	17.68	19.28	5.29	8.18
Raai5000	44.60	5.15	5.02	2.58
Raai568	37.97	17.29	6.17	7.72
Raai588	40.65	9.65	7.37	4.98
Raai5900	35.14	17.48	5.82	6.04
Raai5925	40.93	11.20	4.25	5.35
Raai5950	41.05	16.53	4.89	6.87
Raai5975	49.70	16.95	5.19	6.34
Raai6000	49.05	15.98	4.52	5.61
Raai6025	49.70	6.60	4.67	3.05
Raai6050	46.04	17.79	5.34	6.32
Raai6075	56.09	7.19	5.56	3.19
Raai608	38.23	9.81	5.67	4.38
Raai6100	55.23	6.75	4.66	3.08
Raai628	28.17	10.42	5.07	4.55
Raai648	18.94	17.77	25.62	23.96
Raai6500	23.77	24.66	11.71	12.80
Raai7000	36.25	12.38	5.48	5.93
Raai7050	29.33	14.63	5.23	6.99
Raai7100	29.21	16.91	6.75	6.28

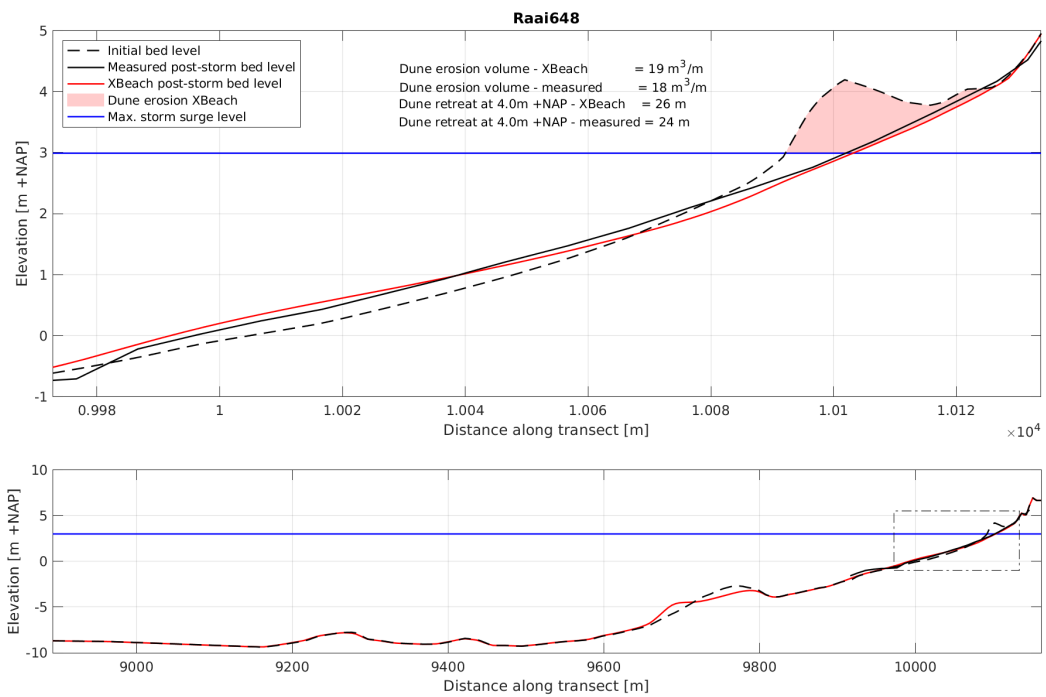


**Figure 4.29:** Cross-section for JarKus profile 648 before and after the 1976 storm based on the measurements and XBeach, including dune erosion volumes and retreat distances.

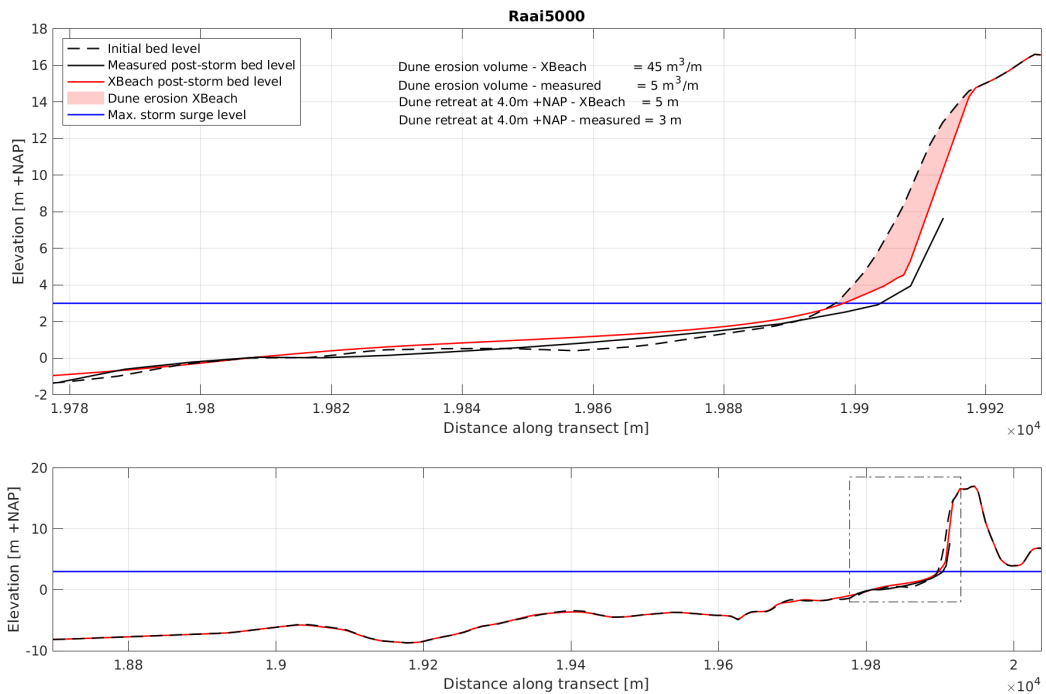


**Figure 4.30:** Cross-section for JarKus profile 5000 before and after the 1976 storm based on the measurements and XBeach, including dune erosion volumes and retreat distances.

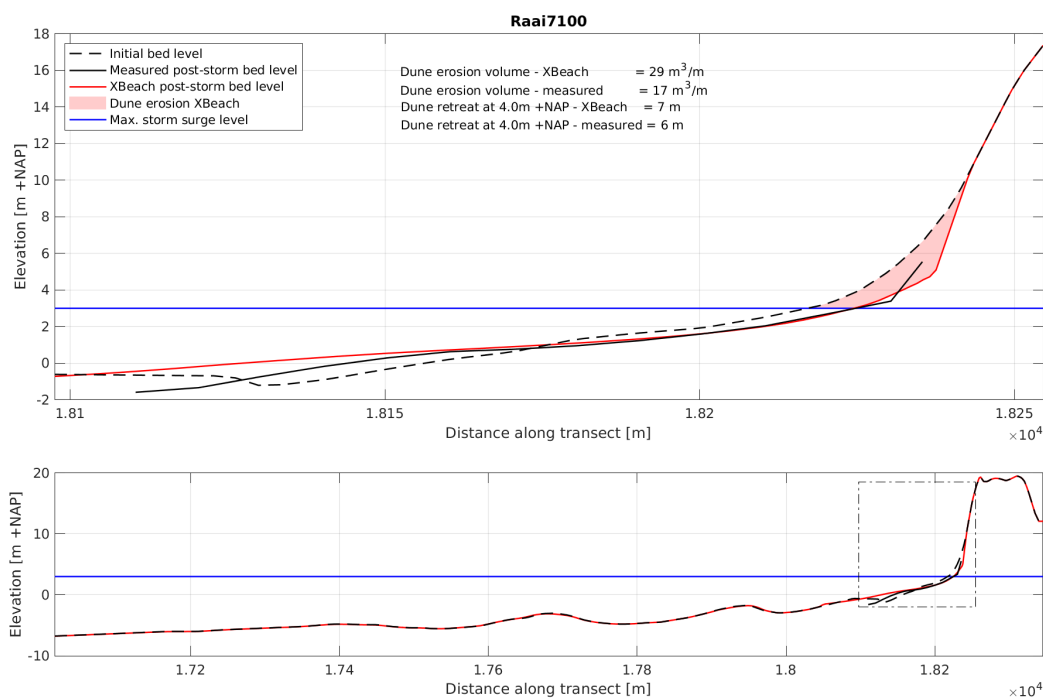


**Figure 4.31:** Cross-section for JarKus profile 7100 before and after the 1976 storm based on the measurements and XBeach, including dune erosion volumes and retreat distances.

## 4.9 Holland 1953

### Experiment description

One of the most memorable storm surges in recent history, is the storm surge in early February of 1953, leading up to the flooding of large areas in the southwest of the Netherlands and resulting in hundreds of casualties. The storm surge was especially disastrous because of the occurrence of the worst case scenario where a storm surge coincides with spring tide. A very strong northwesterly storm and spring tide led to one of the largest natural disasters (called the ‘Watersnoodramp’). It was one of the main causes for the initiation of the Dutch Delta plan, with the primary goal to increase and regulate the water security of the Dutch coast.

Because the event occurred in 1953, the amount of available data is limited. As such, a coastal profile representative for the Dutch coast is applied as pre-storm profile. For the hydrodynamic conditions, a combination of satellite derived reanalysis data, ERA5 (Bell, 2020) and literature (Gerritsen, 2005) is used. Finally, the properties of the simulated post-storm profile will be compared to reported dune erosion (Van thiel de Vries, 2009), reported at around 90 m<sup>3</sup>/m and changes in dune foot location that are available from Ruessink and Jeuken (2002), ranging from 8 to 16 meters along the Dutch coast. Because of this, the main focus of this validation case will be the morphological in nature.

Using the available data, as explained in more detail in the following sections, boundary conditions are reconstructed, representative for the coastal section between Hoek van Holland – Scheveningen (Figure 4.32).

The resulting hydraulic boundary conditions, explained in more detail below, are as follows:

- ◇ The peak surge level consisting of high (spring) tide and storm surge is 4.0 m +NAP.
- ◇ The peak significant wave height  $H_s$  during the storm is 7.3 meters.

- ◇ The maximum wave peak period  $T_p$  is 14.1 seconds.



**Figure 4.32:** Overview of the extent of the southern part of the Dutch coast (Hoek van Holland to IJmuiden) and the location of the ERA5 data.

## Results

Just like the pre-storm profile data, the post-storm data for the 1953 storm event is fairly limited. From [Van thiel de Vries \(2009\)](#), a representative range for the dune erosion above storm surge level along the Dutch coast is available:  $90 \pm 26 \text{ m}^3/\text{m}$  (with  $90 \text{ m}^3/\text{m}$  being the mean of all observations and  $26 \text{ m}^3/\text{m}$  being equal to 1 standard deviation). From [Ruessink and Jeuken \(2002\)](#), the cross-shore displacement of the dunefoot along the Dutch coast through the years is available. Looking at the 1953 timeframe specifically, a noticeable negative displacement (i.e. erosion) can be observed for all locations along the Delta coast (Walcheren and Schouwen) and the Dutch coast (Hoek van Holland to Den Helder). The displacement at Vlieland and Terschelling is less pronounced. Assuming that the entire displacement within this specific measurement interval is the result of the 1953 storm surge, the resulting dunefoot erosion can be deduced. An uncertainty range of  $\pm 1.5 \text{ m}$  is added due to the visual deduction method. The southern-most coastal sections show the largest dune foot erosion of up to  $16.5 \pm 1.5 \text{ m}$ . Towards the north, the dunefoot erosion gradually reduces, down to  $8.5 \pm 1.5 \text{ m}$  at Den Helder, possibly due to the increasing time difference between the peak waves and the peak water level, as was previously discussed. The source does not specifically mention the height at which the retreat is measured, a height of 1 meter above maximum storm surge level (i.e.  $5 \text{ m} + \text{NAP}$ ) is assumed.

In [Figure 4.33](#), the predicted dune erosion due to the 1953-storm is presented and compared to the ranges of observed dune erosion and retreat.

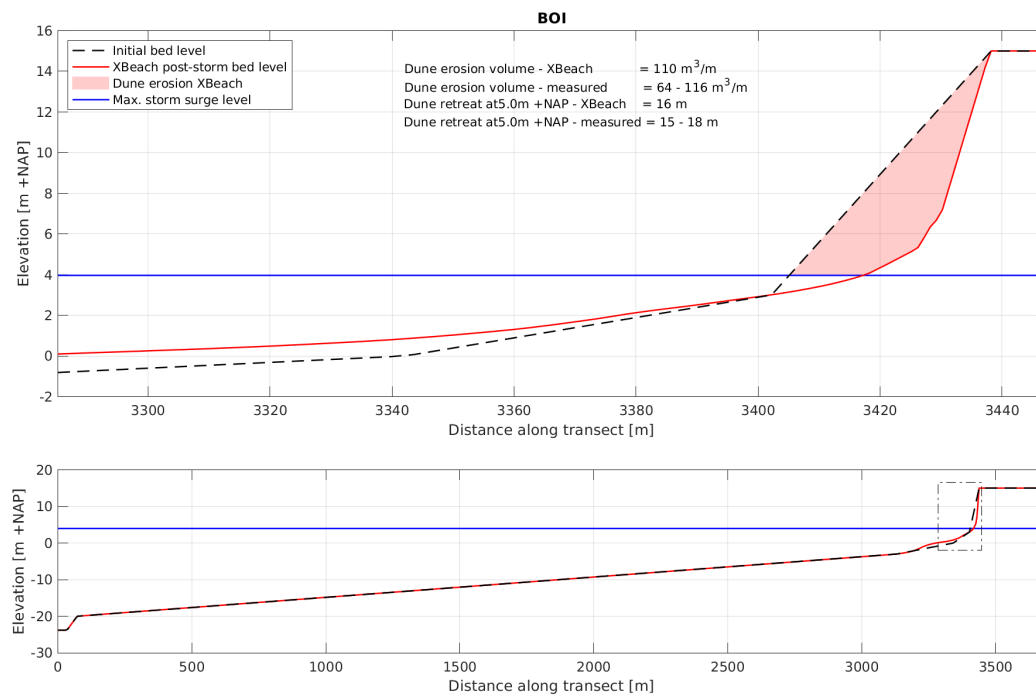


**Figure 4.33:** Pre and post storm surge profile as computed by XBeach. Upper frame shows the dune erosion section, the lower frame shows the entire XBeach profile.

## 5 References

- Arcilla, A. S., J. A. Roelvink, B. A. O'Connor, A. Reniers and J. A. Jimenez, 1994. "The Delta flume '93 experiment." In *Coastal Dynamics*, pages 488–502.
- Bakker, A. de, R. de Goede, L. de Vet, M. de Ridder, M. der Lugt, R. McCall and D. Roelvink, 2021. *BOI Standaard instellingen. Deltares rapport [concept]*. Tech. Rep. 1205758-029-GEO-0009, Deltares.
- Bell, H. H. B. P. D. P. H. A. M. S. J. T. J.-N., B., 2020. "ERA5 hourly data on single levels from 1950 to 1978 (preliminary version)." Retrieved from <https://cds.climate.copernicus-climate.eu/cdsapp/dataset/reanalysisera5-single-levels-preliminary-back-extension?tab=overview>.
- Bertin, X., K. Martins, A. de Bakker, T. Chataigner, T. Guérin, T. Coulombier and O. de Viron, 2020. "Energy transfers and reflection of infragravity waves at a dissipative beach under storm waves." *Journal of Geophysical Research: Oceans* 125 (5): e2019JC015714.
- Boers, M., 1996. *Simulation of a Surf Zone with Barred Beach, Part 1: Wave heights and Wave breaking*. Communications on Hydraulic and Geotechnical Engineering 69-5, Delft University of Technology. 116 p.
- Buster, N. A., J. C. Bernier, O. T. Brenner, K. W. Kelso, T. M. Tuten, J. L. Miselis and P. looking approximately east along Fire, 2018. *Sediment Data From Vibracores Collected in 2016 From Fire Island, New York*. US Department of the Interior, US Geological Survey.
- Carrier, G. F. and H. P. Greenspan, 1958. "Water waves of finite amplitude on a sloping beach." *Journal of Fluid Mechanics* 4: 97–109.
- Clemmensen, L. B., K. Pedersen, A. Murray and J. Heinemeier, 2006. "A 7000-year record of coastal evolution, Vejers, SW Jutland, Denmark." *Bulletin of the Geological Society of Denmark* 53: 1–22.
- De Winter, R., F. Gongriep and B. Ruessink, 2015. "Observations and modeling of alongshore variability in dune erosion at Egmond aan Zee, the Netherlands." *Coastal Engineering* 99: 167–175.
- Degraer, S., A. Volckaert and M. Vincx, 2003. "Macrobenthic zonation patterns along a morphodynamical continuum of macrotidal, low tide bar/rip and ultra-dissipative sandy beaches." *Estuarine, Coastal and Shelf Science* 56 (3-4): 459–468.
- Engelstad, A., B. Ruessink, D. Wesselman, P. Hoekstra, A. Oost and M. van der Vegt, 2017. "Observations of waves and currents during barrier island inundation." *Journal of Geophysical Research: Oceans* 122 (4): 3152–3169.
- Fredericks, H. C. L. E., X., 2016. "Coastal Topography - Fire Island, New York, 07 May 2012 U.S. Geological Survey data release."
- Gerritsen, H., 2005. "What happened in 1953? The Big Flood in the Netherlands in retrospect." *Philosophical Transactions of the Royal Society A: Mathematical, Physical and Engineering Sciences* 363 (1831): 1271–1291.
- Guérin, T., X. Bertin, T. Coulombier and A. de Bakker, 2018. "Impacts of wave-induced circulation in the surf zone on wave setup." *Ocean Modelling* 123: 86–97.
- Hamm, L. and C. Peronnard, 1997. "Wave parameters in the nearshore: A clarification." *Coastal Engineering* 32 (2-3): 119–135.

- Hapke, C. J., O. Brenner, R. Hehre and B. Reynolds, 2013. *Coastal Change from Hurricane Sandy and the 2012-13 Winter Storm Season: Fire Island, New York*. US Department of the Interior, US Geological Survey Reston, Virginia.
- Hillmann, H. T. F., Simon; Blum, 2021. *National Analysis. Germany / Lower Saxony NLWKN - Interreg VB NSR BwN*. Tech. rep., <https://building-with-nature.eu/publications/monitoring-evaluation/>.
- Hillmann, K. Q. E. H. R., S.; Geertsen and B. Frederiksen, 2021. *Influencing the SPR for storm surge events. A cross-border XBeach application. Interreg North Sea Region VB Building with Nature report*. Tech. rep.
- IMDC, 2005. *Hydraulisch Randvoorwaardenboek Vlaamse Kust*. Tech. Rep. I/RA/11226/03.041/KTR, IMDC. In Dutch.
- Kystdirektoratet, 2021. *Calculation of cliff retreat on sandy coasts in Denmark using XBeach*. Tech. rep., Kystdirektoratet.
- Lanckriet, T., K. Trouw, N. Zimmermann, L. Wang, B. De Maerschalck, R. Delgado, T. Verwaest and F. Mostaert, 2015. "Scientific support regarding hydrodynamics and sand transport in the coastal zone: hindcast of the morphological impact of the 5-6 December 2013 storm using XBeach." *WL Rapporten* .
- Jerma, A. N., T. Bulteau, S. Lecacheux and D. Idier, 2015. "Spatial variability of extreme wave height along the Atlantic and channel French coast." *Ocean Engineering* 97: 175–185.
- Lugt, M. A. van der, E. Quataert, A. van Dongeren, M. van Ormondt and C. R. Sherwood, 2019. "Morphodynamic modeling of the response of two barrier islands to Atlantic hurricane forcing." *Estuarine, Coastal and Shelf Science* 229: 106404.
- Roelvink, J. A. and M. J. F. Stive, 1989. "Bar-generating cross-shore flow mechanisms on a beach." *Journal of Geophysical Research* 94 (C4): 4785–4800.
- Ruessink, B. and M. Jeuken, 2002. "Dunefoot dynamics along the Dutch coast." *Earth Surface Processes and Landforms: The Journal of the British Geomorphological Research Group* 27 (10): 1043–1056.
- Ruessink, B. G., H. Michallet, P. Bonneton, D. Mouazé, J. Lara, P. A. Silva and P. Wellens, 2013. "Globex: wave dynamics on a gently sloping laboratory beach." *Proceedings Coastal Dynamics 2013* pages 1351–1362.
- Ruessink, G., C. S. Schwarz, T. D. Price and J. J. Donker, 2019. "A multi-year data set of beach-foredune topography and environmental forcing conditions at Egmond aan Zee, The Netherlands." *Data* 4 (2): 73.
- Saye, S. E. and K. Pye, 2006. "Variations in chemical composition and particle size of dune sediments along the west coast of Jutland, Denmark." *Sedimentary Geology* 183 (3-4): 217–242.
- Schwab, W. C., W. E. Baldwin, C. J. Hapke, E. E. Lentz, P. T. Gayes, J. F. Denny, J. H. List and J. C. Warner, 2013. "Geologic evidence for onshore sediment transport from the inner continental shelf: Fire Island, New York." *Journal of Coastal Research* 29 (3): 526–544.
- Trouw, K., R. Houthuys, T. Lanckriet, N. Zimmermann, L. Wang, B. De Maerschalck, R. Delgado, T. Verwaest and F. Mostaert, 2015. "Wetenschappelijke bijstand zanddynamica: inventarisatie randvoorwaarden en morfologische impact van de Sinterklaasstorm op 6 december 2013." *WL Rapporten* .

- Van Gent, M. R. A. and E. M. Coeveld, 2007. *Influence of collapsed revetments on dune erosion*. Tech. Rep. H4731, Delft Hydraulics.
- Van Gent, M. R. A., J. S. M. Van Thiel de Vries, E. M. Coeveld, J. H. De Vroeg and J. Van de Graaff, 2008. "Large-scale dune erosion tests to study the influence of wave periods." *Coastal Engineering* 55 (12).
- Vellinga, P., 1981. *The functioning of dune revetments during a super storm surge*. Tech. Rep. M1797, Delft Hydraulics. In Dutch.
- Vellinga, P., 1984. *Scale series dune erosion: Large scale tests in Deltaflume*. Tech. Rep. M1263 part III, Delft Hydraulics. In Dutch.
- Vries, J. S. M. Van Thiel de, 2009. *Dune erosion during storm surges*. Ph.D. thesis, Delft University of Technology.
- Vries, J. S. M. Van Thiel de, M. R. A. Van Gent, D. J. R. Walstra and A. J. H. M. Reniers, 2008. "Analysis of dune erosion processes in large-scale flume experiments." *Coastal Engineering* 55 (12).
- Werf, J. Van der, R. Van Santen, M. Van Ormondt, C. Briere and A. Van Dongeren, 2011. "Operational model to simulate storm impact along the Holland Coast." In *Proceedings Coastal Sediments 2011*. Miami, Florida, USA.
- Wesselman, D., R. de Winter, A. Engelstad, R. McCall, A. van Dongeren, P. Hoekstra, A. Oost and M. van der Vegt, 2018. "The effect of tides and storms on the sediment transport across a Dutch barrier island." *Earth Surface Processes and Landforms* 43 (3): 579–592.
- Wijnberg, K. M., 2002. "Environmental controls on decadal morphologic behaviour of the Holland coast." *Marine Geology* 189 (3-4): 227–247.



## A Model Performance Statistics

### A.1 Introduction

In this Appendix the theory behind the Model Performance Statistics (MPS) used in the XBeach skillbed is explained. The MPS are used to quantify the performance of model results based on a comparison with measurement data. Different MPS parameters are used as each parameter has its own characteristics.

First an overview is given of the MPS parameters used in the XBeach skillbed, summarized in table form including some basic characteristics. Consequently, each MPS parameters listed in the overview table is further explained in separate sections.

### A.2 MPS parameters

An overview of the MPS parameters used in the XBeach skillbed is given in [Table A.1](#).

**Table A.1:** MPS parameters

Parameter	Description	Ranges
ME & STD	Mean Error & Standard Deviation	0: perfect prediction
Rel. bias	Systematic error relative to the mean	low value: good performance
Sci	Scatter Index	low values: performance

Each parameter listed in the table is further explained in the following paragraphs.

### A.3 Mean Error & Standard Deviation

The Mean Error (ME) and the Standard Deviation (STD) of the error of a timeseries are a useful measure to quantify model performance for parameters such as wave heights or water levels. The SD is in general not so useful when applied to morphological parameters such as the bed leve evolution.

$$ME = \frac{1}{N} \sum_{i=1}^N (f_{comp.,i} - f_{meas.,i}) \quad (A.1)$$

$$STD = \sqrt{\frac{1}{N-1} \sum_{i=2}^N (f_{comp.,i} - f_{meas.,i} - ME)^2} \quad (A.2)$$

#### A.4 Relative Bias

The Relative Bias (Rel. Bias) is the systematic error relative to the mean. Relative low values of the mean can cause high vales of the Rel. Bias.

$$Rel.Bias = \frac{\sum_{i=1}^N (f_{comp.,i} - f_{meas.,i})}{\sum_{i=1}^N \bar{f}_{meas.}} \quad (A.3)$$

#### A.5 Scatter Index

The Scatter index (SCI) is the standard deviation relative to the mean value of the measured signal. Relative low values of the mean can cause high vales of the SCI.

$$Sci = \frac{\sqrt{\frac{1}{N-1} \sum_{i=2}^N (f_{comp.,i} - f_{meas.,i} - ME)^2}}{\bar{f}_{meas.}} \quad (A.4)$$

## B Morphology indicators

### B.1 Erosion volume

The dune erosion volume is defined as the volume per running meter between the initial bed level and the bed level at a given time. For both the initial bed level and the bed level at a given time, the maximum water level is applied as lower limit (See Figure B.1).

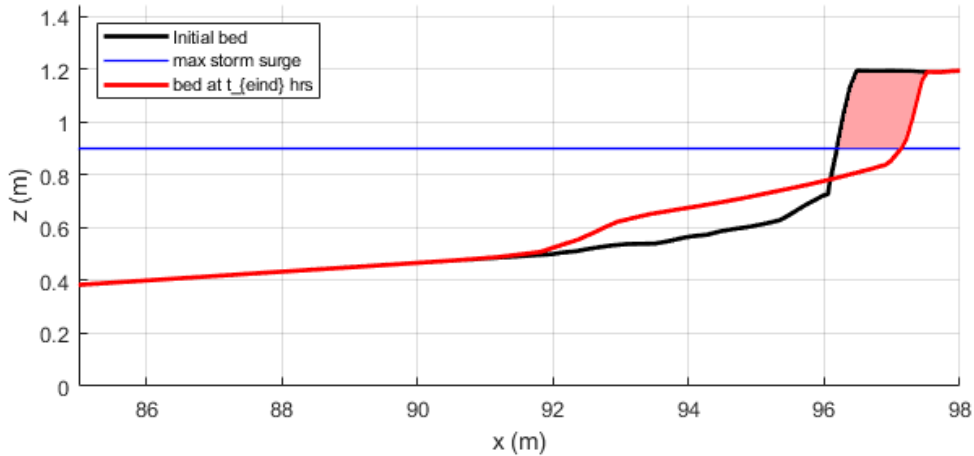


Figure B.1: Definition of erosion volume

### B.2 Dune front retreat

The dune front retreat is defined as the horizontal displacement at a given reference height in the considered time period. The reference height is defined as the 1.5 times the grid resolution below the maximum initial bed level for the lab experiments (See Figure B.2). This height is representative for the dune front and low enough to capture all the dune front of all the observed profiles. The dune height can reduce during an experiment due to erosion. For each of the field cases a different characteristic dune height is applied since the profiles are very different. This definition of the dune retreat for the field cases is given in each section.

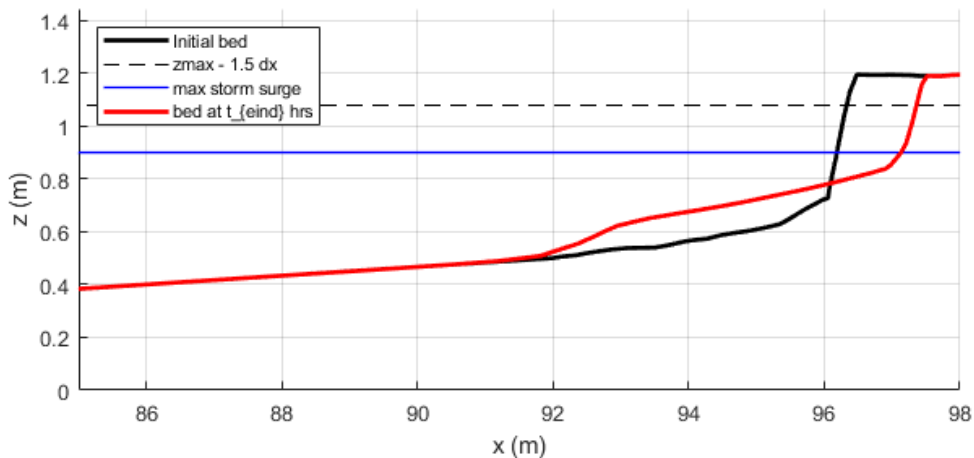
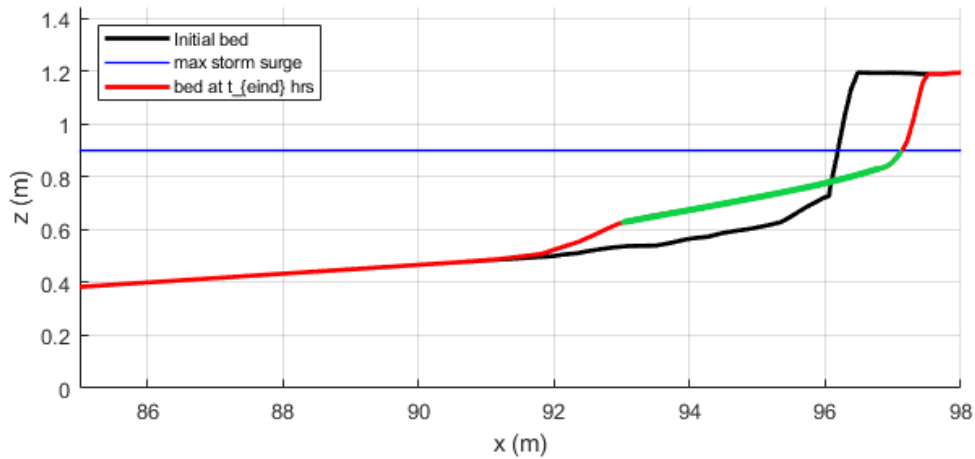


Figure B.2: Dune retreat indicator.

### B.3 Berm slope

The berm slope is defined as the mean slope in the deposition zone. The upper limit is defined as the maximum water level and the lower limit is equal to the most seaward point of the deposition zone, where the deposition is equal to 50% of the maximum vertical deposition (See Figure B.3). The mean of this slope is computed after interpolating the bed level to a uniform grid. This interpolation is required to prevent that the mean berm slope is affected by the spatial variation in the grid.



**Figure B.3:** Berm slope indicator

## C Detailed analysis

This Appendix shows a detailed analysis selected physical experiments for which detailed hydrodynamic and morphodynamic data are available.

### C.1 Deltagoot 2006

In this section, a detailed comparison between simulated physics over an evolving bathymetry and the measurements obtained during the Deltaflume experiment in 2006 (Van Gent *et al.*, 2008) is made.

The observed and computed wave height transformation and the setup are shown in Figure C.1 to Figure C.3. These wave height transformations results in a flow pattern, which affect the sediment transport rates. The comparison of the flow velocities is shown in Figure C.4 and Figure C.5. Note that the comparison of the velocities of test T02 is not shown, because the observed velocities are not available.

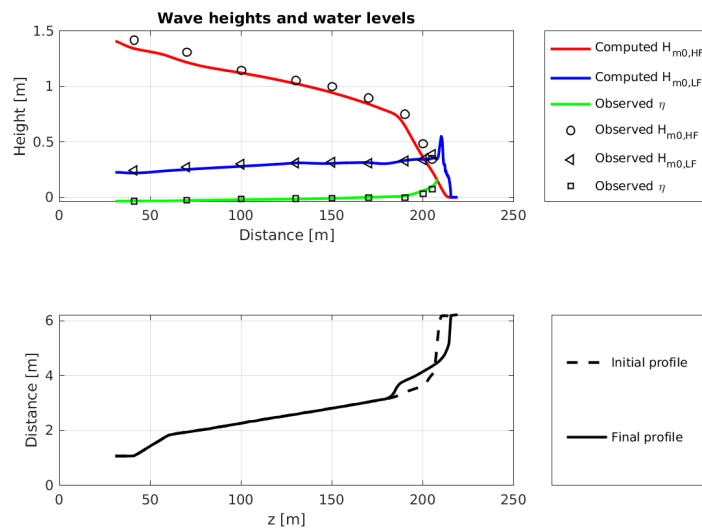


**Figure C.1:** Computed and observed short wave height transformation, infragravity wave height transformation and mean water level (upper panel) for test T01. The lower panel shows the initial and final computed profiles.

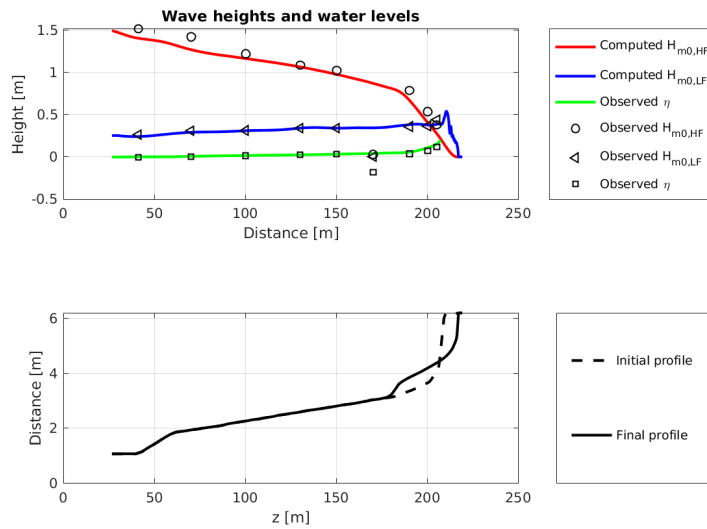


**Figure C.2:** Computed and observed short wave height transformation, infragravity wave height transformation and mean water level (upper panel) for test T02. The lower panel shows the initial and final computed profiles.

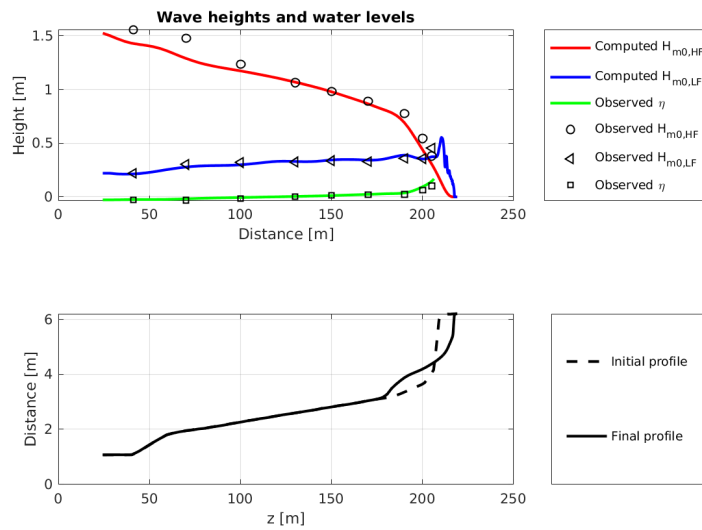


**Figure C.3:** Computed and observed short wave height transformation, infragravity wave height transformation and mean water level (upper panel) for test T03. The lower panel shows the initial and final computed profiles.

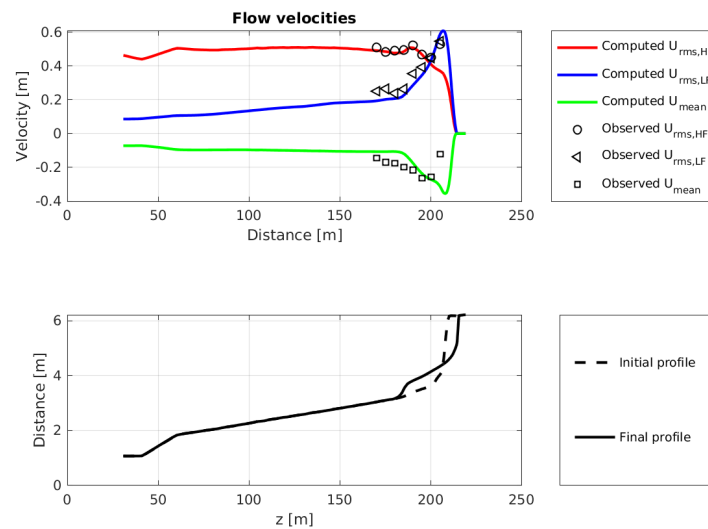


**Figure C.4:** Computed and observed high and low frequency root-mean-squared velocity and mean velocity (upper panel) for test T01. The lower panel shows the initial and final computed profiles.

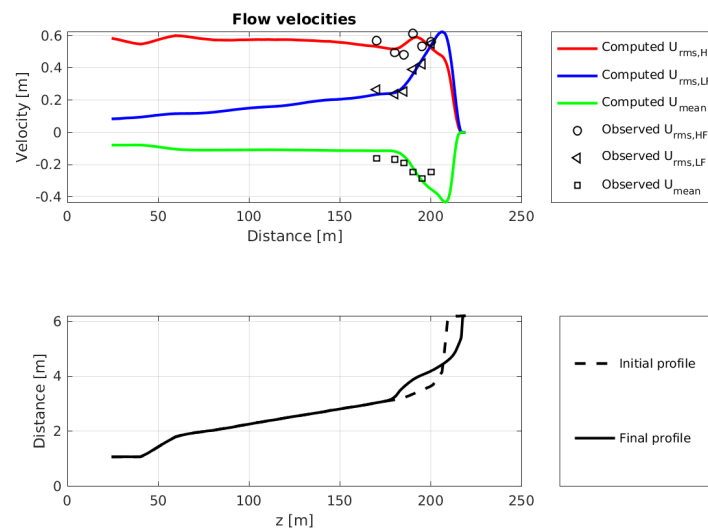


**Figure C.5:** Computed and observed high and low frequency root-mean-squared velocity and mean velocity (upper panel) for test T03. The lower panel shows the initial and final computed profiles.

XBeach does not resolve the short wave shape, but an approximation is applied to include the effects of nonlinear waves on the sediment transport rates. The wave shape which is expressed in terms of skewness, asymmetry is shown in [Figure C.6](#), [Figure C.7](#) and [Figure C.8](#). In general, the wave shape changes when the water depth decreases. In shallow water the waves become more asymmetrical (sawtooth shape) and more skewed (higher peaks), which is also visible in the computed and observed wave shapes.

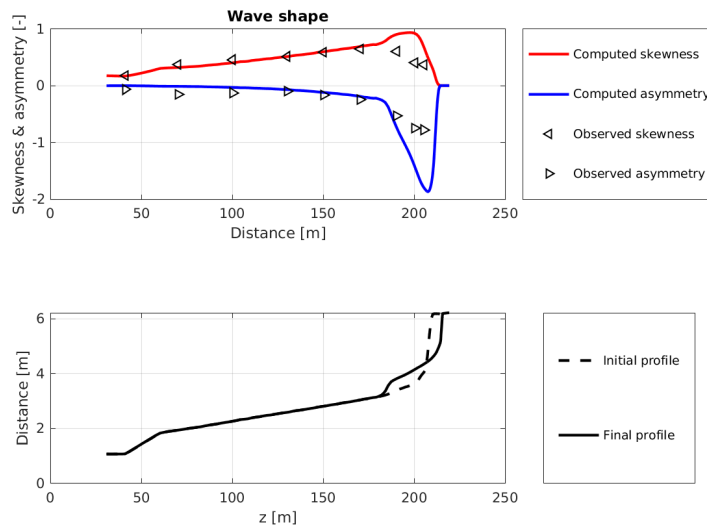


**Figure C.6:** Computed and observed wave shape as a function of the cross-shore distance (upper panel).

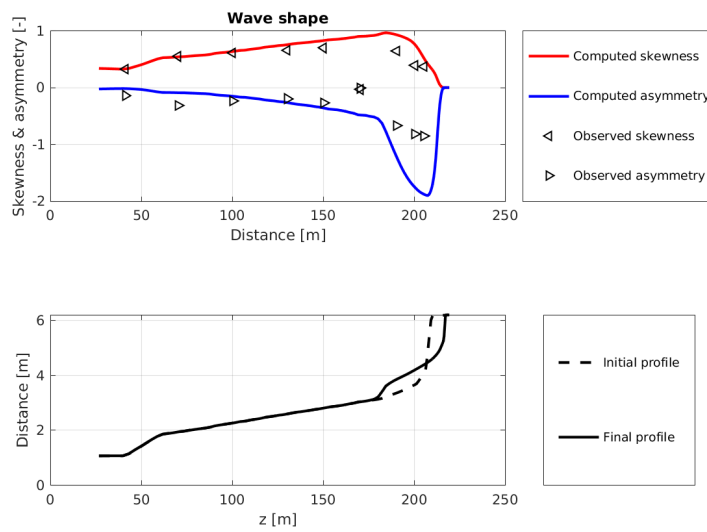


**Figure C.7:** Computed and observed wave shape as a function of the cross-shore distance (upper panel)

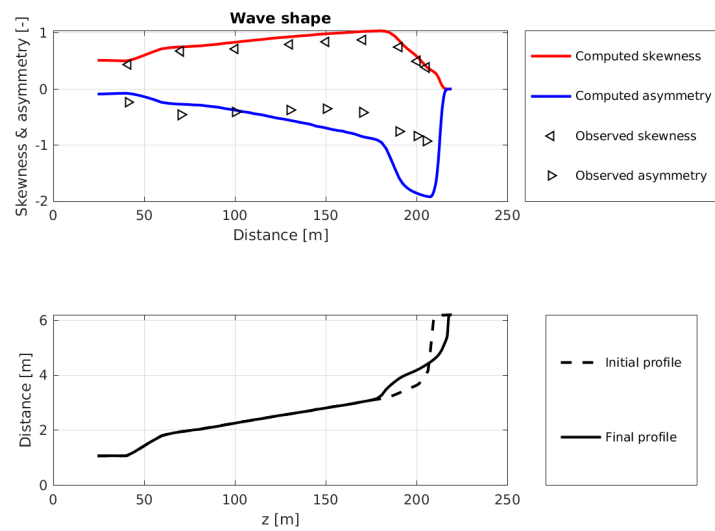


**Figure C.8:** Computed and observed wave shape as a function of the cross-shore distance (upper panel)

The observed and modelled sediment concentrations are shown in Figure ?? and ?. The observed sediment concentrations are not available and, therefore, the results of test T02 are not shown.

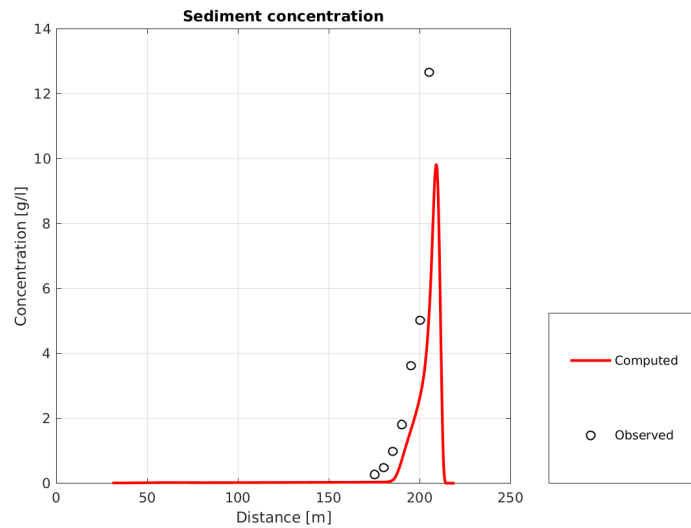


**Figure C.9:** Sediment concentrations

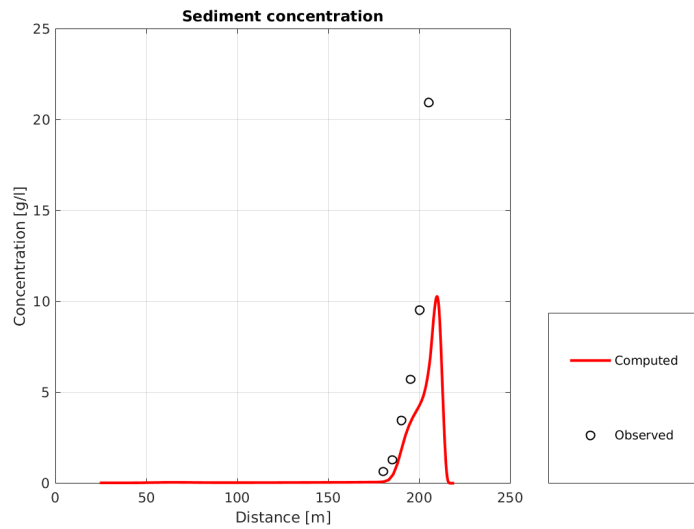


**Figure C.10:** Sediment concentrations

In Figure C.11 to Figure C.13, the observed and computed erosion and sedimentation patterns are compared. The bed level changes clearly show a erosion at the dune front and a deposition on the foreshore. The temporal plot of the erosion volumes is shown in Figure C.14 to Figure C.16.

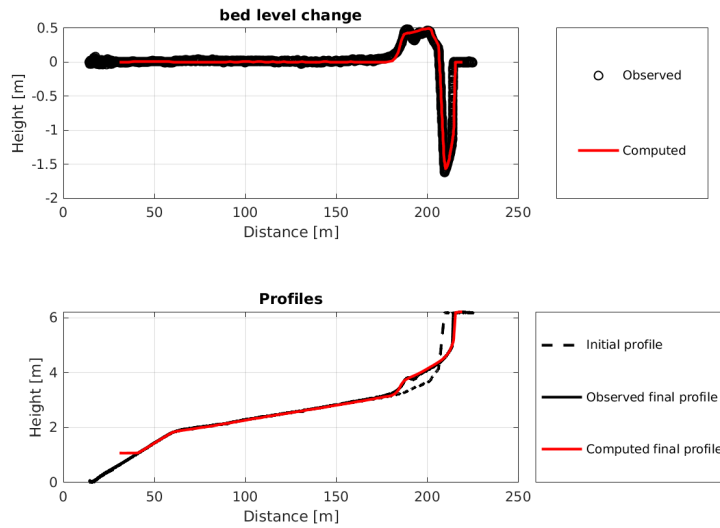


**Figure C.11:** Erosion and sedimentation patterns (upper panel) and profiles (lower panel) for test T01

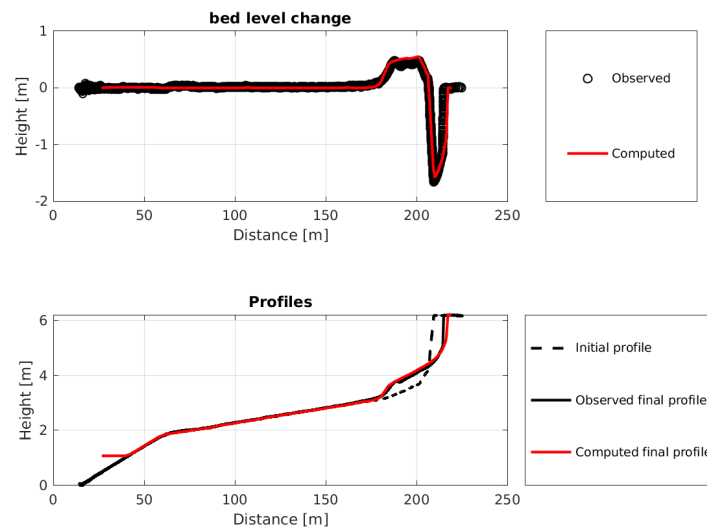


**Figure C.12:** Erosion and sedimentation patterns (upper panel) and profiles (lower panel) for test T02

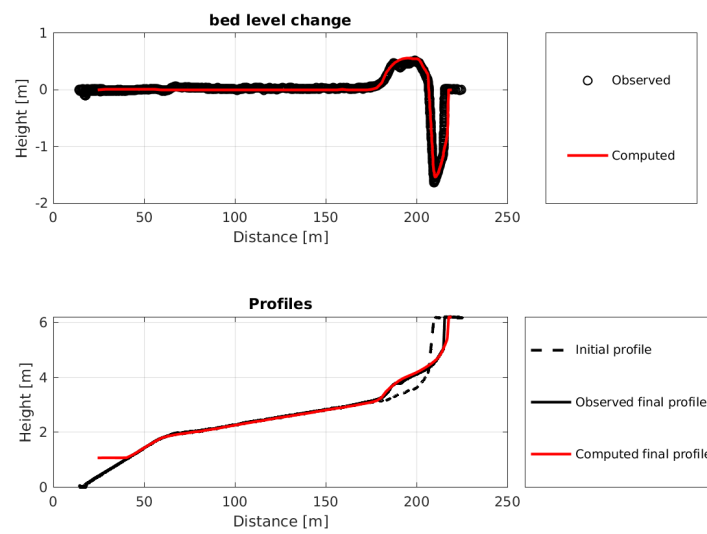


**Figure C.13:** Erosion and sedimentation patterns (upper panel) and profiles (lower panel) for test T03

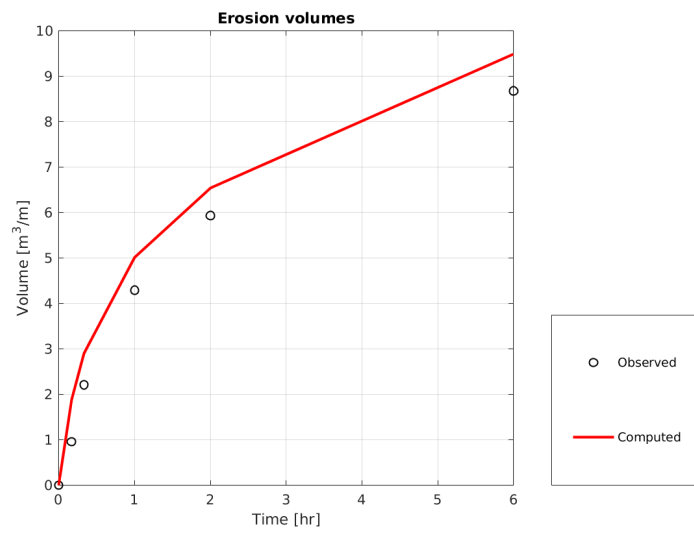


**Figure C.14:** Erosion volumes as a function of time for test T01

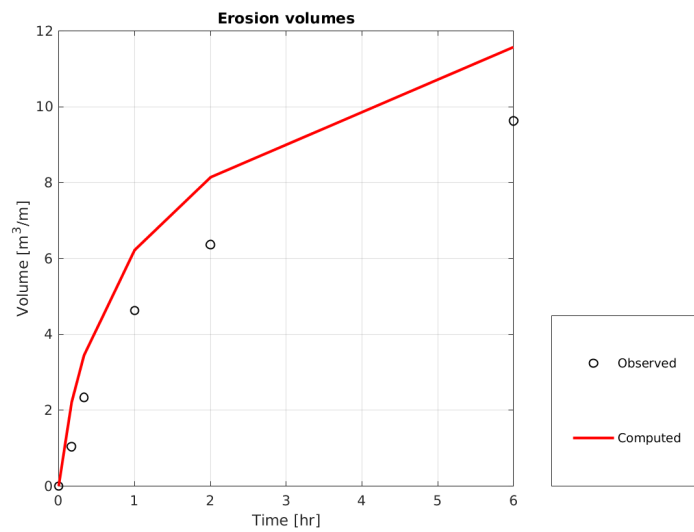


**Figure C.15:** Erosion volumes as a function of time for test T02

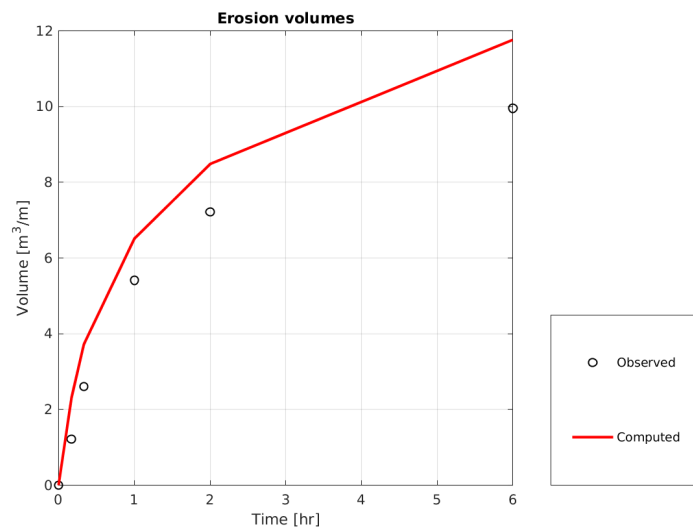


**Figure C.16:** Erosion volumes as a function of time for test T03

## C.2 LIP

This section shows additional detailed comparison of the 2E test of the LIP 11D experiment (Arcilla *et al.*, 1994).

The observed and computed wave height transformation and the setup are shown in Figure C.17. The sedimentation and erosion patterns are shown in Figure C.18 and the erosion volumes as function of the time are shown in Figure C.19.

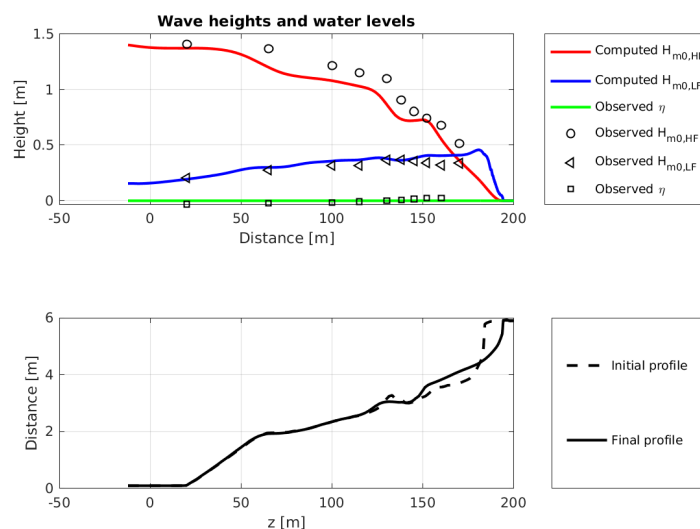


**Figure C.17:** Computed and observed short wave height transformation, infragravity wave height transformation and mean water level (upper panel) for test 2E. The lower panel shows the initial and final computed profiles.

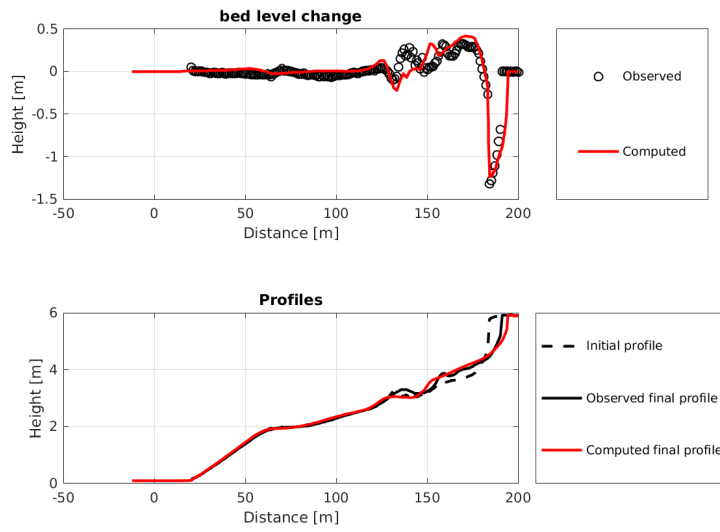


**Figure C.18:** Erosion pattern and volumes and retreat distance during test 2E

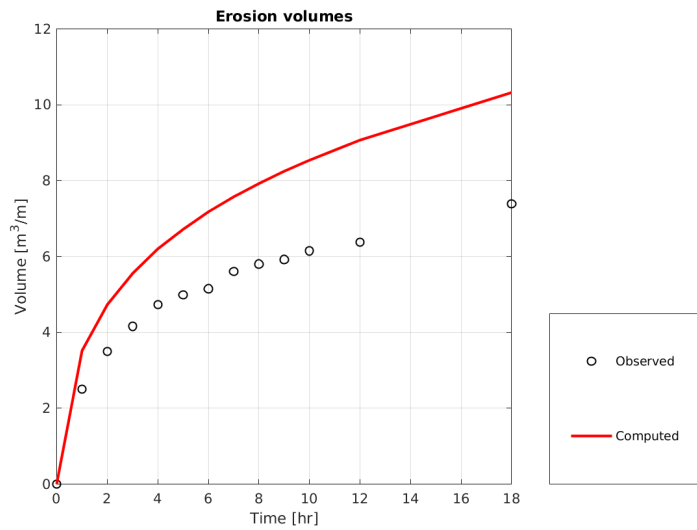


**Figure C.19:** Erosion volumes as a function of time for test E2